FUNDAMENTAL SOLUTIONS OF MULTI-LAYER ELASTIC MEDIA WITH COUPLE STRESS THEORY

Miss Wipavee Wongviboonsin

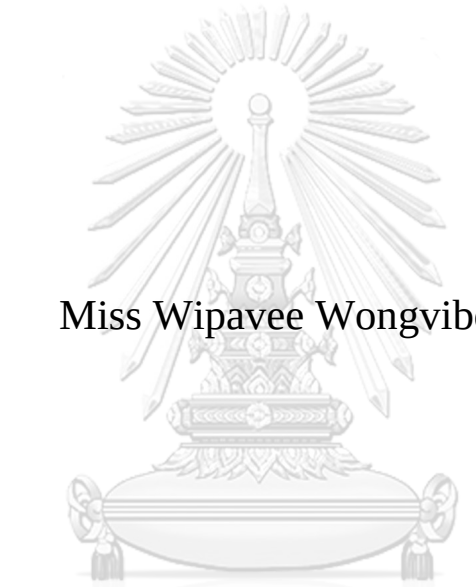

จุฬาลงกรณ์มหาวิทยาลัย
Chulalongkorn University

A Thesis Submitted in Partial Fulfillment of the Requirements
for the Degree of Master of Engineering in Civil Engineering
Department of Civil Engineering
Faculty of Engineering
Chulalongkorn University
Academic Year 2019
Copyright of Chulalongkorn University

ผลเฉลยพื้นฐานของตัวกลางยืดหยุ่นหลายชั้นด้วยทฤษฎีหน่วยแรงคู่ควบ

น.ส.วิภาวี วงษ์วิบูลย์สิน

จุฬาลงกรณ์มหาวิทยาลัย
CHULALONGKORN UNIVERSITY

วิทยานิพนธ์นี้เป็นส่วนหนึ่งของการศึกษาตามหลักสูตรปริญญาวิศวกรรมศาสตรมหาบัณฑิต
สาขาวิชาวิศวกรรมโยธา ภาควิชาวิศวกรรมโยธา
คณะวิศวกรรมศาสตร์ จุฬาลงกรณ์มหาวิทยาลัย
ปีการศึกษา 2562
ลิขสิทธิ์ของจุฬาลงกรณ์มหาวิทยาลัย

Thesis Title	FUNDAMENTAL SOLUTIONS OF MULTI-LAYER ELASTIC MEDIA WITH COUPLE STRESS THEORY
By	Miss Wipavee Wongviboonsin
Field of Study	Civil Engineering
Thesis Advisor	Associate Professor Jaroon Rungamornrat, Ph.D.

Accepted by the Faculty of Engineering, Chulalongkorn University in Partial Fulfillment of the Requirement for the Master of Engineering

..... Dean of the Faculty of Engineering
(Professor SUPOT TEACHAVORASINSKUN, Ph.D.)

THESIS COMMITTEE

..... Chairman
(Professor Teerapong Senjuntichai, Ph.D.)
..... Thesis Advisor
(Associate Professor Jaroon Rungamornrat, Ph.D.)
..... Examiner
(Assistant Professor Watanachai Smittakorn, Ph.D.)
..... External Examiner
(Associate Professor Pornkasem Jongpradist, Ph.D.)

จุฬาลงกรณ์มหาวิทยาลัย
Chulalongkorn University

วิภาวี วงษ์วิบูลย์สิน : ผลเฉลยพื้นฐานของตัวกลางยืดหยุ่นหลายชั้นด้วยทฤษฎีหน่วยแรงคู่ควบ. (FUNDAMENTAL SOLUTIONS OF MULTI-LAYER ELASTIC MEDIA WITH COUPLE STRESS THEORY) อ.ที่ปรึกษาหลัก : รศ. ดร.จรูญ รุ่งอมรรัตน์

วิทยานิพนธ์นี้นำเสนอผลเฉลยพื้นฐานสำหรับตัวกลางหลายชั้นยืดหยุ่นสองมิติภายใต้แรงกระทำที่ผิวโดยพิจารณาอิทธิพลของโครงสร้างวัสดุในระดับไมโครร่วมด้วย แบบจำลองทางคณิตศาสตร์สำหรับจำลองอิทธิพลจากสเกลขนาดเล็กสร้างขึ้นภายใต้กรอบแบบต่อเนื่องผ่านทางทฤษฎีหน่วยแรงคู่ควบ สมการของเนเวียร์แบบทั่วไปซึ่งกำกับสนามการขจัดของแต่วัสดุแต่ละชั้นถูกพัฒนาขึ้นและใช้ระเบียบวิธีการแปลงเชิงปริพันธ์ของฟูริเยร์ในการหาผลเฉลยทั่วไปในสเปซของการแปลง เซตของเงื่อนไขขอบและความต่อเนื่องของปริมาณสนามตามแนวรอยต่อวัสดุนำมาใช้สร้างระบบสมการพีชคณิตเชิงเส้นซึ่งกำกับระดับขั้นความเสรีไม่ทราบค่าของตัวกลางชั้นทั้งหมดในสเปซของการแปลง ปริพันธ์ที่เกิดขึ้นจากการแปลงปริพันธ์ผกผันของฟูริเยร์หาค่าโดยใช้ระเบียบวิธีเชิงตัวเลขที่มีประสิทธิภาพ ผลที่ได้จากการวิเคราะห์ไม่เพียงเพื่อยืนยันความถูกต้องของผลเฉลยที่พัฒนาขึ้นแต่ยังแสดงถึงความสามารถของแบบจำลองทางคณิตศาสตร์ที่เลือกใช้ในการจำลองการขึ้นอยู่กับขนาดเมื่อมาตรความยาวภายในและภายนอกมีค่าใกล้เคียงกัน แบบจำลองตัวกลางหลายชั้นที่สร้างขึ้นยังถูกนำมาใช้ในการศึกษาปัญหาตัวกลางชั้นยืดหยุ่นวางบนฐานแข็งเกร็งซึ่งทำมาจากวัสดุที่มีคุณสมบัติแปรเปลี่ยนตามตำแหน่งได้อีกด้วย

จุฬาลงกรณ์มหาวิทยาลัย
CHULALONGKORN UNIVERSITY

สาขาวิชา	วิศวกรรมโยธา	ลายมือชื่อนิสิต .....
ปีการศึกษา	2562	ลายมือชื่อ อ.ที่ปรึกษาหลัก .....

6070313621 : MAJOR CIVIL ENGINEERING
KEYWOR D: Couple Stresses, Integral Transforms, Multi-layer Media, Size Dependence, Surface Loading

Wipavee Wongviboonsin : FUNDAMENTAL SOLUTIONS OF MULTI-LAYER ELASTIC MEDIA WITH COUPLE STRESS THEORY. Advisor: Assoc. Prof. Jaroon Rungamornrat, Ph.D.

This thesis presents fundamental solutions of a two-dimensional, elastic, multi-layered medium under surface loadings by taking the influence of material micro-structure into account. An underlying mathematical model for simulating such small-scale influence is established within the continuum-based framework via the well-known couple stress theory. For each material layer, the generalized Navier's equation governing the displacement field is established and the method of Fourier integral transform is applied to derive its general solution in a transformed space. A set of boundary conditions and the continuity of fields along the material interfaces are enforced to obtain a system of linear algebraic equations governing all unknown degrees of freedom of the whole layered medium in the transformed space. An efficient quadrature is then adopted to carry out all involved integrals arising from Fourier integral transform inversion. A selected set of results is also reported not only to confirm the validity of established solutions but also to demonstrate the capability of the selected mathematical model to simulate the size-dependency when the external and internal length scales are comparable. An approximation of a functionally graded material rested on a rigid base is also investigated using the same model.

จุฬาลงกรณ์มหาวิทยาลัย
Chulalongkorn University

Field of Study:	Civil Engineering	Student's Signature .....
Academic Year:	2019	Advisor's Signature .....

ACKNOWLEDGEMENTS

I deeply appreciate all the support from my advisor, Assoc. Prof. Jaroon Rungamornrat. His dedication in research works and the helpful guidance led me to the right direction and be able to carry out such an amazing quality research. I am grateful to the committee who patiently listened to my presentation and gave me a useful feedback. Thanks to my friends and seniors who cheered me up during the hard time. Lastly, I would love to express my deep gratitude to my family, the greatest source of energy, that always be there and believe in me.

Wipavee Wongviboonsin

จุฬาลงกรณ์มหาวิทยาลัย
CHULALONGKORN UNIVERSITY

TABLE OF CONTENTS

Page

..... iii

ABSTRACT (THAI) iii

.....iv

ABSTRACT (ENGLISH).....iv

ACKNOWLEDGEMENTS.....v

TABLE OF CONTENTS.....vi

LIST OF FIGURES viii

CHAPTER 1 INTRODUCTION.....1

1.1 Motivation and Significance.....1

1.2 Background and Review.....4

1.3 Objectives 6

1.4 Scopes of Work.....6

1.5 Methodology and Research Procedure 7

1.6 Expected Outputs and Contributions.....8

CHAPTER 2 PROBLEM FORMULATION 9

2.1 Problem Description and Statement 9

2.2 Linearized Couple Stress Theory.....10

2.3 Two-dimensional, Plane-strain Case 14

2.4 Governing Equations in terms of Displacement.....16

CHAPTER 3 SOLUTION PROEDURE 18

3.1 General Solutions for Displacement of Representative Layer 18

3.2 General Solutions for Other Field Quantities 21

3.3 Governing Equations for Whole Layered Medium 23

3.4 Fourier Integral Transform Inversion 26

CHAPTER 4 RESULTS AND DISCUSSION.....27

จุฬาลงกรณ์มหาวิทยาลัย
Chulalongkorn University

4.1 Homogeneous Half-plane 28
4.2. Single Layer Media.....29
4.3. Layer on Half Plane under Uniformly Distributed Loads 40
4.4 Layered Media Consisting of Periodic Bi-materials.....55
4.5 Functionally Graded Layer on Rigid Base 63
CHAPTER 5 CONCLUSION.....72
REFERENCES 74
VITA 79

จุฬาลงกรณ์มหาวิทยาลัย
Chulalongkorn University

LIST OF FIGURES

Page

Figure 2.1 Schematic of two-dimensional layered medium rested on rigid foundation and subjected to surface loading 9

Figure 2.2 Schematic indicating force-stress and couple-stress components for two-dimensional problems 14

Figure 4.1 Normalized normal force stress σ_{xx} and σ_{yy} along the line of symmetry of elastic half-plane under uniformly distributed normal traction. Result reported for $\nu = 0.33$ and $a/\ell_0 = 1$. 29

Figure 4.2 Normalized horizontal displacements u_x at the top surface of a single homogeneous layer under normal concentrated force with $\nu = 0$ 31

Figure 4.3 Normalized vertical displacements u_y at the top surface of a single homogeneous layer under normal concentrated force with $\nu = 0$ 32

Figure 4.4 Normalized rotations ω_z at the top surface of a single homogeneous layer under normal concentrated force with $\nu = 0$ 32

Figure 4.5 Normalized vertical stresses σ_{yy} at the bottom surface of a single homogeneous layer under normal concentrated force with $\nu = 0$ 33

Figure 4.6 Normalized shear stresses σ_{yx} at the bottom surface of a single homogeneous layer under normal concentrated force with $\nu = 0$ 33

Figure 4.7 Normalized couple stresses μ_{yz} at the bottom surface of a single homogeneous layer under normal concentrated force with $\nu = 0$ 34

Figure 4.8 Normalized horizontal displacements u_x at the top surface of a single homogeneous layer under normal concentrated force with $\nu = 0.49$ 34

Figure 4.9 Normalized vertical displacements u_y at the top surface of a single homogeneous layer under normal concentrated force with $\nu = 0.49$ 35

Figure 4.10 Normalized rotations ω_z at the top surface of a single homogeneous layer under normal concentrated force with $\nu = 0.49$ 35

Figure 4.11 Normalized vertical stresses σ_{yy} at the bottom surface of a single homogeneous layer under normal concentrated force with $\nu = 0.49$ 36

จุฬาลงกรณ์มหาวิทยาลัย
Chulalongkorn University

Figure 4.12 Normalized shear stresses σ_{yx} at the bottom surface of a single homogeneous layer under normal concentrated force with $\nu = 0.49$ 36

Figure 4.13 Normalized couple stresses μ_{yz} at the bottom surface of a single homogeneous layer under normal concentrated force with $\nu = 0.49$ 37

Figure 4.14 Normalized vertical stresses σ_{yy} along the line of symmetry of a single layer medium plane under uniformly distributed normal traction. Results are reported for $\nu = 0.33$, $h/a = 1$, $\rho \in \{0,1\}$, and various values of a/ℓ. 37

Figure 4.15 Normalized vertical stresses σ_{yy} at a point $x = 0$ and $y = h/2$ of a single layer medium plane under uniformly distributed normal traction versus the normalized half-length of loading region. Result reported for $\nu = 0.33$, $h/a = 1$, and $\rho \in \{0,1\}$. 38

Figure 4.16 Profile of normalized vertical displacement u_y at $y/h = 0.5$ for a single homogeneous layer medium under uniformly distributed normal traction having with $h = \ell = \ell_0$ and $\nu = 0.5$. 38

Figure 4.17 Profile of normalized vertical stress σ_{yy} at $y/h = 0.5$ for a single homogeneous layer medium under uniformly distributed normal traction having with $h = \ell = \ell_0$ and $\nu = 0.5$. 39

Figure 4.18 Profile of normalized couple stress μ_{xz} at $y/h = 0.5$ for a single homogeneous layer medium under uniformly distributed normal traction having with $h = \ell = \ell_0$ and $\nu = 0.5$. 39

Figure 4.19 Profile of normalized couple stress μ_{yz} at $y/h = 0.5$ for a single homogeneous layer medium under uniformly distributed normal traction having with $h = \ell = \ell_0$ and $\nu = 0.5$. 40

Figure 4.20 Schematics of a layer rested on a half plane under (a) uniformly distributed normal traction, (b) uniformly distributed shear traction, and (c) uniformly distributed couple traction.....41

Figure 4.21 Results for (a) normalized shear stress σ_{xy}, (b) normalized shear stress σ_{yx}, (c) normalized vertical stress σ_{yy}, and (d) normalized couple stress μ_{yz} at the bottom surface of the layer under uniformly distributed normal traction. Results are reported for $\nu = 0.30$, and $a/\ell_0 = 1$. 44

จุฬาลงกรณ์มหาวิทยาลัย
Chulalongkorn University

Figure 4.22 Results for (a) normalized shear stress σ_{xy}, (b) normalized shear stress σ_{yx}, (c) normalized vertical stress σ_{yy}, and (d) normalized couple stress μ_{yz} at the bottom surface of the layer under uniformly distributed shear traction. Results are reported for $\nu = 0.30$, and $a/\ell_0 = 1$. 45

Figure 4.23 Results for (a) normalized shear stress σ_{xy}, (b) normalized shear stress σ_{yx}, (c) normalized vertical stress σ_{yy}, and (d) normalized couple stress μ_{yz} at the bottom surface of the layer under uniformly distributed couple traction. Results are reported for $\nu = 0.30$, and $a/\ell_0 = 1$. 46

Figure 4.24 Results for (a) normalized shear stress σ_{xy}, (b) normalized shear stress σ_{yx}, (c) normalized vertical stress σ_{yy}, and (d) normalized couple stress μ_{yz} at the bottom surface of the layer under uniformly distributed normal traction. Results are reported for $a/h = 1$, $\gamma = 0.5$, $\rho^{(1)} = \rho^{(2)} = 1$, and $\nu^{(1)} = \nu^{(2)} = 0.3$ 47

Figure 4.25 Results for (a) normalized horizontal stress σ_{xx} and (b) normalized vertical stress σ_{yy} along the line of symmetry of the elastic layer under uniformly distributed normal traction. Results are reported for $a/h = 1$, $\gamma = 0.5$, $\rho^{(1)} = \rho^{(2)} = 1$, and $\nu^{(1)} = \nu^{(2)} = 0.3$ 48

Figure 4.26 Results for (a) normalized shear stress σ_{xy}, (b) normalized shear stress σ_{yx}, (c) normalized vertical stress σ_{yy}, and (d) normalized couple stress μ_{yz} at the bottom surface of the layer under uniformly distributed shear traction. Results are reported for $a/h = 1$, $\gamma = 0.5$, $\rho^{(1)} = \rho^{(2)} = 1$, and $\nu^{(1)} = \nu^{(2)} = 0.3$. 49

Figure 4.27 Results for (a) normalized shear stress σ_{xy} and (b) normalized shear stress σ_{yx} along the line of symmetry of the elastic layer under uniformly distributed shear traction. Results are reported for $a/h = 1$, $\gamma = 0.5$, $\rho^{(1)} = \rho^{(2)} = 1$, and $\nu^{(1)} = \nu^{(2)} = 0.3$. 50

Figure 4.28 Results for (a) normalized shear stress σ_{xy}, (b) normalized shear stress σ_{yx}, (c) normalized vertical stress σ_{yy}, and (d) normalized couple stress μ_{yz} at the bottom surface of the layer under uniformly distributed couple traction. Results are reported for $a/h = 1$, $\gamma = 0.5$, $\rho^{(1)} = \rho^{(2)} = 1$, and $\nu^{(1)} = \nu^{(2)} = 0.3$. 51

Figure 4.29 Results for (a) normalized shear stress σ_{yx} and (b) normalized couple stress μ_{yz} along the line of symmetry of the elastic layer under uniformly distributed

จุฬาลงกรณ์มหาวิทยาลัย
Chulalongkorn University

couple traction. Results are reported for $a/h=1$, $\gamma=0.5$, $\rho^{(1)}=\rho^{(2)}=1$, and $\nu^{(1)}=\nu^{(2)}=0.3$. 52

Figure 4.30 Normalized vertical stress σ_{yy} at a selected point $x=0$, $y=h/2$ within the elastic layer under uniformly distributed normal traction versus the normalized half-length of loading region. Results are reported for $\gamma=0.5$, $\rho^{(1)}=\rho^{(2)}=1$, and $\nu^{(1)}=\nu^{(2)}=0.3$. 52

Figure 4.31 Normalized shear stress σ_{yx} at a selected point $x=0$, $y=h/2$ within the elastic layer under uniformly distributed shear traction versus the normalized half-length of loading region. Results are reported for $\gamma=0.5$, $\rho^{(1)}=\rho^{(2)}=1$, and $\nu^{(1)}=\nu^{(2)}=0.3$. 53

Figure 4.32 Normalized couple stress μ_{yz} at a selected point $x=0$, $y=h/2$ within the elastic layer under uniformly distributed couple traction versus the normalized half-length of loading region. Results are reported for $\gamma=0.5$, $\rho^{(1)}=\rho^{(2)}=1$, and $\nu^{(1)}=\nu^{(2)}=0.3$. 53

Figure 4.33 Normalized vertical stress σ_{yy} at a selected point $x=0$, $y=h/2$ within the elastic layer under uniformly distributed normal traction versus the normalized half-length of loading region. Results are reported for $a/h=1$, $\rho^{(1)}=\rho^{(2)}=1$, and $\nu^{(1)}=\nu^{(2)}=0.3$. 54

Figure 4.34 Normalized shear stress σ_{yx} at a selected point $x=0$, $y=h/2$ within the elastic layer under uniformly distributed shear traction versus the normalized half-length of loading region. Results are reported for $a/h=1$, $\rho^{(1)}=\rho^{(2)}=1$, and $\nu^{(1)}=\nu^{(2)}=0.3$ 54

Figure 4.35 Normalized couple stress μ_{yz}/m_0 at a selected point $x=0$, $y=h/2$ within the elastic layer under uniformly distributed couple traction versus the normalized half-length of loading region. Results are reported for $a/h=1$, $\rho^{(1)}=\rho^{(2)}=1$, and $\nu^{(1)}=\nu^{(2)}=0.3$. 55

Figure 4.36 Schematic of two-dimensional layered medium consisting of two different materials arranged alternately and rested on rigid foundation. The layered medium shown is subjected to Hertzian traction over the region $[-a,a]$. 56

Figure 4.37 Normalized horizonal displacement u_x along the top surface of the periodic bi-materials layered medium under Hertzian loading. Results are reported for $a/H=1$, $\rho^{(1)}=\rho^{(2)}=1$, and $\nu^{(1)}=\nu^{(2)}=0.25$ 57

CHULALONGKORN UNIVERSITY

Figure 4.38 Normalized vertical displacement u_y along the top surface of the periodic bi-materials layered medium under Hertzian loading. Results are reported for $a/H=1,\ \rho^{(1)}=\rho^{(2)}=1$, and $\nu^{(1)}=\nu^{(2)}=0.25$ 58

Figure 4.39 Normalized rotation ω_z along the top surface of the periodic bi-materials layered medium under Hertzian loading. Results are reported for $a/H=1$, $\rho^{(1)}=\rho^{(2)}=1$, and $\nu^{(1)}=\nu^{(2)}=0.25$. 58

Figure 4.40 Normalized vertical displacement u_y along line of symmetry the periodic bi-materials layered medium under Hertzian loading. Results are reported for $a/H=1,\ \rho^{(1)}=\rho^{(2)}=1$, and $\nu^{(1)}=\nu^{(2)}=0.25$ 59

Figure 4.41 Normalized horizontal stress σ_{xx} along the bottom surface of the periodic bi-materials layered medium under Hertzian loading. Results are reported for $a/H=1,\ \rho^{(1)}=\rho^{(2)}=1$, and $\nu^{(1)}=\nu^{(2)}=0.25$ 59

Figure 4.42 Normalized shear stress σ_{xy} along the bottom surface of the periodic bi-materials layered medium under Hertzian loading. Results are reported for $a/H=1$, $\rho^{(1)}=\rho^{(2)}=1$, and $\nu^{(1)}=\nu^{(2)}=0.25$. 60

Figure 4.43 Normalized shear stress σ_{yx} along the bottom surface of the periodic bi-materials layered medium under Hertzian loading. Results are reported for $a/H=1$, $\rho^{(1)}=\rho^{(2)}=1$, and $\nu^{(1)}=\nu^{(2)}=0.25$. 60

Figure 4.44 Normalized vertical stress σ_{yy} along the bottom surface of the periodic bi-materials layered medium under Hertzian loading. Results are reported for $a/H=1,\ \rho^{(1)}=\rho^{(2)}=1$, and $\nu^{(1)}=\nu^{(2)}=0.25$ 61

Figure 4.45 Normalized couple stress μ_{xz} along the bottom surface of the periodic bi-materials layered medium under Hertzian loading. Results are reported for $a/H=1$, $\rho^{(1)}=\rho^{(2)}=1$, and $\nu^{(1)}=\nu^{(2)}=0.25$. 61

Figure 4.46 Normalized couple stress μ_{yz} along the bottom surface of the periodic bi-materials layered medium under Hertzian loading. Results are reported for $a/H=1$, $\rho^{(1)}=\rho^{(2)}=1$, and $\nu^{(1)}=\nu^{(2)}=0.25$. 62

Figure 4.47 Normalized vertical stress σ_{yy} along line of symmetry of the periodic bi-materials layered medium under Hertzian loading. Results are reported for $a/H=1$, $\rho^{(1)}=\rho^{(2)}=1$, and $\nu^{(1)}=\nu^{(2)}=0.25$. 62

จุฬาลงกรณ์มหาวิทยาลัย
CHULALONGKORN UNIVERSITY

Figure 4.48 Schematic of two-dimensional layer made of a functionally graded material and subjected to uniformly distributed normal traction p_0. The layer is discretized into N identical sub-layers. 64

Figure 4.49 Normalized vertical displacement u_y at the top surface of (a) small different between $\bar{\mu}_{(0)}$ and $\bar{\mu}_{(1)}$, and (b) large different between $\bar{\mu}_{(0)}$ and $\bar{\mu}_{(1)}$ medium under uniformly distributed normal traction. Results are reported for $a/h=1$, $\nu=0.3$, $\rho=1$, and various grading functions. 65

Figure 4.50 Normalized vertical displacement u_y at the top surface of (a) small different between $\nu_{(0)}$ and $\nu_{(1)}$, and (b) large different between $\nu_{(0)}$ and $\nu_{(1)}$ medium under uniformly distributed normal traction. Results are reported for $a/h=1$, $\bar{\mu}=1$, $\rho=1$, and various grading functions. 66

Figure 4.51 Normalized vertical displacement u_y at the top surface of (a) small different between $\rho_{(0)}$ and $\rho_{(1)}$, and (b) large different between $\rho_{(0)}$ and $\rho_{(1)}$ medium under uniformly distributed normal traction. Results are reported for $a/h=1$, $\bar{\mu}=1$, $\nu=0.3$, and various grading functions. 66

Figure 4.52 Normalized shear stress σ_{yx} at the bottom surface of (a) small different between $\bar{\mu}_{(0)}$ and $\bar{\mu}_{(1)}$, and (b) large different between $\bar{\mu}_{(0)}$ and $\bar{\mu}_{(1)}$ medium under uniformly distributed normal traction. Results are reported for $a/h=1$, $\nu=0.3$, $\rho=1$, and various grading functions. 67

Figure 4.53 Normalized shear stress σ_{yx} at the bottom surface of (a) small different between $\nu_{(0)}$ and $\nu_{(1)}$, and (b) large different between $\nu_{(0)}$ and $\nu_{(1)}$ medium under uniformly distributed normal traction. Results are reported for $a/h=1$, $\bar{\mu}=1$, $\rho=1$, and various grading functions. 67

Figure 4.54 Normalized shear stress σ_{yx} at the bottom surface of (a) small different between $\rho_{(0)}$ and $\rho_{(1)}$, and (b) large different between $\rho_{(0)}$ and $\rho_{(1)}$ medium under uniformly distributed normal traction. Results are reported for $a/h=1$, $\bar{\mu}=1$, $\nu=0.3$, and various grading functions. 68

Figure 4.55 Normalized horizontal stress σ_{xx} along the line of symmetry for (a) small different between $\bar{\mu}_{(0)}$ and $\bar{\mu}_{(1)}$, and (b) large different between $\bar{\mu}_{(0)}$ and $\bar{\mu}_{(1)}$ medium under uniformly distributed normal traction. Results are reported for $a/h=1$, $\nu=0.3$, $\rho=1$, and various grading functions. 68

Figure 4.56 Normalized horizontal stress σ_{xx} along the line of symmetry for (a) small different between $\nu_{(0)}$ and $\nu_{(1)}$, and (b) large different between $\nu_{(0)}$ and $\nu_{(1)}$ medium under uniformly distributed normal traction. Results are reported for $a/h=1$, $\bar{\mu}=1$, $\rho=1$, and various grading functions. 69

Figure 4.57 Normalized horizontal stress σ_{xx} along the line of symmetry for (a) small different between $\rho_{(0)}$ and $\rho_{(1)}$, and (b) large different between $\rho_{(0)}$ and $\rho_{(1)}$ medium under uniformly distributed normal traction. Results are reported for $a/h=1$, $\bar{\mu}=1$, $\nu=0.3$, and various grading functions. 69

Figure 4.58 Normalized vertical stress σ_{yy} along the line of symmetry for (a) small different between $\bar{\mu}_{(0)}$ and $\bar{\mu}_{(1)}$, and (b) large different between $\bar{\mu}_{(0)}$ and $\bar{\mu}_{(1)}$ medium under uniformly distributed normal traction. Results are reported for $a/h=1$, $\nu=0.3$, $\rho=1$, and various grading functions. 70

Figure 4.59 Normalized vertical stress σ_{yy} along the line of symmetry for (a) small different between $\nu_{(0)}$ and $\nu_{(1)}$, and (b) large different between $\nu_{(0)}$ and $\nu_{(1)}$ medium under uniformly distributed normal traction. Results are reported for $a/h=1$, $\bar{\mu}=1$, $\rho=1$, and various grading functions. 70

Figure 4.60 Normalized vertical stress σ_{yy} along the line of symmetry for (a) small different between $\rho_{(0)}$ and $\rho_{(1)}$, and (b) large different between $\rho_{(0)}$ and $\rho_{(1)}$ medium under uniformly distributed normal traction. Results are reported for $a/h=1$, $\bar{\mu}=1$, $\nu=0.3$, and various grading functions. 71

จุฬาลงกรณ์มหาวิทยาลัย
CHULALONGKORN UNIVERSITY

CHAPTER 1
INTRODUCTION

This chapter briefly offers an overview of the proposed research. The key motivation together with the significance of the present study is provided, first, and then followed by the background and review of relevant literatures to not only demonstrate the current growths in the area but also pinpoint the existing current gap of knowledge. The objective, the scope of work, the methodology, and the research procedure for the present investigation are then summarized. Finally, expected outcomes and contribution of the proposed study are clearly addressed.

1.1 Motivation and Significance

Technology in the present time has improved dramatically and due to the fact that the innovations in manufacturing are also develop in the same direction, a lot of instruments with great functions are created. Small-scale materials (e.g., carbon nanotubes, lithium ion, nano-clusters, nano-crystals, etc.) and various tiny devices (e.g., MEMS, NEMS, micro- and nano-sensors, actuators, chips, etc.) have a large reputation in many industrial societies these day; including, natural and medical sciences, engineering, and modern industries. (e.g., Ratner and Ratner 2003, Booker and Boysen 2005, Park et al. 2011, Yang et al. 2016) They are taking over the long-time-used traditional macro-material. The reason regards to its popularity comes from its desirable properties (e.g., Yang et al. 2001, Liao et al. 2005, Peng et al. 2008, Qian et al. 2008). Therefore, many studies on this particular kind of material are undergoing extensively.

To create a better understanding toward nanoscale technology, the following examples of materials and instruments are given. Carbon nanotubes are used as a reinforcement in cement-based materials to control micro-cracks due to its useful physical properties (i.e., tensile strength, bonding force, Young's modulus, and ductility) that is much higher and better than the other reinforcement materials (Han et al. 2011). Nanowires, made of soluble metals, are utilized in the creation of molecular electronics such as transistors and memory devices in electronics (Booker and Boysen

2005). Nanosensor is one of the interesting nanoscale devices that adopts spectroscopic techniques to detect the type of material or its composite as those molecules are excited by a different frequency of light (Booker and Boysen 2005).

The trend of material coating has increased through decades. Apart from being an additional surface for the macro-structures, it has become one of the choice in producing the tiny element as it can maintain the size of the products to be about the same as the without-coating version while its physical features may get modified due to the side-effect of coating. For instance, Nano-coating on glass-like materials that makes it become hydrophilic or hydrophobic matters (Ratner and Ratner 2003). Silicon nitride (SiN_x) coating on Gallium arsenide (GaAs) material in optoelectronic devices that capable of blocking the chemical reaction that could lead to a reducing in its efficiency (Lu et al. 2013). A multiwalled reinforcement in carbon nanotubes has turned out to be one of the popular choices for the armaments due to its significant low values of fracture strengths and smaller failure strains (Peng et al. 2008)

These instruments and materials are usually coated in multiple layers and each layer may provide different material properties which make it become more complicated when the whole behavior of the object has to be defined. The most basic kind of test that often perform to obtain the material property is the indentation test which can be done in a wide ranges of scale, from macro- to micro- or even nano-scale. Unfortunately, as the materials are in micro-range, the test cannot be carried out easily due to its extent. Hence, modeling is chosen, instead, to carry out all the study using capable theories and assumptions.

จุฬาลงกรณ์มหาวิทยาลัย
Chulalongkorn University

In the usual situation, a well-recognized theory, Cauchy continuum or classical theory, is chosen as a core basis in a simulation. But it is evident from several works (e.g., Fleck et al. 1994, Ma and Clarke 1994, Wong et al. 1997, Chong and Lam 1999, Chong et al. 2001), that the behavior of the microscopic structure from the experiment has a completely deviate trend compared to those in macro-scale. This trait is later called size-dependence and it makes many scientists become aware of the significance of the material body's dimension. Therefore, a lot of researches and developments for these small matters have been taken up till dates. Numerous theories can be used for the study on size-dependency effects for such a small-scale medium. One of the

reputable theories that can reflect the scaling effects is couple stress theory which have been used in many applications.

For couple stress theory, couple stress is the main quantity that makes this theory becomes capable of behaviors observation. The same is indisposed for the classical continuum as the couple stress has never appeared in the continuum. This couple stress theory has become more popular from the fact that when there is no association of the couple stresses on the body of material, the theory can simply turn back to be like those results from conventional theory and it is expected to be more accurate and reliable theory as the characteristic length of material has been taken into account. Therefore, couple stress theory has become popular in the present time. Every mechanics problem, such as, dislocation, crack, and indentation, that were solved in classical theory context, can also be developed in the same sense using couple stress theory. For that reason, several publications of the related works and applications using couple stress theory (e.g., Gourgiotis and Georgiadis 2008, Gourgiotis and Georgiadis 2011, Gourgiotis et al. 2011, Itou 2013, Seyyed Fakhrabadi 2015, Baxevanakis et al. 2017, Baxevanakis et al. 2017, Zisis 2018) are released in the last decade.

There were only a few works for the type of problem which a medium's surface exposes to an external excitation in the framework of couple stress theory. As it has been known that the basic of indentation problem came from the idea of loading on the top of the surface, the very first work was introduced as a point load subjected to the half-plane (Muki and Sternberg 1965). Nevertheless, the work did not receive much response. Until recent years, the microscale element trend raise up among industries, these sorts of problem are then once again revisited (Zisis et al. 2014).

As it has been stated before that the multilayer are taking a big step in the modernized industrial community and due to the urge of producing an infinitesimal element, some properties of material has to be determined initially. Since the medium has become more complicated than the homogeneous system, an existing solution that were derived in the past cannot demonstrate the behaviors of these material. Therefore, the fundamental solution for the multilayer media subjected to an arbitrary surface loading is chosen as a topic in this study. The parametric study along with the other interesting characteristic will be investigated, too.

จุฬาลงกรณ์มหาวิทยาลัย
Chulalongkorn University

1.2 Background and Review

Classical continuum has been the core of knowledge in solid mechanics and rooted for a long period of time. Until 1887, Voigt started to propose an idea that polar-forces should acting on the body of continuum as it could be more realistic than the long-time-used conventional theory. But Voigt neither gave a full detail nor a model of his idea (Voigt 1887, Vardoulakis 2019). Two decades later, Cosserat and Cosserat (1909) started to purpose a mathematical model for the theory by adding couple-stresses to the system. The action led to the reconstruction of force-equilibrium equations and forming an additional couple-stress equilibrium equation. The consequence of involving couple stresses in the domain leads to a non-symmetric force-stress tensor which is unusual for the classical theory. Kinematics quantities for this theory are displacements and rotation. The number of degrees of freedom in continuum has increase doubly from three to six which makes the whole theory become much more complicated than the classical theory. In addition, the Cosserats were using microrotation that describe the rotation of each infinitesimal element independently which this trait should not appear in continuum mechanics (Neff 2006, Grekova 2012, Vardoulakis 2019). Therefore, only a few numbers of applications were found during that period.

In 1960s, several researchers brought back the Cosserats theory, developed the constrained rotation for the continuum mechanics and used it instead of the original microrotation (Mindlin and Tiersten 1962, Mindlin 1963, Koiter 1964, Mindlin 1964, Toupin 1964). This theory was latter called linearized couple-stress theory. The developed theory was derived under an acceptable physical explanation and the number of degrees of freedom was reduced to be only three. It is also remarked that the material properties used in this theory need to be restricted with some constrains. Even though, some parts of the theory are left indeterminate, this couple stress theory has been well-recognized by many academics and has been applied to several works in mechanics engineering.

Sometimes later, the works once again revisited, an additional equilibrium equation based on representative volume element was generated to govern the nature of couple stresses (Yang et al. 2002). The relations led to a mathematical conclusion of having symmetrical couple stress tensor, however, the theory still suffer from the

indeterminacy of the spherical part in couple stress tensor and faced some unreal physical conditions due to the improper assumption used during the derivation of an additional equilibrium equations (Münch et al. 2017). Nonetheless, the theory was entitled as ‘modified couple stress theory’ and grouped as one of the indeterminate couple stress theories.

In these recent years Hadjesfandiari and Dargush (2011) went back to the very first indeterminate couple stress theory and claimed that they had found an important characteristic of couple stress tensor that were missed by other researchers. The remarkable point in the discovery was that couple-stresses is a skew-symmetric tensor and with this statement some material parameters was reduced. Furthermore, it had been found that the spherical part that was a problematic issue in the past vanished, and every parameter could be determined and admissible in both mathematical and physical sense unlike all the previous presented theories. This theory was set under the name ‘consistent couple stress theory’. Later, other researchers found that the proposed theory was actually not consistent at all as the boundary conditions were ill-posed from the start. Despite all that, it was not mean that this consistent couple stress theory was all wrong. It was rather a special case of the typical couple stress theory (Neff et al. 2016).

The first work in the area of surface on loading problems in couple stress theory was studied by Muki and Sternberg (1965). Homogeneous isotropic elastic half-plane in plane-strain condition was excited by various types of load (i.e., concentrated normal load, concentrated shear load, uniformly distributed normal load, uniformly distributed shear load) was observed. Moreover, an indentation problem for the same medium was introduced in the final part of the study where a rigid flat-ended punch is applied on the surface.

After the work of Muki and Sternberg, no appearance of work associated in this field of problem were found for decades. Until 2014, another research in the indentation problem was published (Zisis et al. 2014). The solutions were derived through the method of stress function and singular integral. Three types of indenter were selected in the observation including, flat punch, cylindrical indenter, and wedge indenter. Although, the research focused on the indentation, this work showed a good potential in a development of this branch of knowledge in the future. Next, in 2016,

จุฬาลงกรณ์มหาวิทยาลัย
Chulalongkorn University

(Gourgiotis and Zisis solved for the same problem as Zisis et al. (2014) by determining the Green's function through singular integral transform before applied to the indentation for cylindrical rigid punch, rigid wedge, and any punch that generating uniform pressure. The study was remaining in the homogeneous isotropic elastic half-plane. Then, another punching work launched by Karuriya and Bhandakkar (2017) which follow Zisis et al. (2014) scheme but modified the medium to be a finite thickness single layer of homogenous isotropic elastic material having a rigid foundation where it is subjected to a rigid, cylindrical, and wedge punch. More recently, another associated publication investigated on the Burmister's problem for a single layer media that is bonded perfectly to inflexible base (Zisis 2018). Two different sets of boundary condition at the bottom surface of the layer were set as rotation at the bottom is equal to zero and, for the other case, couple stress is equal to zero. These two cases were observed and compared over two different Poisson's ratio value through the results of field quantities

From a framework of all half-plane and layer problems in couple stress theory, it has been found that there is a great possibility of successfully extending the model into the multilayer fashion. More importantly, those set of problem in the half-plane and layer can be utilized as a benchmark solutions for the verification of this soon to be developed solutions as all of them is the special case of the layered problems to ensure the correctness.

จุฬาลงกรณ์มหาวิทยาลัย
CHULALONGKORN UNIVERSITY

1.3 Objectives

The present research aims to (1) develop a set of fundamental solutions of a layered elastic medium under prescribed surface loading by taking into account the length-scale effect and (2) investigate the size dependent behavior of predicted elastic fields.

1.4 Scopes of Work

The research is aimed to be conducted within the following context: (i) a medium is two-dimensional, consists of infinite layers with constant thickness adhered perfectly at the interfaces, and is rested on a rigid foundation; (ii) each layer is made of a homogeneous, isotropic, linearly elastic material with its behavior governed by the linearized couple stress theory (Mindlin and Tiersten 1962, Mindlin 1963, Koiter 1964); the body force and body couple vanish throughout the medium; and the

medium is only excited by a set of arbitrarily distributed, surface loadings. In addition, all involved governing field equations and the corresponding value problem are confined to linear and static cases (i.e., the inertia effect is assumed negligible).

1.5 Methodology and Research Procedure

The methodology and research procedure for the present study can be summarized as shown in the following step:

(1) A two-dimensional, layered medium is first fictitiously partitioned along the material interfaces into a collection of infinite layers of uniform thickness.

(2) A linearized couple stress theory (Mindlin and Tiersten 1962, (Mindlin 1963, Koiter 1964); is adopted to form a set of basic field equations (i.e., equilibrium equations, kinematics, and constitutive laws) of each infinite layer. Equilibrium equations in terms of the displacement in in-plane condition are then derived.

(3) A method of Fourier integral transform is employed to derive a pair of linear ordinary differential equations governing the displacement of each layer in the transform space.

(4) A standard technique in the theory of differential equations is adopted to derive a general solution of the displacement in the transform space. The general solutions for other field quantities in the transformed space such as the rotation, the force stress and the couple stress are then obtained via the direct substitution in the transformed field equations.

(5) Boundary conditions at the top surface of the top layer and at the bottom surface of the bottom layer together with the continuity along the material interfaces are employed to form a set of linear algebraic equations governing all unknown coefficients.

(6) An efficient solution procedure is chosen to determine all unknown coefficients and then, an existing algorithm for carrying out Fourier integral inversion is adopted to determine all field quantities in the physical space.

(7) The proposed solution procedure is implemented in a form of an in-house computer code and then verified by comparing with existing benchmark cases.

(8) Results for some fundamental loading cases are then summarized and reported.

(9) An extensive parametric study is performed to explore the length-scale effect and size dependent behavior of predicted responses.

1.6 Expected Outputs and Contributions

The current work should offer a better understanding in mechanical responses and size dependent behavior of small-scale layered media under surface excitations within the context of theoretical simulations via a couple-stress, linear elasticity theory. An implemented in-house computer code is capable of simulating responses of interest in the level of complexity involved and, in addition, offering an initial estimation/evaluation before conducting any experiments to mainly save cost and time associated with random/trial-and-error processes. Furthermore, results from the present study should provide a fundamental basis for the potential extension of applying the couple stress theory to explore the size dependent behaviors and length-scale effects of other types of boundary value problems such as dislocations, cracks, and indentations.

จุฬาลงกรณ์มหาวิทยาลัย
Chulalongkorn University

CHAPTER 2
PROBLEM FORMULATION

In this chapter, the description and statement of the research problem are stated clearly. Then, the linearized couple stress theory is briefly summarized. Finally, a set of basic field equations governing field quantities for two-dimensional media subjected to a plane-strain condition is established. A pair of governing equations in terms of the in-plane displacement is also summarized.

2.1 Problem Description and Statement

Consider a two-dimensional, infinite, layered medium as depicted in Figure 2.1. The medium consists of N infinite layers with a constant thickness and perfectly bonded along the straight interfaces. A two-dimensional, Cartesian reference coordinate system $\{x, y; O\}$ is chosen such that the origin O is located at the top surface of the 1st layer; the x-axis spans along the infinite direction of the layer; and the y-axis directs downward. The bottom surface of the last layer (i.e., the N^{th} layer) is bonded perfectly to the rigid foundation whereas the top surface of the top layer (i.e.,

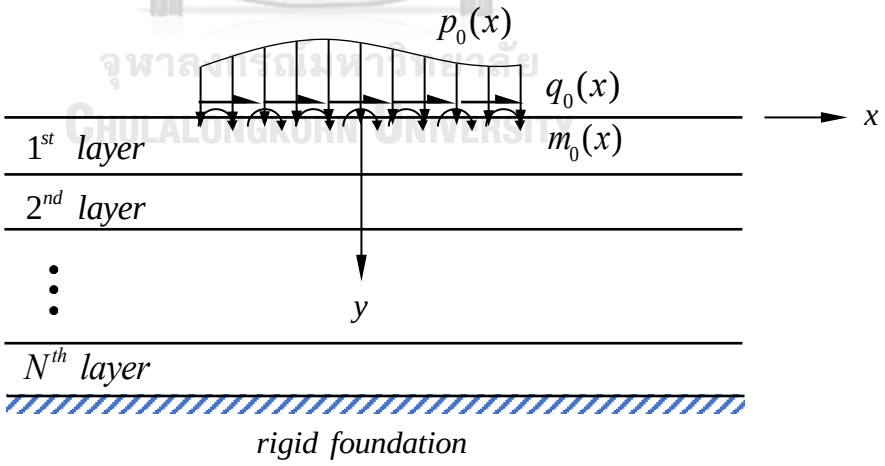

Figure 2.1 Schematic of two-dimensional layered medium rested on rigid foundation and subjected to surface loading

the 1st layer) is subjected to arbitrarily distributed normal traction p_0, arbitrarily distributed shear traction q_0, and arbitrarily distributed couple m_0 over the region $x \in [-a, a]$. Each layer is made of a homogeneous, isotropic, linearly elastic material and subjected to zero body force and body couple. The thickness of the medium in the direction perpendicular to the $x-y$ plane is assumed significantly large such that the plane-strain condition prevails.

A statement of the research problem is to determine the associated elastic field (e.g., the displacement, the rotation, the force stress, and the couple stress) within the layered media due to the applied surface loading. The length-scale effect and size dependency of the predicted response is also of interest.

2.2 Linearized Couple Stress Theory

According to the linearized couple stress theory proposed by Mindlin and Tiersten (1962), Mindlin (1963), and Koiter (1964), equilibrium equations resulting from the conservation of linear and angular momentum are given, in a three-dimensional, Cartesian coordinate system $\{x_1, x_2, x_3; O\}$, by

$$\sigma_{ji,j} + F_i = 0 \tag{1}$$

$$\mu_{ji,j} + \varepsilon_{ijk}\sigma_{jk} + C_i = 0 \tag{2}$$

where σ_{ji} denotes a force-stress tensor; μ_{ji} denotes a couple-stress tensor; ε_{ijk} is a standard permutation tensor; and F_i and C_i are the volumetric body force and the volumetric body couple, respectively; and $f_{,i}$ stands for the spatial derivative of a function f with respect to the coordinate x_i. From here to what follows, standard indicial notation and summation convention apply except stated otherwise.

In the absence of the body force and the body couple throughout the body, the equilibrium equations (1) and (2) become

$$\sigma_{ji,j} = 0 \tag{3}$$

$$\mu_{ji,j} + \varepsilon_{ijk}\sigma_{jk} = 0 \tag{4}$$

The force-stress tensor σ_{ji} can be further rewritten in symmetric and skew-symmetric parts as follows

จุฬาลงกรณ์มหาวิทยาลัย
Chulalongkorn University

$$\sigma_{ji} = \sigma_{(ji)} + \sigma_{[ji]} \tag{5}$$

where the parentheses and bracket are used to designate the symmetric and skew-symmetric parts of the tensor, respectively.

Also, the couple-stress tensor μ_{ji} is decomposed into sphearical part $\mu_{ij}^{(S)}$ and deveatoric part $\mu_{ij}^{(D)}$ as shown

$$\mu_{ji} = \mu_{ij}^{(D)} + \mu_{ij}^{(S)} \tag{6}$$

where the spherical part and deviatoric part of couple stress can be described as

$$\mu_{ij}^{(D)} = m_{ij} \tag{7}$$

$$\mu_{ij}^{(S)} = \frac{1}{3}\delta_{ij}\mu_{kk} \tag{8}$$

It is worth noticing that in the classical, size-independent linear elasticity theory, the couple-stress tensor does not exist or vanishes, and the force-stress tensor is essentially symmetric.

By substituting (6)-(8) into (3) and (4), it yields one equilibrium equation as

$$\sigma_{(jk),j} - \frac{1}{2}\varepsilon_{jkl} m_{il,ji} = 0 \tag{9}$$

Note particularly that the spherical part of the couple stress tensor is eliminated from the equation as $\varepsilon_{jkl}((1/3)\delta_{ij}\mu_{kk})_{,ji} = 0$ and the spherical part itself is left indeterminate in linearized couple stress theory.

The force traction t_i and the moment traction m_i on the smooth boundary relate to the force-stresses and couple-stresses through

$$t_i = \sigma_{ji} n_j \tag{10}$$

$$m_i = \mu_{ji} n_j \tag{11}$$

However, according to the theory, the boundary conditions at any point in continuum or at any smooth section can be specified a priori but only five of them (i.e., three force-tractions and two couple-tractions) are eligible as following expression

$$P_i^{(n)} = \sigma_{ji} n_j - \frac{1}{2}\varepsilon_{ijk} n_j m_{(nn),k} \tag{12}$$

$$R_i^{(n)} = m_{ji} n_j - m_{(nn)} n_i \tag{13}$$

where $m_{(nn)} = n_i n_j m_{ij}$ is the normal component of the deviatoric part of couple stress tensor.

The gradient of the displacement vector u_i, denoted by $u_{i,j}$, can be also decomposed into symmetric and skew-symmetric parts as

$$u_{i,j} = u_{(i,j)} + u_{[i,j]} \tag{14}$$

where the symmetric part $u_{(i,j)}$ and the anti-symmetric part $u_{[i,j]}$ are recognized as the infinitesimal strain tensor ε_{ij} and the infinitesimal rotation tensor ω_{ij}

$$u_{(i,j)} = \varepsilon_{ij} = \frac{1}{2}(u_{i,j} + u_{j,i}) \tag{15}$$

$$u_{[i,j]} = \omega_{ij} = \frac{1}{2}(u_{i,j} - u_{j,i}) \tag{16}$$

It is important to remark that in couple stress theory, the rotation tensor ω_{ij} is used as the measure of the curvature of a material element. Due to the skew symmetry of ω_{ij}, it can be represented in terms of an axial vector, called the rotation vector ω_i, as

$$\omega_i = \frac{1}{2}\varepsilon_{ijk}\omega_{kj} = \frac{1}{2}\varepsilon_{ijk}u_{k,j} \tag{17}$$

$$\omega_{ji} = \varepsilon_{ijk}\omega_k \tag{18}$$

$$d\omega_i = \omega_{i,j}dx_i \tag{19}$$

จุฬาลงกรณ์มหาวิทยาลัย
Chulalongkorn University

The gradient of the rotation tensor can also be decomposed into symmetric and skew-symmetric parts as

$$\omega_{i,j} = \omega_{(i,j)} + \omega_{[i,j]} \tag{20}$$

$$\omega_{(i,j)} = \frac{1}{2}(\omega_{i,j} + \omega_{j,i}) \equiv \chi_{ij} \tag{21}$$

$$\omega_{[i,j]} = \frac{1}{2}(\omega_{i,j} - \omega_{j,i}) \equiv \kappa_{ij} \tag{22}$$

The symmetric part χ_{ij} can be viewed as the infinitesimal strain of the rotation tensor whereas the skew-symmetric part κ_{ij} is termed the curvature tensor. Due to the characteristic of the skew-symmetric tensor κ_{ij}, all its diagonal entries vanish and this is therefore suitable for the curvature measure; in particular, it results directly from

the rotation tensor that produces no elongation in the material element. Similar to the rotation tensor ω_{ij}, the curvature tensor κ_{ij} can also be represented in terms of an axial vector, called the curvature vector κ_i, as

$$\kappa_i = \frac{1}{2}\varepsilon_{ijk}\kappa_{kj} = \frac{1}{2}\varepsilon_{ijk}\omega_{k,j} = \frac{1}{2}\omega_{ji,j} \tag{23}$$

$$\kappa_{ji} = \varepsilon_{ijk}\kappa_k \tag{24}$$

For the case of isotropic, linearly elastic materials, the strain-energy density function taken the presence of the couple stress into account becomes

$$W \equiv W\left(\varepsilon_{ij}, \kappa_{ij}\right) = \frac{1}{2}\lambda\varepsilon_{ii}\varepsilon_{jj} + \mu\varepsilon_{ij}\varepsilon_{ij} + 2\eta\kappa_{ij}\kappa_{ij} + 2\eta'\kappa_{ij}\kappa_{ji} \tag{25}$$

where λ and μ are Lamé constans defined in the same fashion as that in the size independent classical continuum and η together with η' denote the material constant accounting for the couple-stress effect which is responsible for the length-scale effect. Via the existence of $W\left(\varepsilon_{ij}, \kappa_{ij}\right)$, the constitutive relation for the force-stress and the couple stress tensor can be readily established with the final expressions:

$$\sigma_{(ij)} = \frac{\partial W}{\partial \varepsilon_{ij}} = \lambda\delta_{ij}\varepsilon_{kk} + 2\mu\varepsilon_{ij} \tag{26}$$

$$m_{ij} = \frac{\partial W}{\partial \kappa_{ij}} = 4\eta\kappa_{ij} + 4\eta'\kappa_{ji} \tag{27}$$

จุฬาลงกรณ์มหาวิทยาลัย
Chulalongkorn University

The material constant η can be related to the elastic shear modulus μ by

$$\frac{\eta}{\mu} = \ell^2 \tag{28}$$

where ℓ is termed the internal characteristic length of a material.

For the positive definiteness of the stored energy density function, all material constants must obey

$$3\lambda + 2\mu > 0 \tag{29a}$$

$$\mu > 0 \tag{29b}$$

$$\eta > 0 \tag{29c}$$

$$-1 < \frac{\eta'}{\eta} < 1 \tag{29d}$$

2.3 Two-dimensional, Plane-strain Case

A set of basic field equations for a two-dimensional body subjected to a plane-strain condition can be readily obtained from that presented in the previous section. Stress components involved in this problem are shown in Figure 2.2. A two-dimensional, Cartesian reference coordinate system $\{x, y; O\}$ and standard notation and convention for the force-stress components and the couple-stress components are shown schematically in Figure 2.2.

For the case of zero body force and body couple, the force and moment equilibrium equations are given explicitly, for this particular case, by

$$\frac{\partial \sigma_{xx}}{\partial x} + \frac{\partial \sigma_{yx}}{\partial y} = 0 \tag{30a}$$

$$\frac{\partial \sigma_{xy}}{\partial x} + \frac{\partial \sigma_{yy}}{\partial y} = 0 \tag{30b}$$

$$\frac{\partial \mu_{xz}}{\partial x} + \frac{\partial \mu_{yz}}{\partial y} + \sigma_{xy} - \sigma_{yx} = 0 \tag{30c}$$

จุฬาลงกรณ์มหาวิทยาลัย
CHULALONGKORN UNIVERSITY

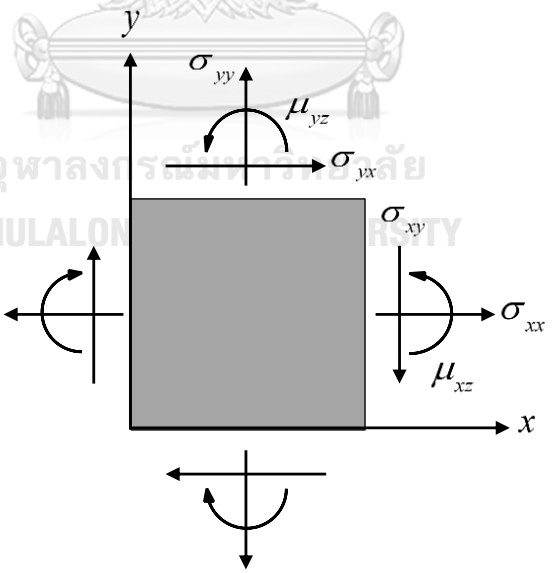

Figure 2.2 Schematic indicating force-stress and couple-stress components for two-dimensional problems

where $\{\sigma_{xx},\sigma_{xy},\sigma_{yx},\sigma_{yy}\}$ are in-plane components of the force-stress tensor and $\{\mu_{xz},\mu_{yz}\}$ are non-zero components of the couple stress tensor as indicated in Figure 2.2 The in-plane displacements u_x and u_y, the rotation normal $x-y$ plane ω_z, the infinitesimal in-plane strain components $\{\varepsilon_{xx},\varepsilon_{xy}=\varepsilon_{yx},\varepsilon_{yy}\}$ and the curvatures κ_{xz} and κ_{yz} are related for the plane-strain condition via the following linearized kinematics

$$\varepsilon_{xx}=\frac{\partial u_x}{\partial x} \tag{31a}$$

$$\varepsilon_{xy}=\frac{1}{2}\left(\frac{\partial u_x}{\partial y}+\frac{\partial u_y}{\partial x}\right) \tag{31b}$$

$$\varepsilon_{yy}=\frac{\partial u_y}{\partial y} \tag{31c}$$

$$\omega_z=\frac{1}{2}\left(\frac{\partial u_y}{\partial x}-\frac{\partial u_x}{\partial y}\right) \tag{32}$$

$$\kappa_{yz}=\frac{\partial \omega_z}{\partial y} \tag{33a}$$

$$\kappa_{xz}=\frac{\partial \omega_z}{\partial x} \tag{33b}$$

The compatibility conditions to ensure the existence of the in-plane displacement u_x, u_y and the rotation ω_z are given by

$$\frac{\partial^2 \varepsilon_{xx}}{\partial y^2}+\frac{\partial^2 \varepsilon_{yy}}{\partial x^2}=2\frac{\partial^2 \varepsilon_{xy}}{\partial x \partial y} \tag{34a}$$

$$\frac{\partial \kappa_{yz}}{\partial x}=\frac{\partial \kappa_{xz}}{\partial y} \tag{34b}$$

$$\frac{\partial \omega_z}{\partial x}=\frac{\partial \varepsilon_{xy}}{\partial x}-\frac{\partial \varepsilon_{xx}}{\partial y} \tag{34c}$$

$$\frac{\partial \omega_z}{\partial y}=\frac{\partial \varepsilon_{yy}}{\partial x}-\frac{\partial \varepsilon_{xy}}{\partial y} \tag{34d}$$

The constitutive relations relating the force-stress tensor, the couple-stress tensor, the infinitesimal strain tensor, and the rotation take the form

จุฬาลงกรณ์มหาวิทยาลัย
Chulalongkorn University

$$\mu_{yz} = 4\eta\kappa_{yz} = 4\eta\frac{\partial\omega_z}{\partial y} \tag{35a}$$

$$\mu_{xz} = 4\eta\kappa_{xz} = 4\eta\frac{\partial\omega_z}{\partial x} \tag{35b}$$

$$\sigma_{xx} = \frac{2\mu}{1-2\nu}[(1-\nu)\varepsilon_{xx} + \nu\varepsilon_{yy}] \tag{36a}$$

$$\sigma_{yy} = \frac{2\mu}{1-2\nu}[\nu\varepsilon_{xx} + (1-\nu)\varepsilon_{yy}] \tag{36b}$$

$$\sigma_{xy} = 2\mu\varepsilon_{xy} - 2\eta\Delta\omega \tag{36c}$$

$$\sigma_{yx} = 2\mu\varepsilon_{xy} + 2\eta\Delta\omega \tag{36d}$$

where Δ denotes the two-dimensional Laplacian operator and ν is the Poisson's ratio.

2.4 Governing Equations in terms of Displacement

By substituting (31)-(33) into (35)-(36), it leads to the expressions of the force stress and couple stress in terms of the in-plane displacements u_x and u_y

$$\sigma_{xx} = \frac{2\mu}{1-2\nu}\left((1-\nu)\frac{\partial u_x}{\partial x} + \nu\frac{\partial u_y}{\partial y}\right) \tag{37}$$

$$\sigma_{xx} = \frac{2\mu}{1-2\nu}\left(\nu\frac{\partial u_x}{\partial x} + (1-\nu)\frac{\partial u_y}{\partial y}\right) \tag{38}$$

$$\sigma_{xy} = \mu\left(\frac{\partial u_x}{\partial y} + \frac{\partial u_y}{\partial x}\right) - \eta\Delta\left(\frac{\partial u_y}{\partial x} - \frac{\partial u_x}{\partial y}\right) \tag{39}$$

$$\sigma_{yx} = \mu\left(\frac{\partial u_x}{\partial y} + \frac{\partial u_y}{\partial x}\right) + \eta\Delta\left(\frac{\partial u_y}{\partial x} - \frac{\partial u_x}{\partial y}\right) \tag{40}$$

$$\mu_{xz} = 2\eta\left(\frac{\partial^2 u_y}{\partial x^2} - \frac{\partial^2 u_x}{\partial x\partial y}\right) \tag{41}$$

$$\mu_{yz} = 2\eta\left(\frac{\partial^2 u_y}{\partial x\partial y} - \frac{\partial^2 u_x}{\partial y^2}\right) \tag{42}$$

Upon substituting (37)-(40) into the force equilibrium equations (30a) and (30b), it gives rise to a pair of equilibrium equations in terms of displacements

จุฬาลงกรณ์มหาวิทยาลัย
Chulalongkorn University

$$\frac{\partial}{\partial x}\left(\frac{2\mu}{1-2\nu}\left((1-\nu)\frac{\partial u_x}{\partial x}+\nu\frac{\partial u_y}{\partial y}\right)\right)+\frac{\partial}{\partial y}\left(\mu\left(\frac{\partial u_x}{\partial y}+\frac{\partial u_y}{\partial x}\right)+\eta\Delta\left(\frac{\partial u_y}{\partial x}-\frac{\partial u_x}{\partial y}\right)\right)=0 \qquad (43)$$

$$\frac{\partial}{\partial x}\left(\mu\left(\frac{\partial u_x}{\partial y}+\frac{\partial u_y}{\partial x}\right)-\eta\Delta\left(\frac{\partial u_y}{\partial x}-\frac{\partial u_x}{\partial y}\right)\right)+\frac{\partial}{\partial y}\left(\frac{2\mu}{1-2\nu}\left(\nu\frac{\partial u_x}{\partial x}+(1-\nu)\frac{\partial u_y}{\partial y}\right)\right)=0 \qquad (44)$$

Terms associated with the Laplacian operator Δ can be further expanded to obtain

$$\eta\Delta\left(\frac{\partial u_y}{\partial x}-\frac{\partial u_x}{\partial y}\right)=\eta\left(\frac{\partial^3 u_y}{\partial x^3}-\frac{\partial^3 u_x}{\partial x^2\partial y}+\frac{\partial^3 u_y}{\partial y^2\partial x}-\frac{\partial^3 u_x}{\partial y^3}\right) \qquad (45)$$

It is important to remark that the moment equilibrium equation (30c) is not employed here as the key governing equation but it provides the sufficient conditions for determining the skew-symmetric part of the force-stress tensor in terms of the couple-stress tensor. By substituting (45) into (43) and (44), it leads to a two-dimensional version of Navier's equations for the linearized couple stress theory

$$\begin{bmatrix}\alpha\partial_x^2+\partial_y^2-\bar{\eta}(\partial_x^2\partial_y^2+\partial_y^4) & \beta\partial_x\partial_y+\bar{\eta}(\partial_x^3\partial_y+\partial_x\partial_y^3)\\ \beta\partial_x\partial_y+\bar{\eta}(\partial_x^3\partial_y+\partial_x\partial_y^3) & \partial_x^2+\alpha\partial_y^2-\bar{\eta}(\partial_x^4+\partial_x^2\partial_y^2)\end{bmatrix}\begin{Bmatrix}u_x\\ u_y\end{Bmatrix}=\begin{Bmatrix}0\\ 0\end{Bmatrix} \qquad (46)$$

where $\alpha=2(1-\nu)/(1-2\nu)$, $\beta=1/(1-2\nu)$, $\bar{\eta}=\eta/\mu$, $\partial_x=\partial/\partial x$, $\partial_x^n=\partial^n/\partial x^n$, $\partial_y=\partial/\partial y$, and $\partial_y^n=\partial^n/\partial y^n$.

จุฬาลงกรณ์มหาวิทยาลัย
Chulalongkorn University

CHAPTER 3
SOLUTION PROEDURE

This chapter presents the development of a general solution of the displacement for a representative infinite layer via the method of Fourier integral transform. The general solutions in the transformed space for other field quantities such as the rotation, the force stress and the couple stress are also established for the representative layer. Finally, the boundary conditions at top surface and bottom surface of the layered medium together with the continuity conditions along the material interfaces and the general solutions for each layer are employed to form a system of linear algebraic equations governing the unknown constants.

3.1 General Solutions for Displacement of Representative Layer

To determine the general solution of (48) for a representative infinite layer occupying a region $x \in (-\infty, \infty), y \in [a,b]$, it is appealing to employ the method of Fourier integral transform (e.g., Sneddon (1951); Karasudhi (1991); Asaro and Lubarda (2006); Sadd (2014). Fourier integral transform of any function $f = f(x,y)$ defined over the region $x \in (-\infty, \infty), y \in [a,b]$ and its inverse with respect to the coordinate x are defined by

จุฬาลงกรณ์มหาวิทยาลัย
Chulalongkorn University

$$\bar{f}(\xi, y) = \int_{-\infty}^{\infty} f(x,y) e^{i\xi x} dx \tag{47a}$$

$$f(x,y) = \frac{1}{2\pi} \int_{-\infty}^{\infty} \bar{f}(\xi, y) e^{-i\xi x} d\xi \tag{47b}$$

By applying Fourier integral transform with respect to the coordinate x to the system (46), it leads to the following system of linear, ordinary differential equations with respect to the coordinate y:

$$\begin{bmatrix} -\alpha\xi^2 + (1+\bar{\eta}\xi^2)D_y^2 - \bar{\eta}D_y^4 & -i\xi[(\beta - \bar{\eta}\xi^2)D_y + \bar{\eta}D_y^3] \\ -i\xi[(\beta - \bar{\eta}\xi^2)D_y + \bar{\eta}D_y^3] & -\xi^2(1+\bar{\eta}\xi^2) + (\alpha + \bar{\eta}\xi^2)D_y^2 \end{bmatrix} \begin{Bmatrix} \bar{u}_x \\ \bar{u}_y \end{Bmatrix} = \begin{Bmatrix} 0 \\ 0 \end{Bmatrix} \tag{48}$$

The general solution of (48) can be obtained via a standard procedure in a theory of differential equations; i.e., the general solution can be assumed in the following form

$$\begin{Bmatrix} \bar{u}_x \\ \bar{u}_y \end{Bmatrix} = \begin{Bmatrix} A \\ B \end{Bmatrix} e^{\gamma y} \tag{49}$$

where $A, B,$ and γ are unknown constants. Upon substituting (49) into the system (48) and then carrying out all involved differentiations, it leads to

$$e^{\gamma y}\begin{bmatrix} -\alpha\xi^2 + (1+\bar{\eta}\xi^2)\gamma^2 - \bar{\eta}\gamma^4 & -i\xi[(\beta - \bar{\eta}\xi^2)\gamma + \bar{\eta}\gamma^3] \\ -i\xi[(\beta - \bar{\eta}\xi^2)\gamma + \bar{\eta}\gamma^3] & -\xi^2(1+\bar{\eta}\xi^2) + (\alpha + \bar{\eta}\xi^2)\gamma^2 \end{bmatrix}\begin{Bmatrix} A \\ B \end{Bmatrix} = \begin{Bmatrix} 0 \\ 0 \end{Bmatrix} \tag{50}$$

Since the system (50) is valid for all $y \in [a,b]$, the unknown constants A, B must satisfy

$$\begin{bmatrix} -\alpha\xi^2 + (1+\bar{\eta}\xi^2)\gamma^2 - \bar{\eta}\gamma^4 & -i\xi[(\beta - \bar{\eta}\xi^2)\gamma + \bar{\eta}\gamma^3] \\ -i\xi[(\beta - \bar{\eta}\xi^2)\gamma + \bar{\eta}\gamma^3] & -\xi^2(1+\bar{\eta}\xi^2) + (\alpha + \bar{\eta}\xi^2)\gamma^2 \end{bmatrix}\begin{Bmatrix} A \\ B \end{Bmatrix} = \begin{Bmatrix} 0 \\ 0 \end{Bmatrix} \tag{51}$$

For the system (51) to admit nontrivial solutions for the unknown constants A, B, the coefficient matrix must be singular, i.e.,

$$\det\begin{bmatrix} -\alpha\xi^2 + (1+\bar{\eta}\xi^2)\gamma^2 - \bar{\eta}\gamma^4 & -i\xi[(\beta - \bar{\eta}\xi^2)\gamma + \bar{\eta}\gamma^3] \\ -i\xi[(\beta - \bar{\eta}\xi^2)\gamma + \bar{\eta}\gamma^3] & -\xi^2(1+\bar{\eta}\xi^2) + (\alpha + \bar{\eta}\xi^2)\gamma^2 \end{bmatrix} = 0 \tag{52}$$

By carrying out the determinant on the left hand side of (52), it yields the following algebraic equation for the parameter γ:

$$\alpha(\gamma^2 - \xi^2)^2\left[\bar{\eta}(\gamma^2 - \xi^2) - 1\right] = 0 \tag{53}$$

The characteristic equation (53) yields following four different roots

$$\gamma_1 = |\xi| \tag{54a}$$

$$\gamma_2 = -|\xi| \tag{54b}$$

$$\gamma_3 = \zeta \tag{54c}$$

$$\gamma_4 = -\zeta \tag{54d}$$

where $|\xi|$ denotes the absolute value of ξ and

$$\zeta = \sqrt{\xi^2 + \frac{1}{\bar{\eta}}} \tag{55}$$

It is worth noting that the first two roots γ_1, γ_2 are of multiplicity 2. By taking care of the presence of repeated roots, the complete general solution of (46) takes the form

จุฬาลงกรณ์มหาวิทยาลัย
CHULALONGKORN UNIVERSITY

$$\begin{Bmatrix}\bar{u}_x\\ \bar{u}_y\end{Bmatrix}=\left[\begin{Bmatrix}A_{11}\\ B_{11}\end{Bmatrix}+\begin{Bmatrix}A_{11}\\ B_{11}\end{Bmatrix}y\right]e^{\gamma_1 y}+\left[\begin{Bmatrix}A_{21}\\ B_{21}\end{Bmatrix}+\begin{Bmatrix}A_{22}\\ B_{22}\end{Bmatrix}y\right]e^{\gamma_2 y}+\begin{Bmatrix}A_3\\ B_3\end{Bmatrix}e^{\gamma_3 y}+\begin{Bmatrix}A_4\\ B_4\end{Bmatrix}e^{\gamma_4 y} \tag{56}$$

where A_{ij}, B_{ij} $(i, j = 1, 2)$ and A_i, B_i $(i = 3, 4)$ are unknown functions of the transform parameter ξ. By substituting (56) into (48), it leads to the relationship among all unknown functions as follows:

$$\begin{aligned}
&e^{|\xi|y}\left(\beta\begin{bmatrix}-\xi^2 & -i\xi|\xi|\\ -i\xi|\xi| & \xi^2\end{bmatrix}\begin{Bmatrix}A_{11}\\ B_{11}\end{Bmatrix}+\begin{bmatrix}2(1-\bar{\eta}\xi^2)|\xi| & -i\xi(\beta+2\bar{\eta}\xi^2)\\ -i\xi(\beta+2\bar{\eta}\xi^2) & 2(\alpha+\bar{\eta}\xi^2)|\xi|\end{bmatrix}\begin{Bmatrix}A_{12}\\ B_{12}\end{Bmatrix}\right)\\
&+e^{-|\xi|y}\left(\beta\begin{bmatrix}-\xi^2 & -i\xi|\xi|\\ -i\xi|\xi| & \xi^2\end{bmatrix}\begin{Bmatrix}A_{21}\\ B_{21}\end{Bmatrix}+\begin{bmatrix}2(1-\bar{\eta}\xi^2)|\xi| & -i\xi(\beta+2\bar{\eta}\xi^2)\\ -i\xi(\beta+2\bar{\eta}\xi^2) & 2(\alpha+\bar{\eta}\xi^2)|\xi|\end{bmatrix}\begin{Bmatrix}A_{22}\\ B_{22}\end{Bmatrix}\right)\\
&+\beta y e^{|\xi|y}\begin{bmatrix}-\xi^2 & -i\xi|\xi|\\ -i\xi|\xi| & \xi^2\end{bmatrix}\begin{Bmatrix}A_{12}\\ B_{12}\end{Bmatrix}+\beta y e^{-|\xi|y}\begin{bmatrix}-\xi^2 & -i\xi|\xi|\\ -i\xi|\xi| & \xi^2\end{bmatrix}\begin{Bmatrix}A_{22}\\ B_{22}\end{Bmatrix}\\
&+\alpha e^{\zeta y}\begin{bmatrix}-\xi^2 & -i\xi\zeta\\ -i\xi\zeta & -\zeta^2\end{bmatrix}\begin{Bmatrix}A_3\\ B_3\end{Bmatrix}+\alpha e^{-\zeta y}\begin{bmatrix}-\xi^2 & i\xi\zeta\\ i\xi\zeta & -\zeta^2\end{bmatrix}\begin{Bmatrix}A_4\\ B_4\end{Bmatrix}=\begin{Bmatrix}0\\ 0\end{Bmatrix}
\end{aligned} \tag{57}$$

where the fact that $\beta = \alpha - 1$ has been utilized. Since (57) must valid for all $y \in [a, b]$, it reduces to six systems of homogenous equations:

$$\beta\begin{bmatrix}-\xi^2 & -i\xi|\xi|\\ -i\xi|\xi| & \xi^2\end{bmatrix}\begin{Bmatrix}A_{11}\\ B_{11}\end{Bmatrix}+\begin{bmatrix}2(1-\bar{\eta}\xi^2)|\xi| & -i\xi(\beta+2\bar{\eta}\xi^2)\\ -i\xi(\beta+2\bar{\eta}\xi^2) & 2(\alpha+\bar{\eta}\xi^2)|\xi|\end{bmatrix}\begin{Bmatrix}A_{12}\\ B_{12}\end{Bmatrix}=\begin{Bmatrix}0\\ 0\end{Bmatrix} \tag{58a}$$

$$\beta\begin{bmatrix}-\xi^2 & -i\xi|\xi|\\ -i\xi|\xi| & \xi^2\end{bmatrix}\begin{Bmatrix}A_{21}\\ B_{21}\end{Bmatrix}+\begin{bmatrix}2(1-\bar{\eta}\xi^2)|\xi| & -i\xi(\beta+2\bar{\eta}\xi^2)\\ -i\xi(\beta+2\bar{\eta}\xi^2) & 2(\alpha+\bar{\eta}\xi^2)|\xi|\end{bmatrix}\begin{Bmatrix}A_{22}\\ B_{22}\end{Bmatrix}=\begin{Bmatrix}0\\ 0\end{Bmatrix} \tag{58b}$$

$$\begin{bmatrix}-\xi^2 & -i\xi|\xi|\\ -i\xi|\xi| & \xi^2\end{bmatrix}\begin{Bmatrix}A_{12}\\ B_{12}\end{Bmatrix}=\begin{Bmatrix}0\\ 0\end{Bmatrix} \tag{58c}$$

$$\begin{bmatrix}-\xi^2 & -i\xi|\xi|\\ -i\xi|\xi| & \xi^2\end{bmatrix}\begin{Bmatrix}A_{22}\\ B_{22}\end{Bmatrix}=\begin{Bmatrix}0\\ 0\end{Bmatrix} \tag{58d}$$

$$\begin{bmatrix}-\xi^2 & -i\xi\zeta\\ -i\xi\zeta & -\zeta^2\end{bmatrix}\begin{Bmatrix}A_3\\ B_3\end{Bmatrix}=\begin{Bmatrix}0\\ 0\end{Bmatrix} \tag{58e}$$

$$\begin{bmatrix}-\xi^2 & i\xi\zeta\\ i\xi\zeta & -\zeta^2\end{bmatrix}\begin{Bmatrix}A_4\\ B_4\end{Bmatrix}=\begin{Bmatrix}0\\ 0\end{Bmatrix} \tag{58f}$$

Solving (58) leads to following relations among all unknown functions

$$A_{11} = -i|\xi|C_1 - i\kappa C_2 \tag{59a}$$

จุฬาลงกรณ์มหาวิทยาลัย
Chulalongkorn University

$$B_{11} = \xi C_1 \tag{59b}$$

$$A_{12} = -i|\xi| C_2 \tag{59c}$$

$$B_{12} = \xi C_2 \tag{59d}$$

$$A_{21} = i|\xi| C_3 - i\kappa C_4 \tag{59e}$$

$$B_{21} = \xi C_3 \tag{59f}$$

$$A_{22} = i|\xi| C_4 \tag{59g}$$

$$B_{22} = \xi C_4 \tag{59h}$$

$$A_3 = -i\zeta C_5 \tag{59i}$$

$$B_3 = \xi C_5 \tag{59j}$$

$$A_4 = i\zeta C_6 \tag{59k}$$

$$B_4 = \xi C_6 \tag{59l}$$

where C_i $(i = 1,2,..,6)$ are independent unknown functions of ξ and $\kappa = 3 - 4\nu$. Substituting (59) into (56) leads to the general solution for the displacement in the transformed space

$$\begin{Bmatrix} \bar{u}_x \\ \bar{u}_y \end{Bmatrix} = C_1 \begin{Bmatrix} -i|\xi| \\ \xi \end{Bmatrix} e^{|\xi|y} + C_2 \begin{Bmatrix} -i\left[\kappa + |\xi| y\right] e^{|\xi|y} \\ \xi y e^{|\xi|y} \end{Bmatrix} + C_3 \begin{Bmatrix} i|\xi| \\ \xi \end{Bmatrix} e^{-|\xi|y} + C_4 \begin{Bmatrix} -i\left[\kappa - |\xi| y\right] e^{-|\xi|y} \\ \xi y e^{-|\xi|y} \end{Bmatrix}$$
$$+ C_5 \begin{Bmatrix} -i\zeta \\ \xi \end{Bmatrix} e^{\zeta y} + C_6 \begin{Bmatrix} i\zeta \\ \xi \end{Bmatrix} e^{-\zeta y} \tag{60}$$

จุฬาลงกรณ์มหาวิทยาลัย
Chulalongkorn University

3.2 General Solutions for Other Field Quantities

By using the general solution for the displacement (60), the general solution for the rotation, the force stress, and the couple stress components in the transformed space can also be obtained. First, by taking Fourier integral transform to the field equations (32) and (37)-(42), it leads to

$$\bar{\omega}_z = \frac{1}{2}\left(-i\xi \bar{u}_y - \frac{d\bar{u}_x}{dy} \right) \tag{61}$$

$$\bar{\sigma}_{xx} = \frac{2\mu}{1-2\nu}\left(\nu \frac{d\bar{u}_y}{dy} - (1-\nu) i\xi \bar{u}_x \right) \tag{62}$$

$$\bar{\sigma}_{yy} = \frac{2\mu}{1-2\nu}\left((1-\nu)\frac{d\bar{u}_y}{dy} - \nu i\xi\bar{u}_x\right) \tag{63}$$

$$\bar{\sigma}_{xy} = \mu\left(\frac{d\bar{u}_x}{dy} - i\xi\bar{u}_y\right) - \eta\left(i\xi^3\bar{u}_y + \xi^2\frac{d\bar{u}_x}{dy} - i\xi\frac{d^2\bar{u}_y}{dy^2} - \frac{d^3\bar{u}_x}{dy^3}\right) \tag{64}$$

$$\bar{\sigma}_{yx} = \mu\left(\frac{d\bar{u}_x}{dy} - i\xi\bar{u}_y\right) + \eta\left(i\xi^3\bar{u}_y + \xi^2\frac{d\bar{u}_x}{dy} - i\xi\frac{d^2\bar{u}_y}{dy^2} - \frac{d^3\bar{u}_x}{dy^3}\right) \tag{65}$$

$$\bar{\mu}_{xz} = 2\eta\left(i\xi\frac{d\bar{u}_x}{dy} - \xi^2\bar{u}_y\right) \tag{66}$$

$$\bar{\mu}_{yz} = -2\eta\left(i\xi\frac{d\bar{u}_y}{dy} + \frac{d^2\bar{u}_x}{dy^2}\right) \tag{67}$$

Next, by substituting the general solution (60) into (61)-(67), it gives rise to

$$\bar{\omega}_z = \frac{i}{2}((\kappa|\xi| + |\xi|)e^{|\xi|y}C_2 - (\kappa|\xi| + |\xi|)e^{-|\xi|y}C_4 + (\zeta^2 - \xi^2)e^{\zeta y}C_5 + (\zeta^2 - \xi^2)e^{-\zeta y}C_6 \tag{68}$$

$$\begin{aligned}\bar{\sigma}_{xx} = {} & -2\mu(\xi|\xi|e^{|\xi|y}C_1 + ((3-2\nu)\xi + \xi|\xi|y)e^{|\xi|y}C_2 - \xi|\xi|e^{-|\xi|y}C_3 \\ & + ((3-2\nu)\xi - \xi|\xi|y)e^{-|\xi|y}C_4 + \xi\zeta e^{\zeta y}C_5 - \xi\zeta e^{-\zeta y}C_6)\end{aligned} \tag{69}$$

$$\begin{aligned}\bar{\sigma}_{yy} = {} & 2\mu(\xi|\xi|e^{|\xi|y}C_1 + ((1-2\nu)\xi + \xi|\xi|y)e^{|\xi|y}C_2 - \xi|\xi|e^{-|\xi|y}C_3 \\ & + ((1-2\nu)\xi - \xi|\xi|y)e^{-|\xi|y}C_4 + \xi\zeta e^{\zeta y}C_5 - \xi\zeta e^{-\zeta y}C_6)\end{aligned} \tag{70}$$

$$\begin{aligned}\bar{\sigma}_{xy} = {} & -i\mu(2\xi^2 e^{|\xi|y}C_1 + (\kappa|\xi| + 2\xi^2 y + |\xi|)e^{|\xi|y}C_2 + 2\xi^2 e^{-|\xi|y}C_3 \\ & - (\kappa|\xi| - 2\xi^2 y + |\xi|)e^{-|\xi|y}C_4 + ((\zeta^2 + \xi^2) + \bar{\eta}(\zeta^2 - \xi^2)^2)e^{\zeta y}C_5 \\ & + ((\zeta^2 + \xi^2) + \bar{\eta}(\zeta^2 - \xi^2)^2)e^{-\zeta y}C_6)\end{aligned} \tag{71}$$

$$\begin{aligned}\bar{\sigma}_{yx} = {} & -i\mu(2\xi^2 e^{|\xi|y}C_1 + (\kappa|\xi| + 2\xi^2 y + |\xi|)e^{|\xi|y}C_2 + 2\xi^2 e^{-|\xi|y}C_3 \\ & - (\kappa|\xi| - 2\xi^2 y + |\xi|)e^{-|\xi|y}C_4 + ((\zeta^2 + \xi^2) - \bar{\eta}(\zeta^2 - \xi^2)^2)e^{\zeta y}C_5 \\ & + ((\zeta^2 + \xi^2) - \bar{\eta}(\zeta^2 - \xi^2)^2)e^{-\zeta y}C_6))\end{aligned} \tag{72}$$

$$\begin{aligned}\bar{\mu}_{xz} = {} & 2\eta((\kappa+1)\xi|\xi|e^{|\xi|y}C_2 - (\kappa+1)\xi|\xi|e^{-|\xi|y}C_4 \\ & - (\xi^3 - \xi\zeta^2)e^{\zeta y}C_5 - (\xi^3 - \xi\zeta^2)e^{-\zeta y}C_6)\end{aligned} \tag{73}$$

$$\begin{aligned}\bar{\mu}_{yz} = {} & 2i\eta((\kappa+1)\xi^2 e^{|\xi|y}C_2 + (\kappa+1)\xi^2 e^{-|\xi|y}C_4 \\ & - (\xi^2\zeta - \zeta^3)e^{\zeta y}C_5 + (\xi^2\zeta - \zeta^3)e^{-\zeta y}C_6)\end{aligned} \tag{74}$$

จุฬาลงกรณ์มหาวิทยาลัย
Chulalongkorn University

Once the unknown functions C_i $(i=1,2,...,6)$ are determined, the general solutions (60) and (68)-(74) can be used together with Fourier integral transform inversion to achieve the field quantities in the physical space.

3.3 Governing Equations for Whole Layered Medium

To obtain the complete solution of the elastic field within the layered medium shown in Figure 2.1, it is evident that the six unknown functions C_i $(i=1,2,...,6)$ for each layer must be determined. To differentiate the unknown functions for each layer, the superscript "(k)" is then added to designate the k^{th} layer, i.e., $C_i^{(k)}$ $(i=1,2,...,6;k=1,2,...,N)$. For a layered medium consisting of N layers, the total number of unknown functions $C_i^{(k)}$ to be determined is equal to $6N$. To provide sufficient conditions, the boundary conditions at the top surface and bottom of the medium and the continuity along the material interfaces must be enforced. More specifically, the boundary conditions on the top surface of the 1^{th} layer, the boundary conditions on bottom surface of the N^{th} layer, and the continuity conditions along the material interface connecting the k^{th} and $(k+1)^{th}$ layers for $k=1,2,...,N-1$ are given, respectively, by

$$\sigma_{yy}^{(1)}\Big|_{y=a^{(1)}} = p_0 \tag{75a}$$

$$\sigma_{yx}^{(1)}\Big|_{y=a^{(1)}} = q_0 \tag{75b}$$

$$\mu_{yz}^{(1)}\Big|_{y=a^{(1)}} = m_0 \tag{75c}$$

$$u_x^{(N)}\Big|_{y=b^{(N)}} = 0 \tag{76a}$$

$$u_y^{(N)}\Big|_{y=b^{(N)}} = 0 \tag{76b}$$

$$\mu_{yz}^{(N)}\Big|_{y=b^{(N)}} = 0 \text{ or } \omega_z^{(N)}\Big|_{y=b^{(N)}} = 0 \tag{76c}$$

$$u_x^{(k)}\Big|_{y=b^{(k)}} = u_x^{(k+1)}\Big|_{y=a^{(k+1)}} \tag{77a}$$

$$u_y^{(k)}\Big|_{y=b^{(k)}} = u_y^{(k+1)}\Big|_{y=a^{(k+1)}} \tag{77b}$$

$$\omega_z^{(k)}\Big|_{y=b^{(k)}} = \omega_z^{(k+1)}\Big|_{y=a^{(k+1)}} \tag{77c}$$

จุฬาลงกรณ์มหาวิทยาลัย
Chulalongkorn University

$$\sigma_{yy}^{(k)}\Big|_{y=b^{(k)}} = \sigma_{yy}^{(k+1)}\Big|_{y=a^{(k+1)}} \tag{77d}$$

$$\sigma_{yx}^{(k)}\Big|_{y=b^{(k)}} = \sigma_{yx}^{(k+1)}\Big|_{y=a^{(k+1)}} \tag{77e}$$

$$\mu_{yz}^{(k)}\Big|_{y=b^{(k)}} = \mu_{yz}^{(k+1)}\Big|_{y=a^{(k+1)}} \tag{77f}$$

where $a^{(k)}$ and $b^{(k)}$ denote the y-coordinates of the top and bottom surface of the k^{th} layer. By taking Fourier integral transform of (75)-(77) with respect to the coordinate x, it yields

$$\bar{\sigma}_{yy}^{(1)}\Big|_{y=a^{(1)}} = \bar{p}_0 \tag{78a}$$

$$\bar{\sigma}_{yx}^{(1)}\Big|_{y=a^{(1)}} = \bar{q}_0 \tag{78b}$$

$$\bar{\mu}_{yz}^{(1)}\Big|_{y=a^{(1)}} = \bar{m}_0 \tag{78c}$$

$$\bar{u}_{x}^{(N)}\Big|_{y=b^{(N)}} = 0 \tag{79a}$$

$$\bar{u}_{y}^{(N)}\Big|_{y=b^{(N)}} = 0 \tag{79b}$$

$$\bar{\mu}_{yz}^{(N)}\Big|_{y=b^{(N)}} = 0 \text{ or } \bar{\omega}_{z}^{(N)}\Big|_{y=b^{(N)}} = 0 \tag{79c}$$

$$\bar{u}_{x}^{(k)}\Big|_{y=b^{(k)}} = \bar{u}_{x}^{(k+1)}\Big|_{y=a^{(k+1)}} \tag{80a}$$

$$\bar{u}_{y}^{(k)}\Big|_{y=b^{(k)}} = \bar{u}_{y}^{(k+1)}\Big|_{y=a^{(k+1)}} \tag{80b}$$

$$\bar{\omega}_{z}^{(k)}\Big|_{y=b^{(k)}} = \bar{\omega}_{z}^{(k+1)}\Big|_{y=a^{(k+1)}} \tag{80c}$$

$$\bar{\sigma}_{yy}^{(k)}\Big|_{y=b^{(k)}} = \bar{\sigma}_{yy}^{(k+1)}\Big|_{y=a^{(k+1)}} \tag{80d}$$

$$\bar{\sigma}_{yx}^{(k)}\Big|_{y=b^{(k)}} = \bar{\sigma}_{yx}^{(k+1)}\Big|_{y=a^{(k+1)}} \tag{80e}$$

$$\bar{\mu}_{yz}^{(k)}\Big|_{y=b^{(k)}} = \bar{\mu}_{yz}^{(k+1)}\Big|_{y=a^{(k+1)}} \tag{80f}$$

where the "bar" is employed to designate the transformed function. From the general solutions of the representative layer established in Section 3.1 and Section 3.2, the transformed quantities $\bar{u}_x^{(k)}$, $\bar{u}_y^{(k)}$, $\bar{\omega}_z^{(k)}$, $\bar{\sigma}_{yy}^{(k)}$, $\bar{\sigma}_{yx}^{(k)}$, and $\bar{\mu}_{yz}^{(k)}$ at the top and bottom surfaces of the k^{th} layer can be obtained as

จุฬาลงกรณ์มหาวิทยาลัย
Chulalongkorn University

$$\begin{Bmatrix} \bar{u}_x^{(k)}(y=a^{(k)}) \\ \bar{u}_y^{(k)}(y=a^{(k)}) \\ \bar{\omega}_z^{(k)}(y=a^{(k)}) \\ \bar{u}_x^{(k)}(y=b^{(k)}) \\ \bar{u}_y^{(k)}(y=b^{(k)}) \\ \bar{\omega}_z^{(k)}(y=b^{(k)}) \end{Bmatrix} = \mathbf{M}^{(k)}(\xi) \begin{Bmatrix} C_1^{(k)} \\ C_2^{(k)} \\ C_3^{(k)} \\ C_4^{(k)} \\ C_5^{(k)} \\ C_6^{(k)} \end{Bmatrix} \tag{81}$$

$$\begin{Bmatrix} \bar{\sigma}_{yx}^{(k)}(y=a^{(k)}) \\ \bar{\sigma}_{yy}^{(k)}(y=a^{(k)}) \\ \bar{\mu}_{yz}^{(k)}(y=a^{(k)}) \\ \bar{\sigma}_{yx}^{(k)}(y=b^{(k)}) \\ \bar{\sigma}_{yy}^{(k)}(y=b^{(k)}) \\ \bar{\mu}_{yz}^{(k)}(y=b^{(k)}) \end{Bmatrix} = \mathbf{N}^{(k)}(\xi) \begin{Bmatrix} C_1^{(k)} \\ C_2^{(k)} \\ C_3^{(k)} \\ C_4^{(k)} \\ C_5^{(k)} \\ C_6^{(k)} \end{Bmatrix} \tag{82}$$

where $\mathbf{M}^{(k)}$ and $\mathbf{N}^{(k)}$ are known 6x6-matrices of the k^{th} layer whose entries depends on the transform parameter ξ. Note in particular that the explicit expression of both $\mathbf{M}^{(k)}$ and $\mathbf{N}^{(k)}$ can be readily established from the general solutions of the displacement, rotation, force stress and couple stress presented in the previous sections. By enforcing the three boundary conditions (78), the three boundary conditions (79), and the six continuity conditions (80) for all $N-1$ material interfaces together with the results (83) and (84), it leads to a system of $6N$ linear algebraic equations governing the $6N$ unknowns $C_i^{(k)}$ $(i=1,2,...,6; k=1,2,...,N)$ in the transformed space. An efficient linear solved is then selected to determine the root $C_i^{(k)}$.

จุฬาลงกรณ์มหาวิทยาลัย
Chulalongkorn University

Another efficient means to determine the unknown functions $C_i^{(k)}$ based on the direct stiffness scheme can also be employed. First, the system of six linear equations (81) is inverted to obtain the functions $C_i^{(k)}$ in terms of the transformed displacements and rotations at the top and bottom surfaces and then the results are substituted in (82), this yields

$$\begin{Bmatrix} \bar{\sigma}_{yx}^{(k)}(y=a^{(k)}) \\ \bar{\sigma}_{yy}^{(k)}(y=a^{(k)}) \\ \bar{\mu}_{yz}^{(k)}(y=a^{(k)}) \\ \bar{\sigma}_{yx}^{(k)}(y=b^{(k)}) \\ \bar{\sigma}_{yy}^{(k)}(y=b^{(k)}) \\ \bar{\mu}_{yz}^{(k)}(y=b^{(k)}) \end{Bmatrix} = \mathbf{N}^{(k)}(\xi)(\mathbf{M}^{(k)}(\xi))^{-1} \begin{Bmatrix} \bar{u}_{x}^{(k)}(y=a^{(k)}) \\ \bar{u}_{y}^{(k)}(y=a^{(k)}) \\ \bar{\omega}_{z}^{(k)}(y=a^{(k)}) \\ \bar{u}_{x}^{(k)}(y=b^{(k)}) \\ \bar{u}_{y}^{(k)}(y=b^{(k)}) \\ \bar{\omega}_{z}^{(k)}(y=b^{(k)}) \end{Bmatrix} = \mathbf{K}^{(k)}(\xi) \begin{Bmatrix} \bar{u}_{x}^{(k)}(y=a^{(k)}) \\ \bar{u}_{y}^{(k)}(y=a^{(k)}) \\ \bar{\omega}_{z}^{(k)}(y=a^{(k)}) \\ \bar{u}_{x}^{(k)}(y=b^{(k)}) \\ \bar{u}_{y}^{(k)}(y=b^{(k)}) \\ \bar{\omega}_{z}^{(k)}(y=b^{(k)}) \end{Bmatrix} \quad (83)$$

where $\mathbf{K}^{(k)}(\xi)$ is termed the stiffness matrix of the k^{th} layer in the transformed space defined by

$$\mathbf{K}^{(k)}(\xi) = \mathbf{N}^{(k)}(\xi)(\mathbf{M}^{(k)}(\xi))^{-1} \quad (84)$$

It is evident that the unknown functions $C_i^{(k)}$ are eliminated and the stiffness equations (83) indicate the relationship among the transformed quantities on the boundaries of the layer. By choosing the displacements and rotations at the boundaries of each layer as the primary unknowns together with the continuity of the displacements and rotations at the material interfaces, the total number of independent unknowns now reduces to $3N$ (i.e., the displacements and rotations at the top surface of all layers $\bar{u}_x^{(k)}(y=a^{(k)})$, $\bar{u}_y^{(k)}(y=a^{(k)})$, and $\bar{\omega}_z^{(k)}(y=a^{(k)})$ for $k=1,2,...,N$). A system of $3N$ linear algebraic equations governing all those unknowns can be formed from the natural boundary conditions (78) and the continuity conditions (80d)-(80f) for all $N-1$ material interfaces. Once the displacements and rotations at the top surface and material interfaces are determined, the unknown functions $C_i^{(k)}$ for each layer can be obtained from (81).

3.4 Fourier Integral Transform Inversion

Once the unknown functions $C_i^{(k)}$ for each layer are determined, the displacements, the rotation, the force stress and the couple stress within the layered medium in the transformed space are known. Then, Fourier integral transform inversion formula (47b) is utilized to obtain the integral formula for the elastic field in the physical space. An efficient algorithm (e.g., the direct evaluation of the integral via an efficient quadrature rule and the so-called fast Fourier transform algorithm) is then selected to perform such inversion.

CHAPTER 4
RESULTS AND DISCUSSION

A computer code has been implemented, under the platform of FORTRAN90, using the proposed scheme presented in Chapter 3 for a general multi-layer elastic medium subjected to arbitrary surface loading and fully bonded to the rigid base. The flow of the implemented code can be briefly summarized as follows. Once all essential information (e.g., geometry of the medium, loading conditions, material properties, etc.) is inserted into the input interface, the stiffness matrix of each layer is first constructed, for each value of the transform parameter, via the proper numerical scheme for the matrix inversion. The stiffness matrices for all layers together with the continuity and equilibrium conditions along the material interfaces and the prescribed surface loadings are then assembled to form the stiffness equation for the whole medium. The unknown displacements and rotations at all material interfaces, for each value of the transform parameter, are obtained by numerically solving a system of linear equations. Such information is then used to determine the unknown coefficients for each layer and, subsequently, all field quantities including the displacements, the rotation, the force stresses and the couple stresses in the transformed space can be readily obtained from the direct substitution. To obtain the elastic field at any point in the physical space, the Fourier integral inversion is applied, and this can be achieved in a separate efficient routine based mainly on Gaussian quadrature.

To verify the implemented computer code, two problems, one associated with a half-plane subjected to a uniformly distributed normal traction and the other corresponding to a single layer medium under the normal point force, are considered. For the half-plane case, computed results are benchmarked with the classical solution where the couple stresses are fully ignored whereas for the single layer medium, results reported by Zisis (2018) are used as the basis for the comparison. To further verify the implemented routine for handling the multi-layer medium via the direct stiffness scheme, the single layer medium is fictitiously partitioned into several layers with the same material properties and the multi-layer scheme is applied to construct the solution and then compared with the available reference solution. Once the

solution scheme is fully tested, extensive results are obtained for various cases and reported to demonstrate the characteristic of predicted solution and size dependence behavior for a wide range of internal and external length scales.

For the purpose of discussion of material length-scale effects and the comparison of results with those predicted by the size-independent continuum theory (i.e., the classical theory of linear elasticity), a reference material characteristic length ℓ_0 is introduced such that $\ell = \rho\ell_0$ where ρ is a non-dimensional parameter. In this sense, results predicted by the classical linear elasticity must be recovered as the parameter ρ approaches zero. In addition, the reference shear modulus μ_0 is also introduced for the normalization of the shear modulus of different layers where $\bar{\mu} = \mu / \mu_0$.

4.1 Homogeneous Half-plane

Consider an elastic half-plane subjected to a uniformly distributed normal traction p_0 on its surface over the region $[-a, a]$. To simulate this scenario within the context of the current formulation (a layered medium perfectly bonded to a rigid base), a single layer model is employed and the thickness of the layer h is chosen to be sufficiently large in comparison with the half length of the loading region a (i.e., $h/a = 1000$). Results of the normalized normal force-stress components along the line of symmetry (i.e., $x = 0$) are reported as a function of the normalized coordinate y/a as shown in Figure 4.1 for $a/\ell_0 = 1$, $\nu = 0.33$, and various values of the parameter ρ together with the exact classical solution. The result is seen that as ρ approaches zero (i.e., the material length scale is much smaller than the size of loading region), obtained results converge to the classical solution In addition, for the case that the length of the loading region is comparable to the material characteristic length ℓ, the force stresses predicted by the couple stress theory significantly deviate from that predicted by the classical continuum.

จุฬาลงกรณ์มหาวิทยาลัย
Chulalongkorn University

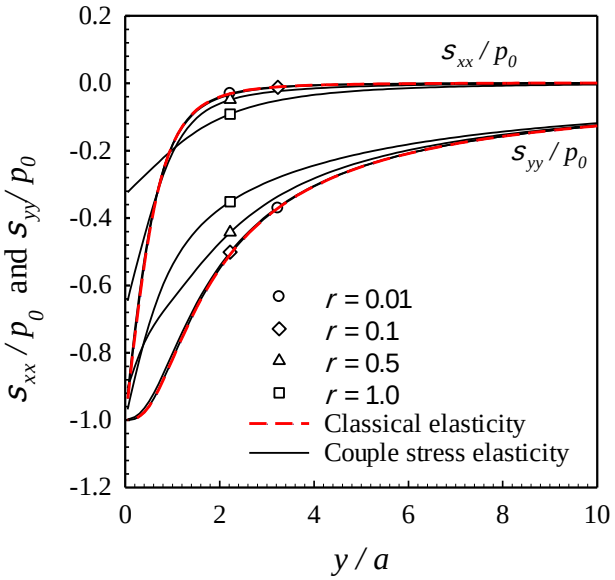

Figure 4.1 Normalized normal force stress σ_{xx} and σ_{yy} along the line of symmetry of elastic half-plane under uniformly distributed normal traction. Result reported for $\nu = 0.33$ and $a/\ell_0 = 1$.

4.2. Single Layer Media

Now, consider a single homogeneous layer medium of thickness h perfectly bonded to a rigid base. To allow the comparison with results reported in Zisis (2018), a particular surface loading condition associated with a concentrated normal point force and two values of Poisson's ratio (i.e., $\nu = 0.00$ and $\nu = 0.49$) are considered in the simulations. Computed results for the displacement and rotation at the top surface and the force stress and couple stress components at the bottom surface are reported along with the reference solutions in Figures 4.2-4.13 for various values of the ratio h/ℓ. It is seen that the excellent agreement between the present results and the benchmark solutions is apparent. In addition, this set of results clearly indicates that by taking the material micro-structure into consideration (via the presence of couple stresses), the field quantities are noticeably different from those predicted by the size-independent elasticity theory, especially when the characteristic material length scale becomes comparable to the thickness of the layer. The larger the material length scale, the

stronger the size-dependent effect. Note also that as the ratio h/ℓ increases (i.e., the external length scale becomes larger than the internal length scale), the couple stress components start decaying and finally approaching zero as h/ℓ reaching infinity.

Next, the response of a single layer medium subjected to a uniformly distributed normal traction p_0 over the region $[-a,a]$ is investigated. In the numerical study, the thickness of the layer is taken as $h/\ell_0 = 1$ and, to facilitate the investigation of the size dependency of predicted solutions, various values of the normalized half-length of the loading region a/ℓ_0 are considered. A selected set of results associated with the normalized vertical stress σ_{yy} along the line of symmetry is reported in Figure 4.14 for both $\rho = 0$ and $\rho = 1$. It is evident that solutions predicted by the couple stress theory become size dependent and significantly deviates from the classical solution (which is clearly size independent) as the size of the loading region reduces to be comparable to the material length scale ℓ.

To further confirm the size-dependent behavior of predicted response due to the presence of couple stress with $\rho \neq 0$, the normalized vertical stress σ_{yy} at a selected point, $x = 0$ and $y = h/2$, is also reported as a function of the normalized half-length of the loading region as shown in Figure 4.15. It is seen that the solution predicted by the couple stress theory is size-dependent for a wide range of a/ℓ_0. In particular, as a/ℓ_0 increases, the predicted solution decays monotonically and finally converges to the classical case. Note also that in the neighborhood of $a/\ell_0 = 0$, results obtained from the couple stress theory is nearly constant and this implies the size independent behavior as observed in the classical case. While the size dependent characteristic disappears as the size of the loading region is much smaller than the material length scale, the influence of couple stresses is still significant and cannot be ignored in modeling.

To additionally verify the validity of implemented code usage for multi-layer media, the same single homogenous layer medium subjected to a uniformly distributed normal traction p_0 over the region $[-a,a]$ is resolved by using the multi-layer scheme. In the simulations, Poisson's ratio $\nu = 0.5$, the material length scale

จุฬาลงกรณ์มหาวิทยาลัย
Chulalongkorn University

$\ell = \ell_0$ and the overall thickness $h = \ell_0$ are considered. The layer is devided into 2, 4, and 10 identical layers with the same material properties. Results for certain field quantities at certain locations within the medium, generated by a single-layer, 2-layer, 4-layer, and 10-layer models, are reported in Figures 4.16-4.19. It is seen that results from all four models are identical and this should confirm the correctness of the multi-layer scheme.

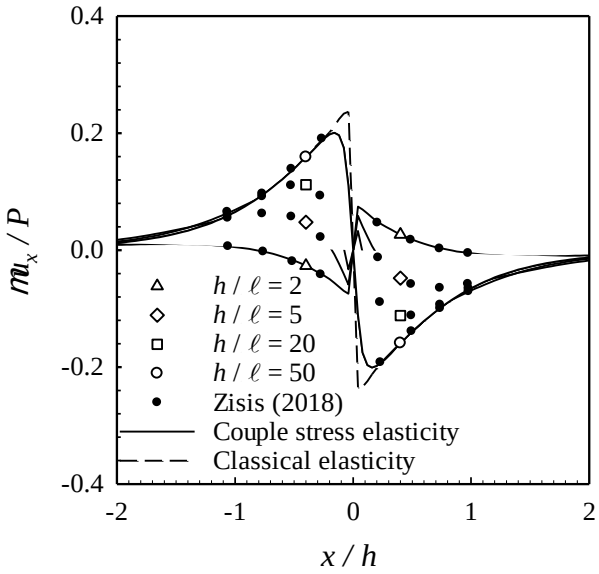

Figure 4.2 Normalized horizontal displacements u_x at the top surface of a single homogeneous layer under normal concentrated force with $\nu = 0$.

จุฬาลงกรณ์มหาวิทยาลัย
CHULALONGKORN UNIVERSITY

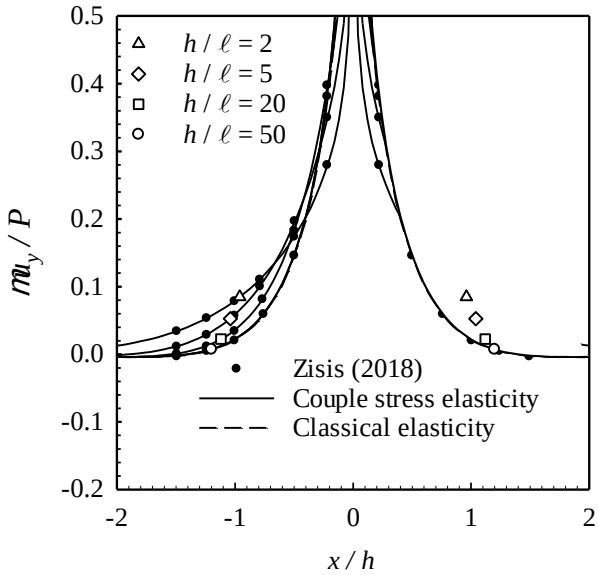

Figure 4.3 Normalized vertical displacements u_y at the top surface of a single homogeneous layer under normal concentrated force with $\nu = 0$.

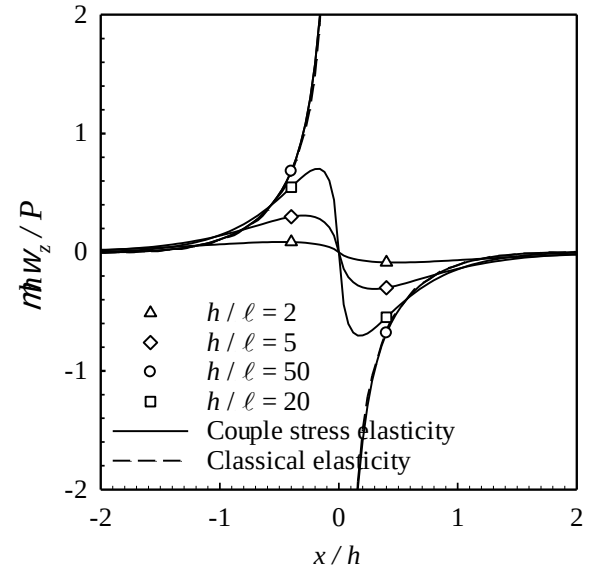

Figure 4.4 Normalized rotations ω_z at the top surface of a single homogeneous layer under normal concentrated force with $\nu = 0$.

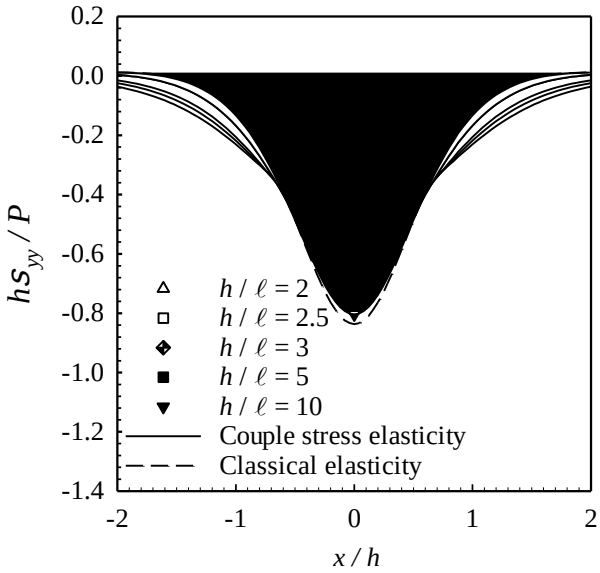

Figure 4.5 Normalized vertical stresses σ_{yy} at the bottom surface of a single homogeneous layer under normal concentrated force with $\nu = 0$.

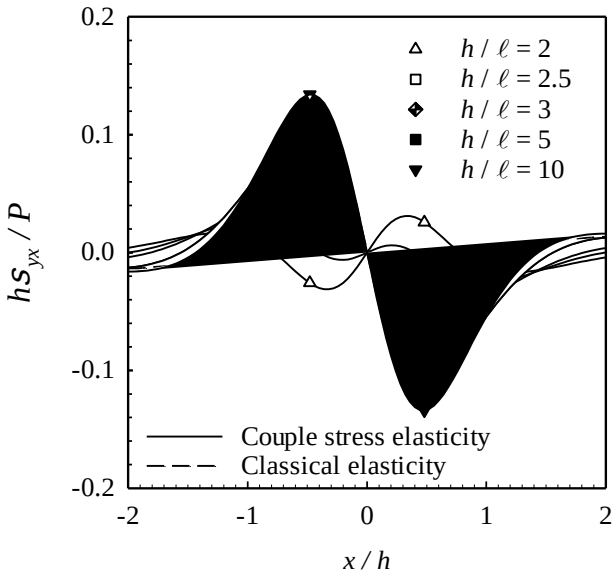

Figure 4.6 Normalized shear stresses σ_{yx} at the bottom surface of a single homogeneous layer under normal concentrated force with $\nu = 0$.

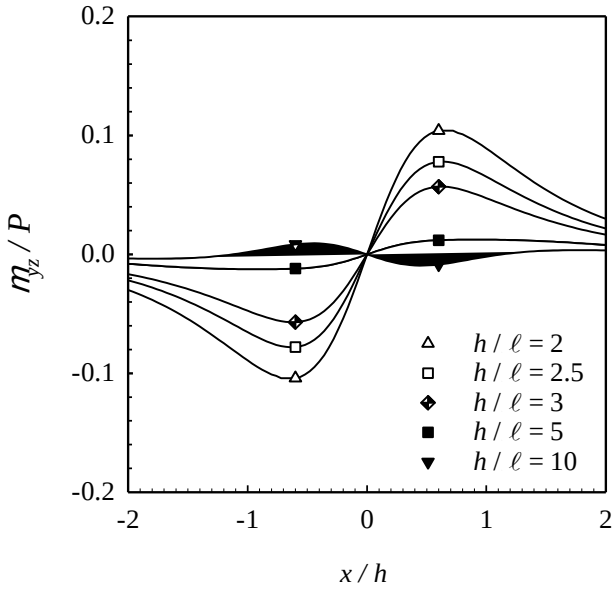

Figure 4.7 Normalized couple stresses μ_{yz} at the bottom surface of a single homogeneous layer under normal concentrated force with $\nu = 0$.

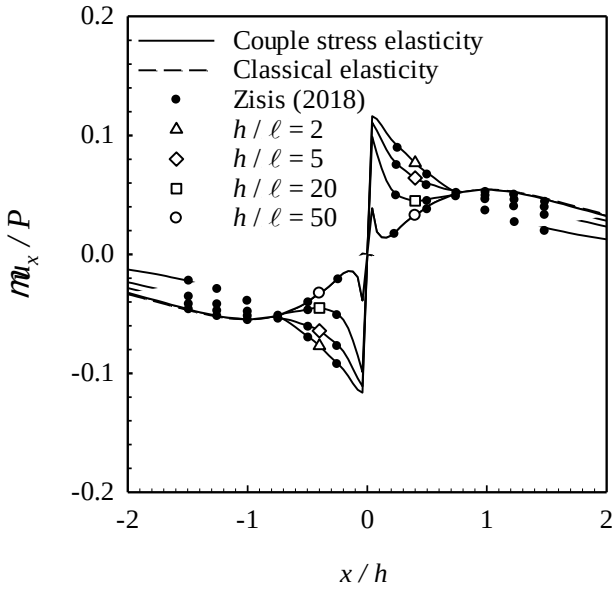

Figure 4.8 Normalized horizontal displacements u_x at the top surface of a single homogeneous layer under normal concentrated force with $\nu = 0.49$.

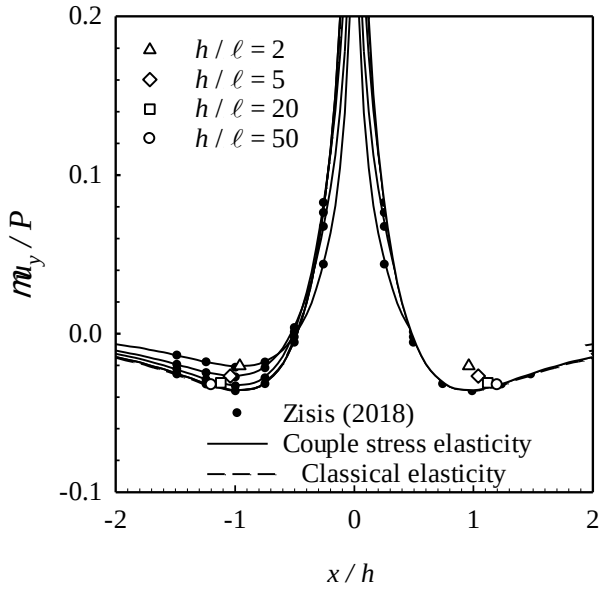

Figure 4.9 Normalized vertical displacements u_y at the top surface of a single homogeneous layer under normal concentrated force with $\nu = 0.49$.

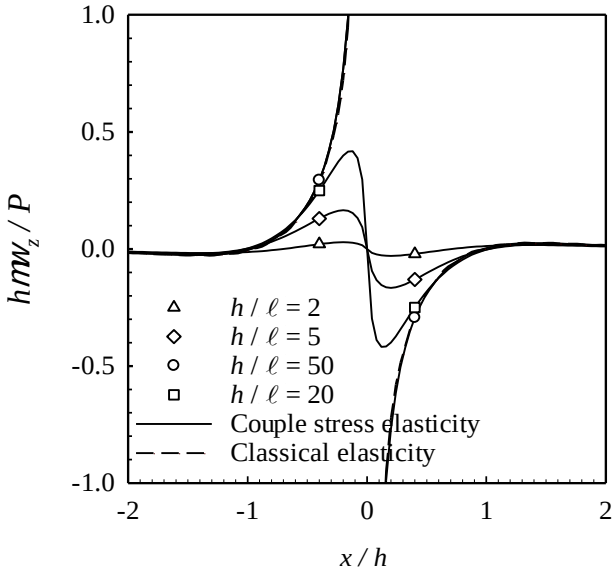

Figure 4.10 Normalized rotations ω_z at the top surface of a single homogeneous layer under normal concentrated force with $\nu = 0.49$.

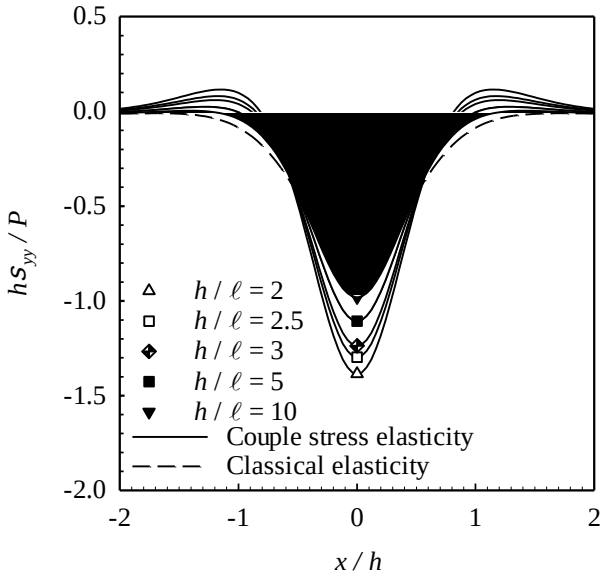

Figure 4.11 Normalized vertical stresses σ_{yy} at the bottom surface of a single homogeneous layer under normal concentrated force with $\nu = 0.49$.

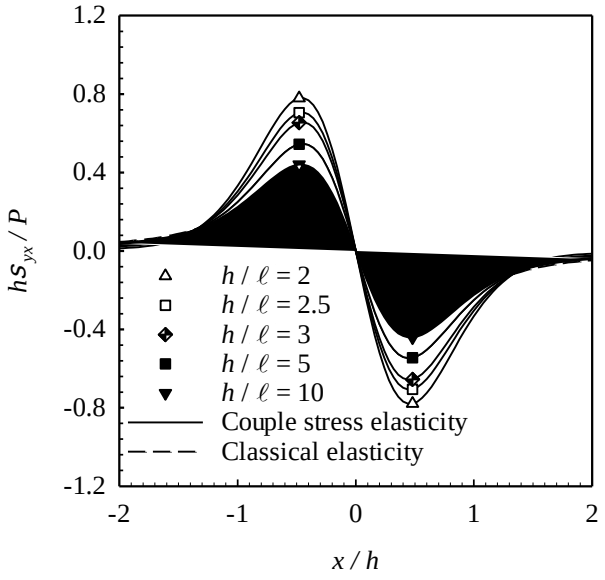

Figure 4.12 Normalized shear stresses σ_{yx} at the bottom surface of a single homogeneous layer under normal concentrated force with $\nu = 0.49$.

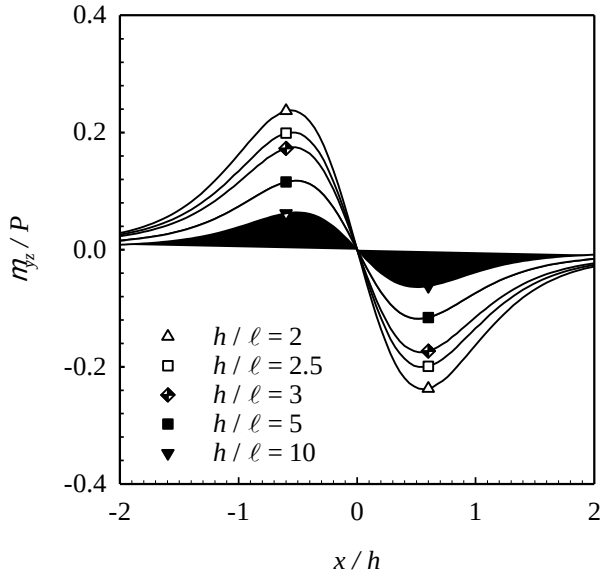

Figure 4.13 Normalized couple stresses μ_{yz} at the bottom surface of a single homogeneous layer under normal concentrated force with $\nu = 0.49$.

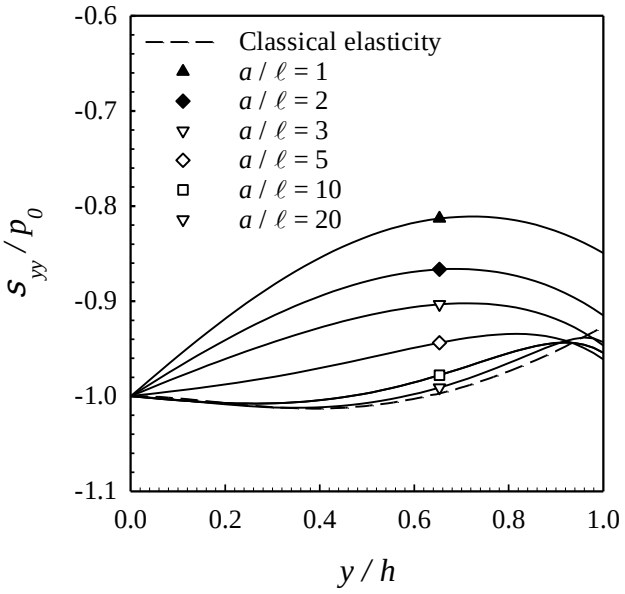

Figure 4.14 Normalized vertical stresses σ_{yy} along the line of symmetry of a single layer medium plane under uniformly distributed normal traction. Results are reported for $\nu = 0.33$, $h / a = 1$, $\rho \in \{0,1\}$, and various values of a / ℓ.

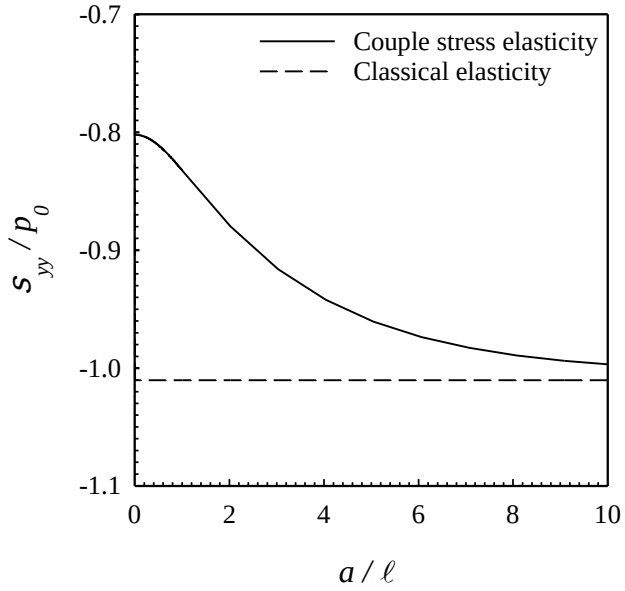

Figure 4.15 Normalized vertical stresses σ_{yy} at a point $x=0$ and $y=h/2$ of a single layer medium plane under uniformly distributed normal traction versus the normalized half-length of loading region. Result reported for $\nu=0.33$, $h/a=1$, and $\rho\in\{0,1\}$.

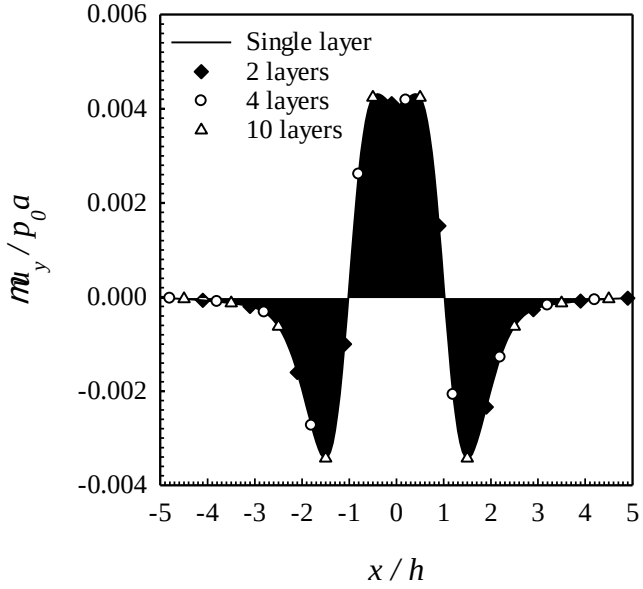

Figure 4.16 Profile of normalized vertical displacement u_y at $y/h=0.5$ for a single homogeneous layer medium under uniformly distributed normal traction having with $h=\ell=\ell_0$ and $\nu=0.5$.

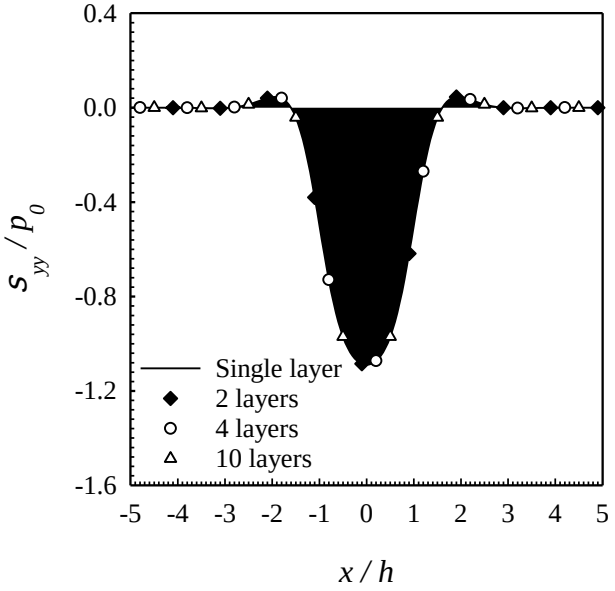

Figure 4.17 Profile of normalized vertical stress σ_{yy} at $y/h = 0.5$ for a single homogeneous layer medium under uniformly distributed normal traction having with $h = \ell = \ell_0$ and $\nu = 0.5$.

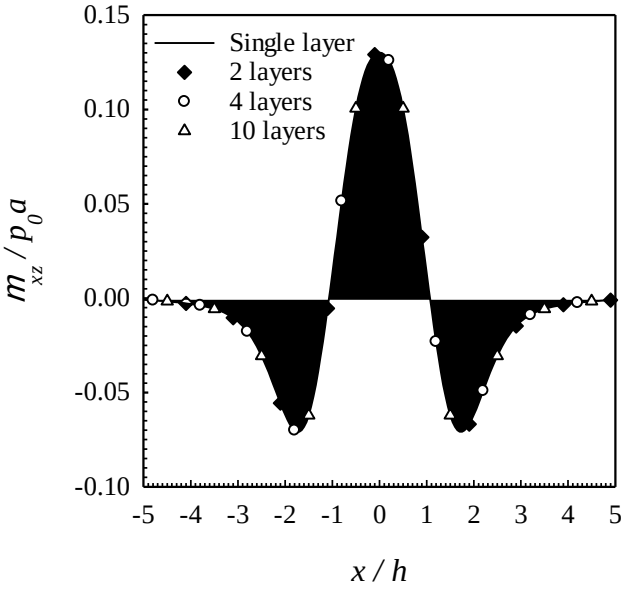

Figure 4.18 Profile of normalized couple stress μ_{xz} at $y/h = 0.5$ for a single homogeneous layer medium under uniformly distributed normal traction having with $h = \ell = \ell_0$ and $\nu = 0.5$.

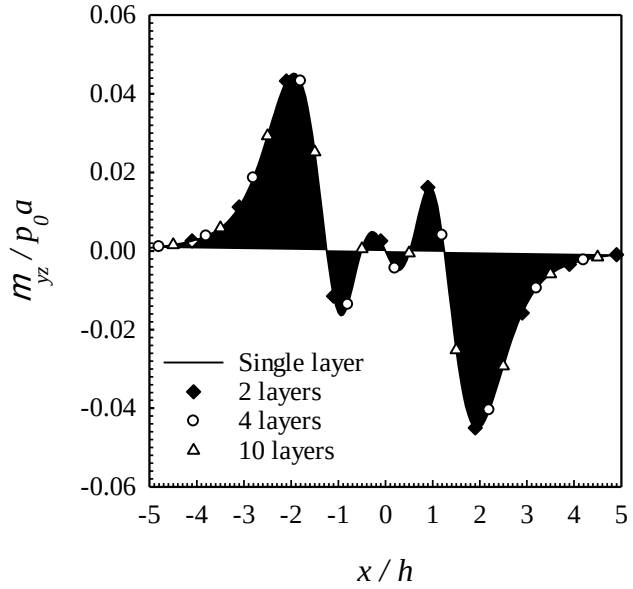

Figure 4.19 Profile of normalized couple stress μ_{yz} at $y/h = 0.5$ for a single homogeneous layer medium under uniformly distributed normal traction having with $h = \ell = \ell_0$ and $\nu = 0.5$.

4.3. Layer on Half Plane under Uniformly Distributed Loads

Now, the elastic response of a single elastic layer rested on a half plane, as illustrated in Figure 4.20, is fully investigated. The shear modulus, Poison's ratio and the normalized length scale of material for the layer and the half plane are denoted by $\mu^{(1)}, \nu^{(1)}, \rho^{(1)}$ and $\mu^{(2)}, \nu^{(2)}, \rho^{(2)}$, respectively. Three representative surface loadings including a uniformly distributed normal traction p_0 (see Figure 4.20(a)), a uniformly distributed shear traction q_0 (see Figure 4.20(b)), and a uniformly distributed couple traction m_0 (see Figure 3 Figure 4.20(c)) acting over a finite region $[-a, a]$ are considered in the numerical investigation. To explore the influence of the material contrast (in terms of the shear modulus) on predicted elastic fields, simulations are gone through for various values of the shear modulus ratio $\gamma = \mu^{(1)}/\mu^{(2)}$ while Poisson's ratio and the normalized length scale of the material for both the layer and the half plane are taken to be identical (i.e., $\nu^{(1)} = \nu^{(2)} = \nu$ and $\rho^{(1)} = \rho^{(2)} = 1$).

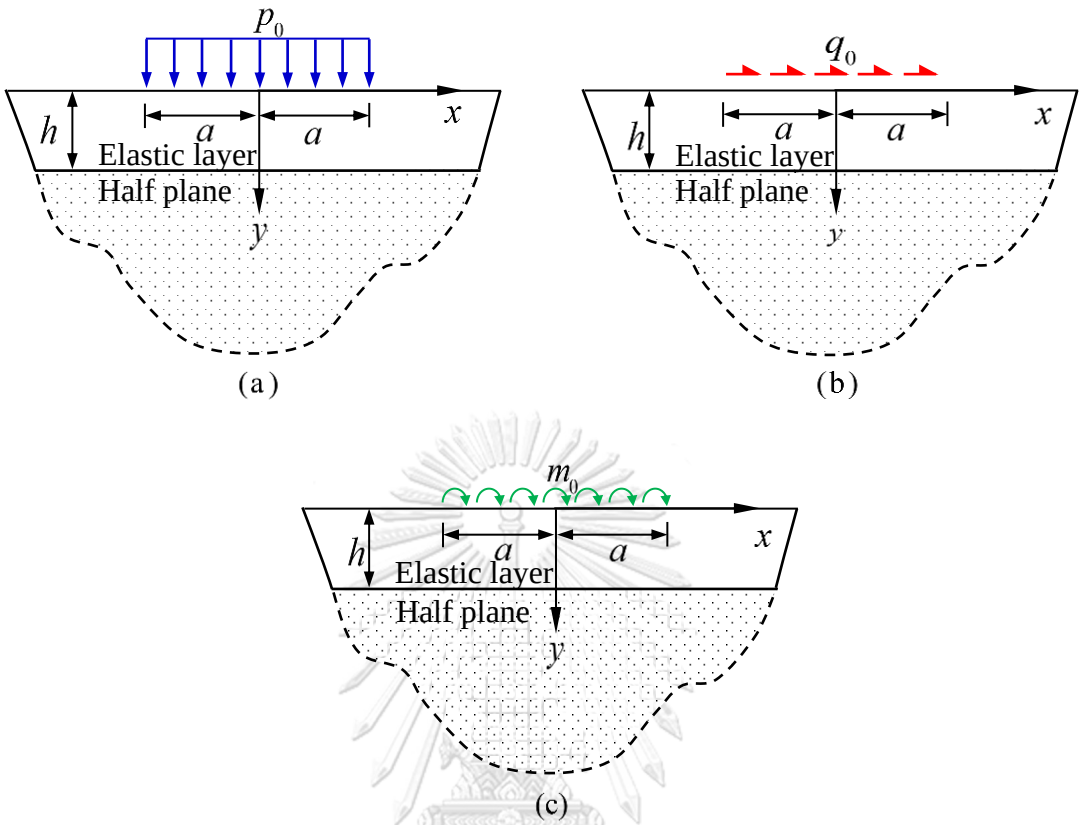

Figure 4.20 Schematics of a layer rested on a half plane under (a) uniformly distributed normal traction, (b) uniformly distributed shear traction, and (c) uniformly distributed couple traction.

จุฬาลงกรณ์มหาวิทยาลัย
Chulalongkorn University

In the numerical study, the following parameters $\nu = 0.30$, $\rho = 1$ and $\bar{a} = a/\ell_0 = 1$ are employed. Representative results for the force stress and the couple stress at the bottom surface of the layer (i.e., at $y = h$) are reported, as a function of the normalized coordinate x/h, in Figures 4.21, 4.22, and 4.23 for the first, second and third type of loading conditions, respectively. It is seen, from these results, that the shear modulus ratio γ has the strong effect on both the value and the distribution of the elastic field within the layer for all three loading cases. In particular, the displacements and stresses start exhibiting deviation from those for the case of an elastic layer rested on an elastic foundation (i.e., $\gamma = 0$) as the ratio γ increases from zero. Clearly, such discrepancy is still significant when the shear modulus of the half

plane is comparable to that of the layer or the ratio γ falls in the practical range in surface coating applications. Note also that results for the case $\gamma = 0$ does not always constitute the upper or lower bound solution and this, as a result, implies the need, in the modeling, to properly handling the finite modulus of the substrate below the layer.

The size dependent characteristic of predicted elastic responses due to the presence of couple stresses is further investigated. In the simulations, the thickness of the layer, the shear modulus ratio, the normalized length scale, and Poisson's ration are taken as $a/h = 1$, $\gamma = 0.5$, $\rho^{(1)} = \rho^{(2)} = 1$, and $\nu^{(1)} = \nu^{(2)} = 0.3$ while the normalized half-length of the loading region $\bar{a} = a/\ell_0$ is varied. Results for the normalized forces stresses σ_{xy}, σ_{yx} and σ_{yy} and normalized couple stress μ_{yz} at the bottom of the elastic layer (i.e., along $y = h/2$) are reported in Figures 4.24, 4.26 and 4.28 for all three types of surface loading. In addition, the normalized force stresses σ_{xx} and σ_{yy}, the normalized shear stresses σ_{xy} and σ_{yx}, and the normalized force stress σ_{yx} and couple stress μ_{yz} along the line of symmetry (i.e., along $x = 0$) are reported in Figures 4.25, 4.27 and 4.29 for the first, second and third loading conditions. Results for the force stresses predicted by the classical elasticity (without couple stresses) are also included for sake of comparison and discussion. It is evident from this set of results that both the force stresses and couple stresses predicted from the couple stress theory become size dependent and deviates from the classical solution. This observation is in contrast to the characteristic of the classical solution. As the size of the loading region is sufficiently small and comparable to the material length scale ℓ, the discrepancy of the two solutions can be significant. On the contrary, results for all types of loading converge to those from the classical elasticity as a is sufficiently large in comparison with ℓ.

To further explore the influence of the ratio a/h on the size dependency of predicted responses due to the presence of the couple stresses ($\rho \neq 0$), certain stress components at a selected point $x = 0$, $y = h/2$ are reported as a function of the normalized half-length of the loading region a/ℓ_0 in Figures 4.30-4.32 for all three loading cases. It is seen again that the solution predicted by the couple stress theory is size dependent for a wide range of a/ℓ. In particular, as a/ℓ increases, the predicted

solution reduces monotonically and finally converges to the classical case. In addition, in the neighborhood of $a/\ell = 0$, the result obtained from the couple stress theory is nearly constant and this also implies the size independent behavior as observed in the classical case. Although the size dependent characteristic disappears as the size of the loading region is much smaller than the material length scale, the influence of the couple stresses is still significant (indicating by the discrepancy of the two solutions) and cannot be ignored in the modeling. Note also that the smaller the value of the ratio a/h, the larger the discrepancy between the classical solution and that from the couple stress theory.

Finally, the influence of the material contrast on the size dependent behavior is also demonstrated via predicted results for stresses at a representative point within the layer. In particular, the vertical stress σ_{yy} (for the first loading case), the shear stress σ_{yx} (for the second loading case) and the couple stress μ_{yz} (for the third loading case) at $x = 0$, $y = h/2$ are reported in Figures 4.33, 4.34 and 4.35, respectively, for $a/h = 1$, $\nu = 0.30$ and various values of the shear modulus ratio $\gamma = \mu^{(1)}/\mu^{(2)}$. As can be seen from these results, the ratio γ does not alter the size dependent characteristic of the predicted solutions except that the larger the magnitude of the predicted stresses is observed as γ decreases.

จุฬาลงกรณ์มหาวิทยาลัย
Chulalongkorn University

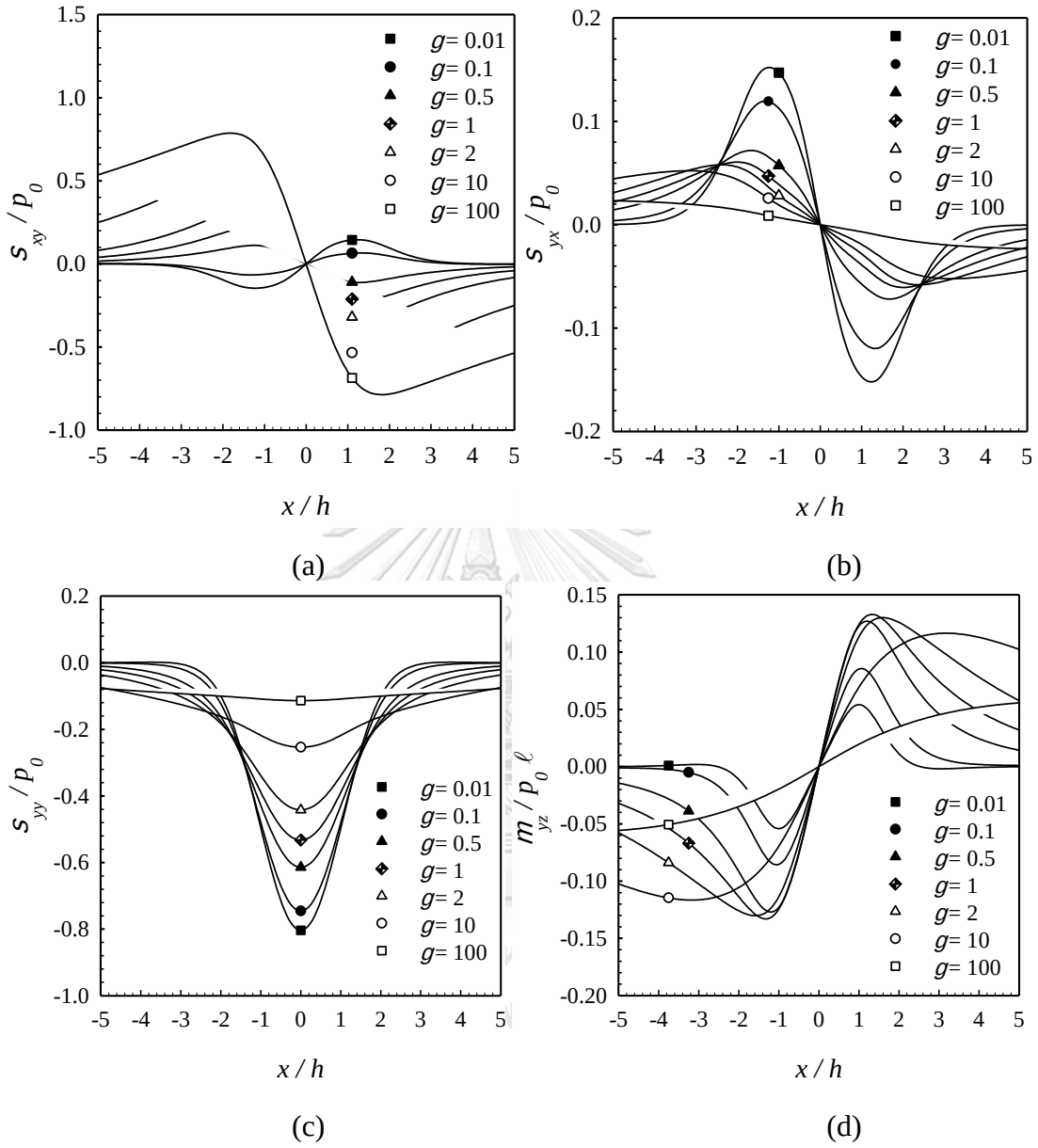

Figure 4.21 Results for (a) normalized shear stress σ_{xy}, (b) normalized shear stress σ_{yx}, (c) normalized vertical stress σ_{yy}, and (d) normalized couple stress μ_{yz} at the bottom surface of the layer under uniformly distributed normal traction. Results are reported for $\nu = 0.30$, and $a/\ell_0 = 1$.

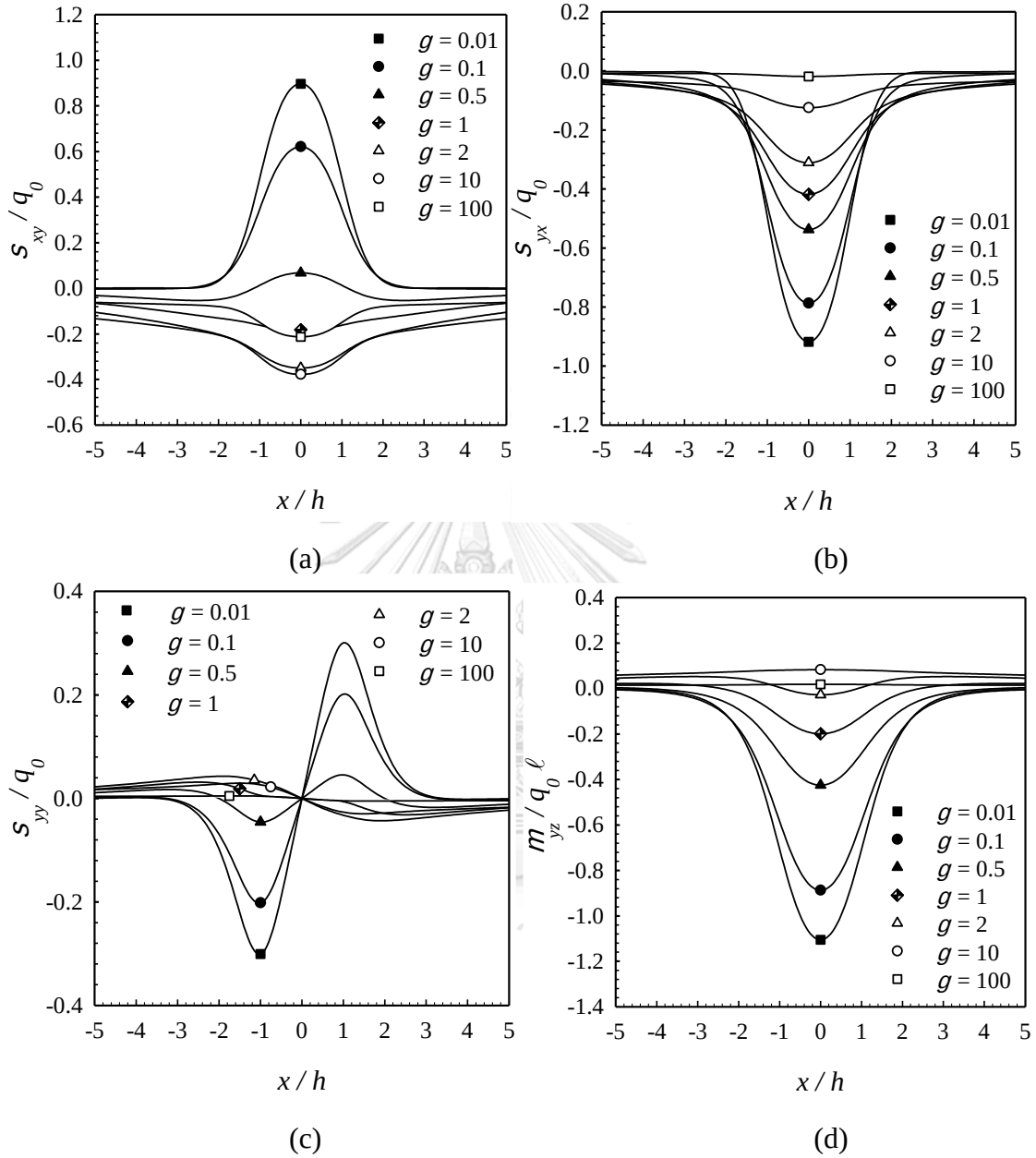

Figure 4.22 Results for (a) normalized shear stress σ_{xy}, (b) normalized shear stress σ_{yx}, (c) normalized vertical stress σ_{yy}, and (d) normalized couple stress μ_{yz} at the bottom surface of the layer under uniformly distributed shear traction. Results are reported for $\nu = 0.30$, and $a/\ell_0 = 1$.

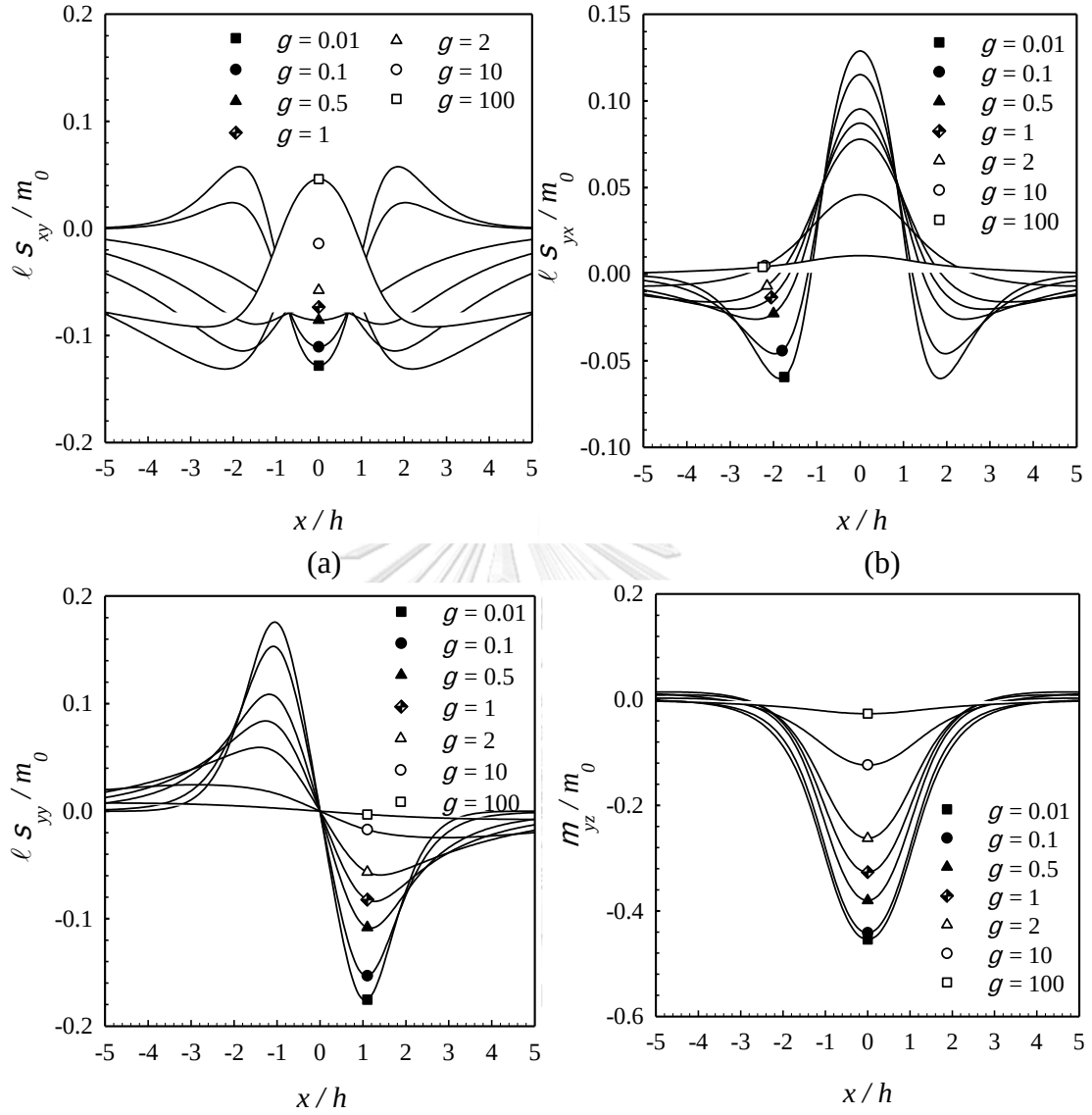

Figure 4.23 Results for (a) normalized shear stress σ_{xy}, (b) normalized shear stress σ_{yx}, (c) normalized vertical stress σ_{yy}, and (d) normalized couple stress μ_{yz} at the bottom surface of the layer under uniformly distributed couple traction. Results are reported for $\nu = 0.30$, and $a/\ell_0 = 1$.

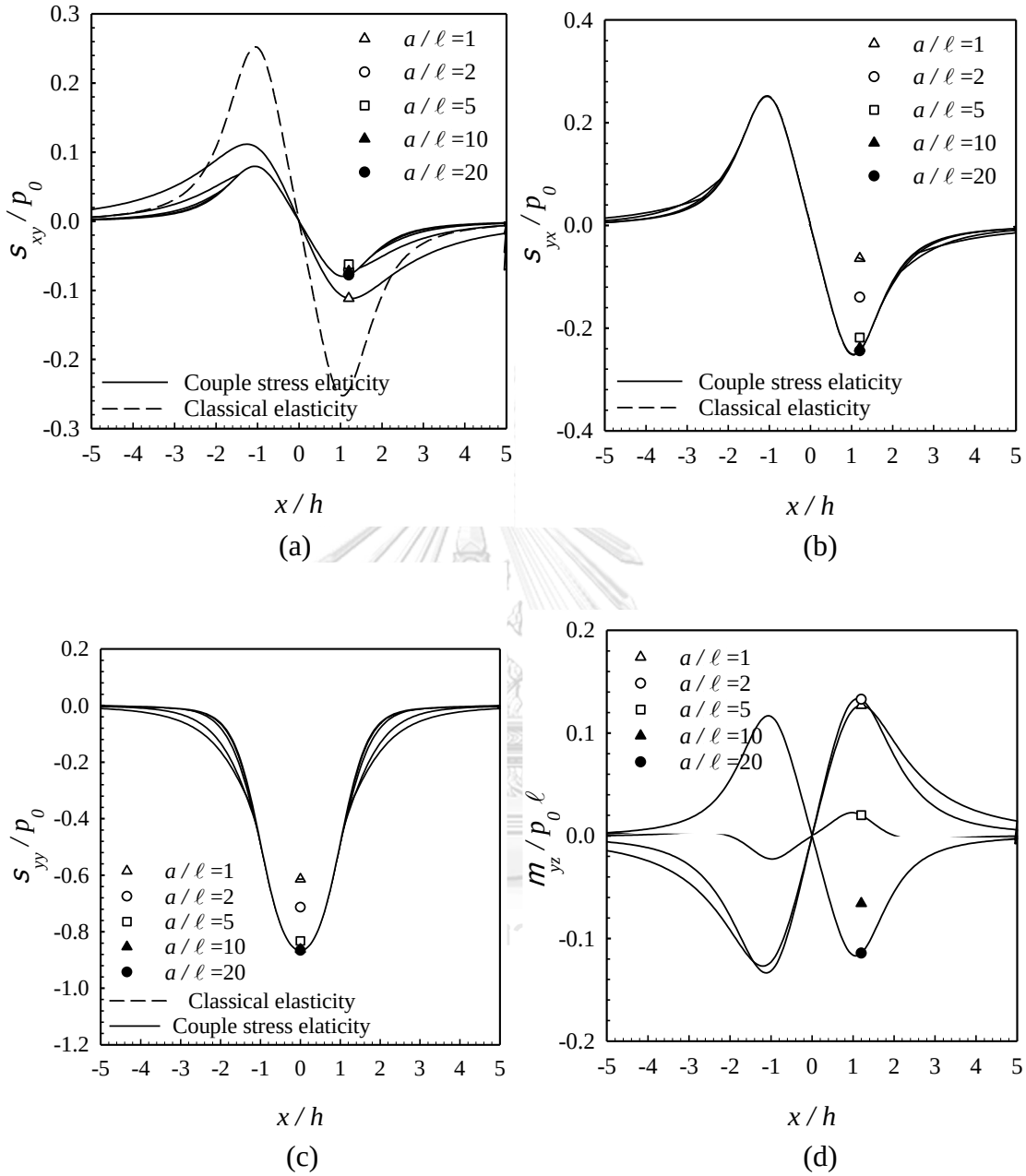

Figure 4.24 Results for (a) normalized shear stress σ_{xy}, (b) normalized shear stress σ_{yx}, (c) normalized vertical stress σ_{yy}, and (d) normalized couple stress μ_{yz} at the bottom surface of the layer under uniformly distributed normal traction. Results are reported for $a/h=1$, $\gamma=0.5$, $\rho^{(1)}=\rho^{(2)}=1$, and $\nu^{(1)}=\nu^{(2)}=0.3$.

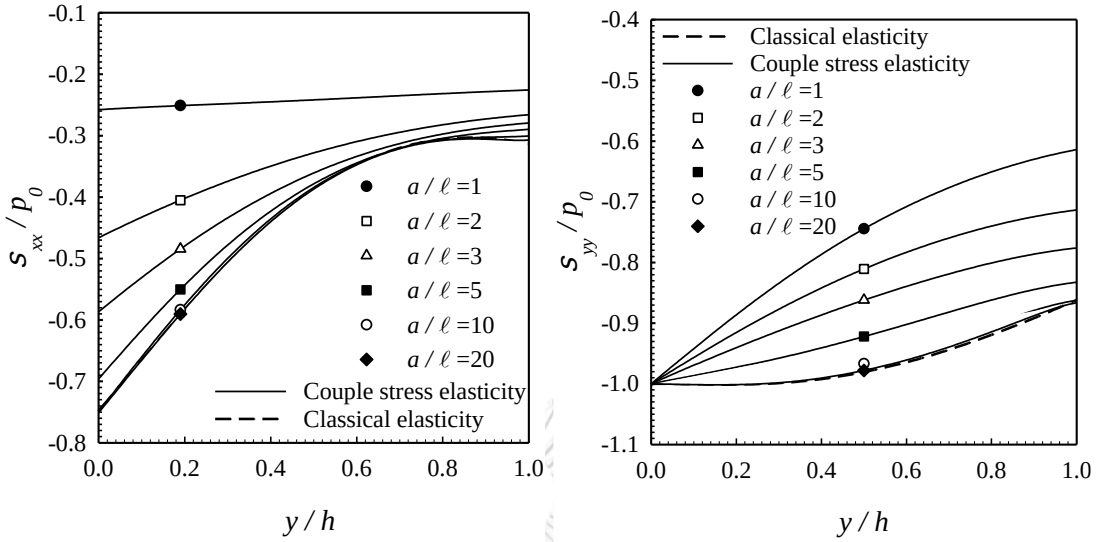

(a) (b)

Figure 4.25 Results for (a) normalized horizontal stress σ_{xx} and (b) normalized vertical stress σ_{yy} along the line of symmetry of the elastic layer under uniformly distributed normal traction. Results are reported for $a/h=1$, $\gamma=0.5$, $\rho^{(1)}=\rho^{(2)}=1$, and $\nu^{(1)}=\nu^{(2)}=0.3$.

จุฬาลงกรณ์มหาวิทยาลัย
CHULALONGKORN UNIVERSITY

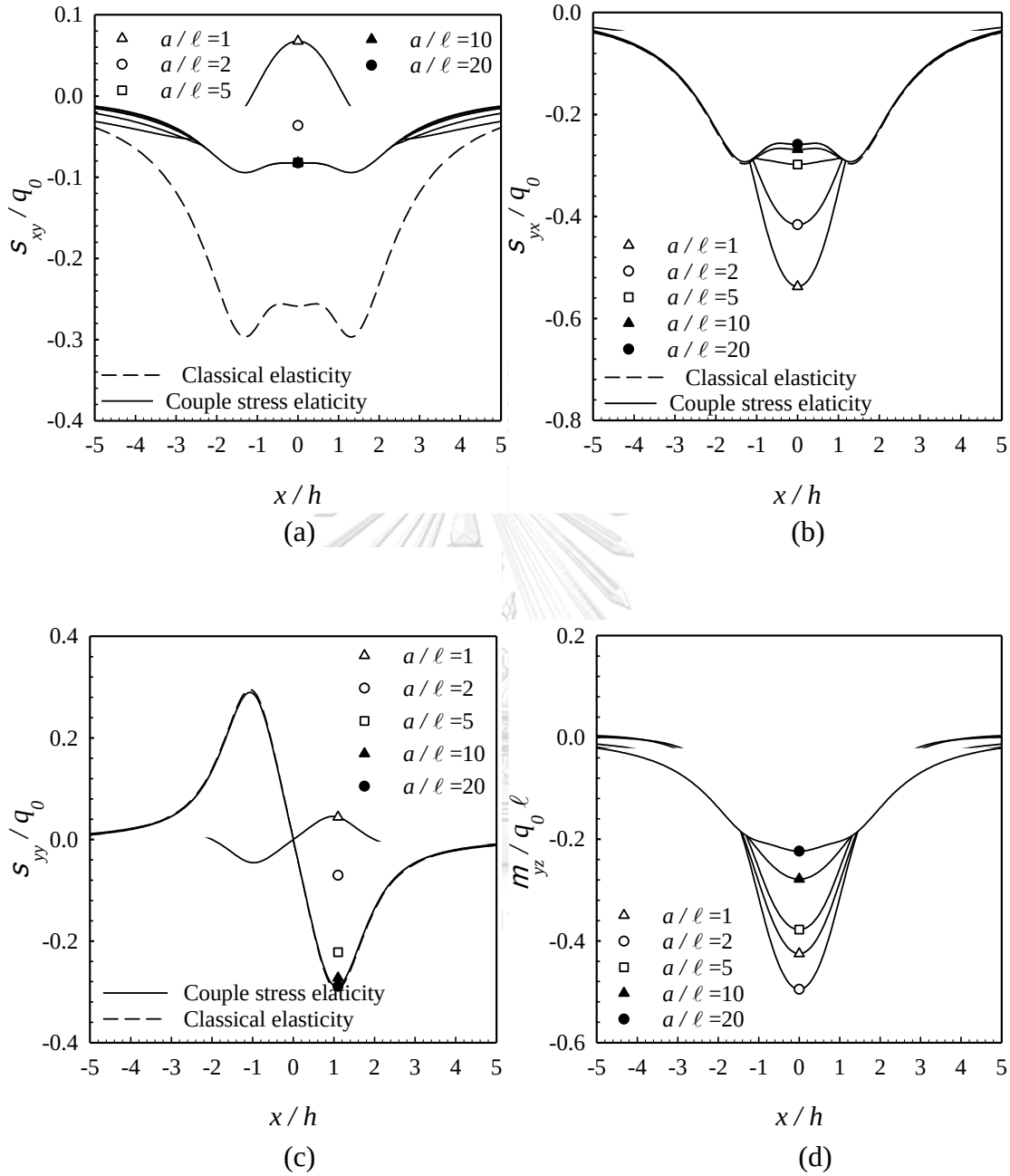

Figure 4.26 Results for (a) normalized shear stress σ_{xy}, (b) normalized shear stress σ_{yx}, (c) normalized vertical stress σ_{yy}, and (d) normalized couple stress μ_{yz} at the bottom surface of the layer under uniformly distributed shear traction. Results are reported for $a/h=1$, $\gamma=0.5$, $\rho^{(1)}=\rho^{(2)}=1$, and $\nu^{(1)}=\nu^{(2)}=0.3$.

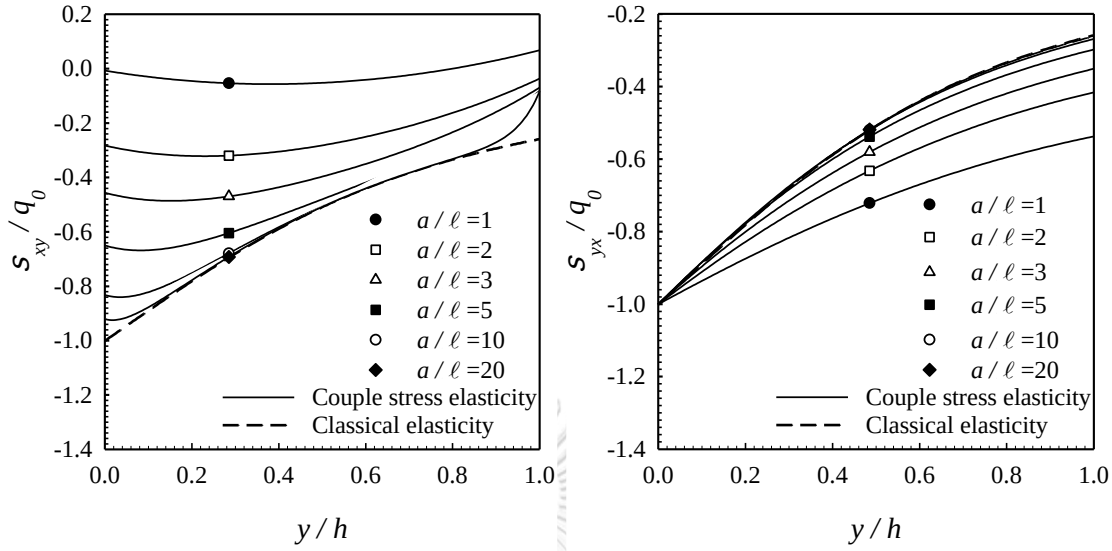

Figure 4.27 Results for (a) normalized shear stress σ_{xy} and (b) normalized shear stress σ_{yx} along the line of symmetry of the elastic layer under uniformly distributed shear traction. Results are reported for $a/h=1$, $\gamma=0.5$, $\rho^{(1)}=\rho^{(2)}=1$, and $\nu^{(1)}=\nu^{(2)}=0.3$.

จุฬาลงกรณ์มหาวิทยาลัย
Chulalongkorn University

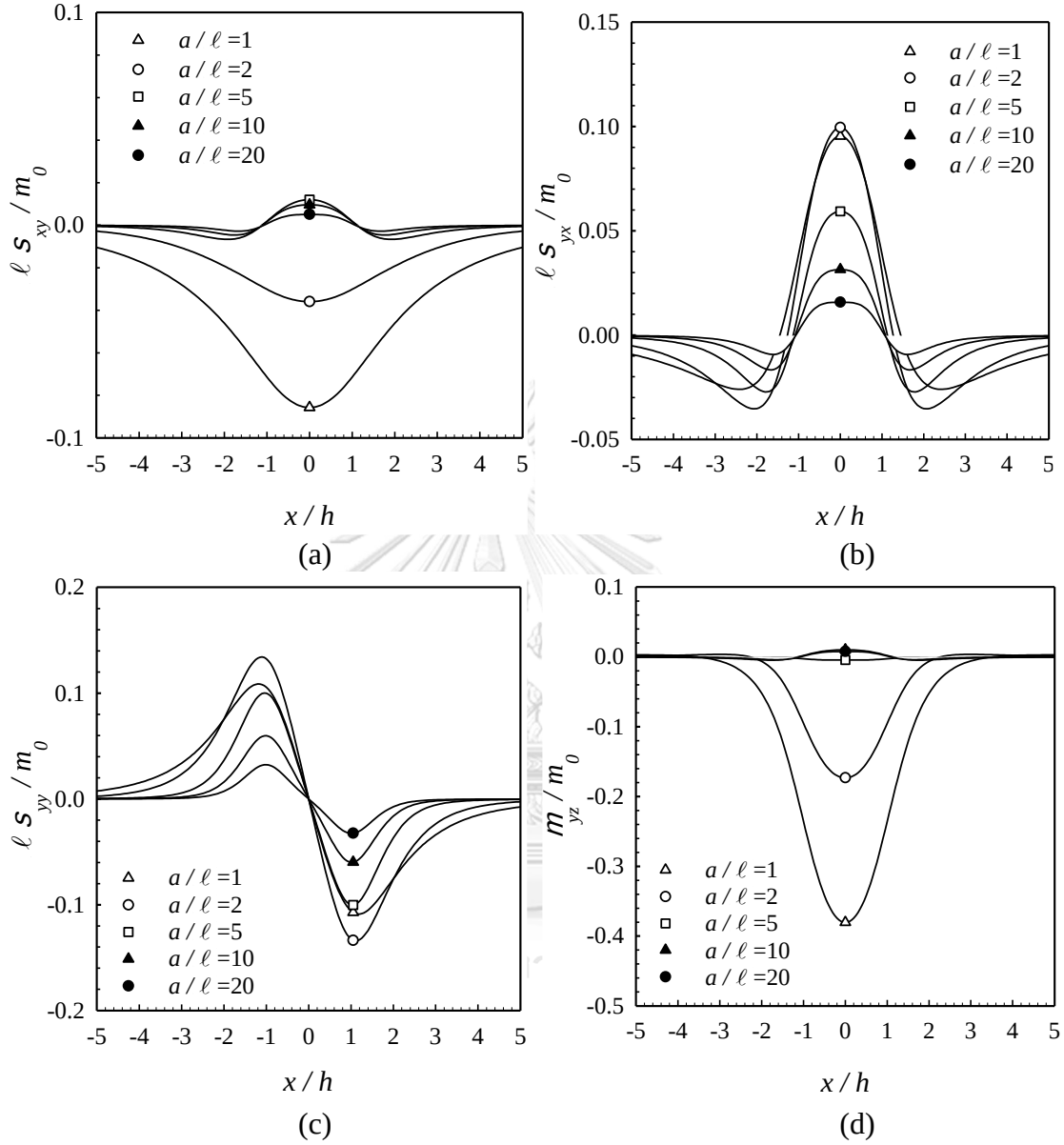

Figure 4.28 Results for (a) normalized shear stress σ_{xy}, (b) normalized shear stress σ_{yx}, (c) normalized vertical stress σ_{yy}, and (d) normalized couple stress μ_{yz} at the bottom surface of the layer under uniformly distributed couple traction. Results are reported for $a/h = 1$, $\gamma = 0.5$, $\rho^{(1)} = \rho^{(2)} = 1$, and $\nu^{(1)} = \nu^{(2)} = 0.3$.

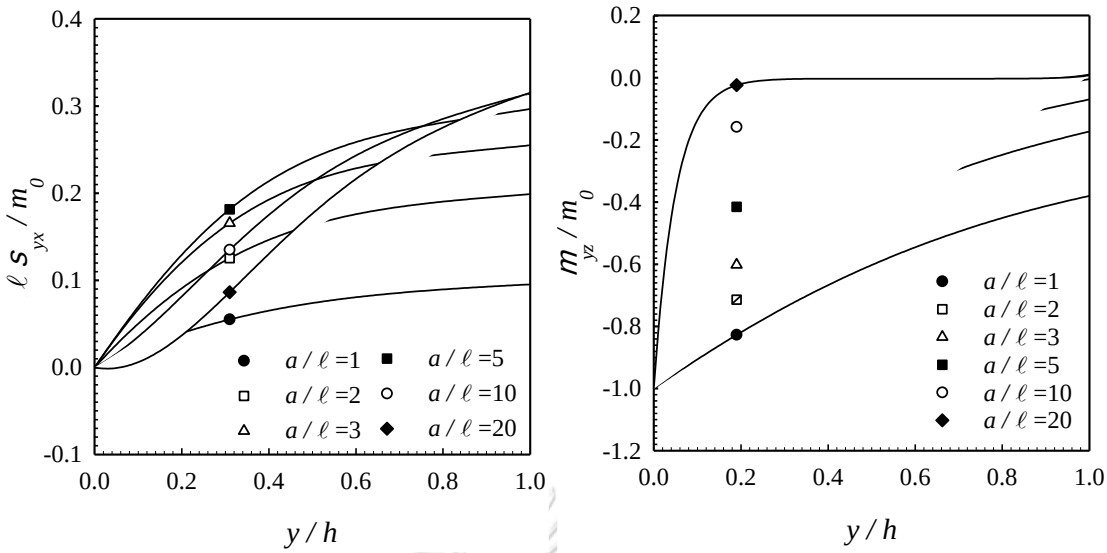

(a) (b)

Figure 4.29 Results for (a) normalized shear stress σ_{yx} and (b) normalized couple stress μ_{yz} along the line of symmetry of the elastic layer under uniformly distributed couple traction. Results are reported for $a/h = 1$, $\gamma = 0.5$, $\rho^{(1)} = \rho^{(2)} = 1$, and $\nu^{(1)} = \nu^{(2)} = 0.3$.

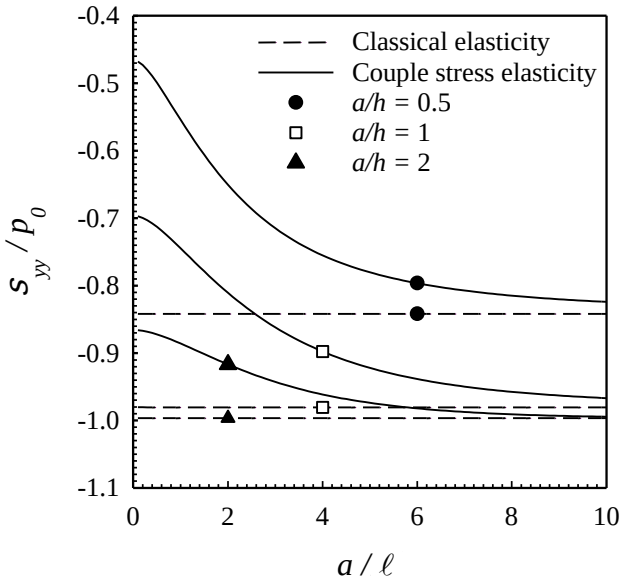

Figure 4.30 Normalized vertical stress σ_{yy} at a selected point $x = 0$, $y = h/2$ within the elastic layer under uniformly distributed normal traction versus the normalized half-length of loading region. Results are reported for $\gamma = 0.5$, $\rho^{(1)} = \rho^{(2)} = 1$, and $\nu^{(1)} = \nu^{(2)} = 0.3$.

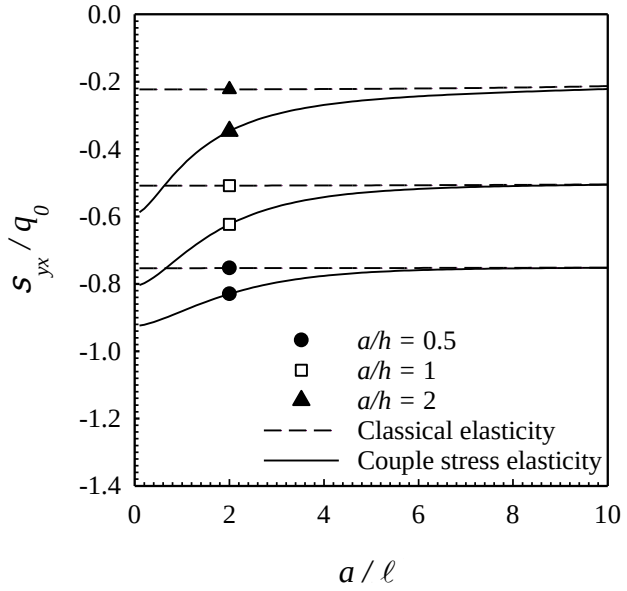

Figure 4.31 Normalized shear stress σ_{yx} at a selected point $x = 0$, $y = h/2$ within the elastic layer under uniformly distributed shear traction versus the normalized half-length of loading region. Results are reported for $\gamma = 0.5$, $\rho^{(1)} = \rho^{(2)} = 1$, and $\nu^{(1)} = \nu^{(2)} = 0.3$.

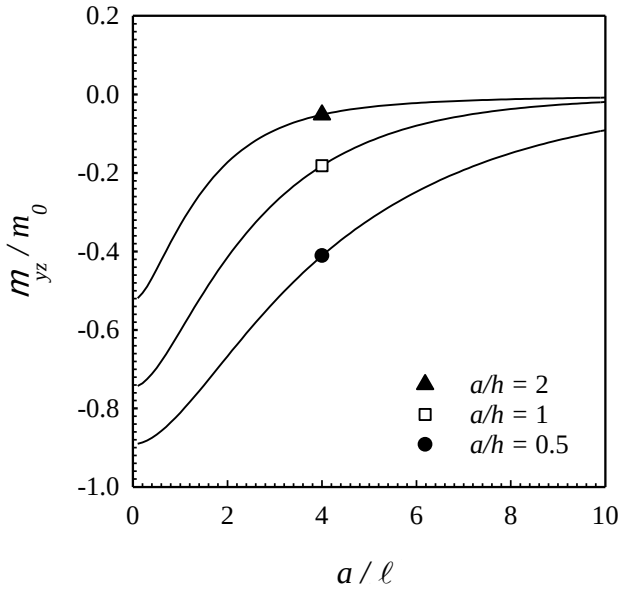

Figure 4.32 Normalized couple stress μ_{yz} at a selected point $x = 0$, $y = h/2$ within the elastic layer under uniformly distributed couple traction versus the normalized half-length of loading region. Results are reported for $\gamma = 0.5$, $\rho^{(1)} = \rho^{(2)} = 1$, and $\nu^{(1)} = \nu^{(2)} = 0.3$.

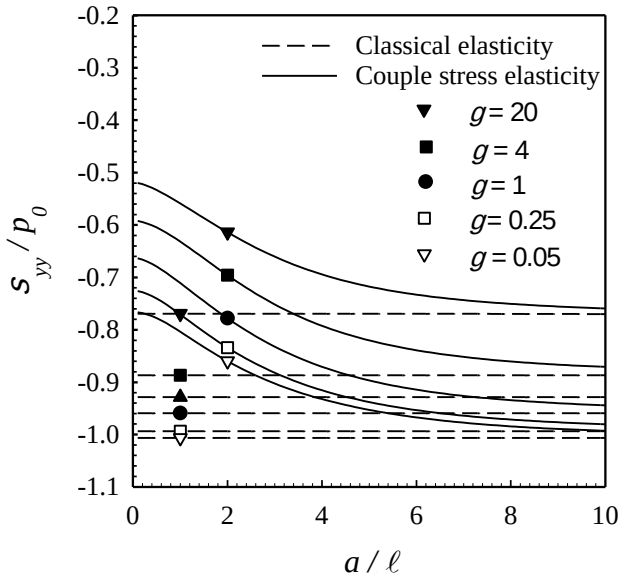

Figure 4.33 Normalized vertical stress σ_{yy} at a selected point $x=0$, $y=h/2$ within the elastic layer under uniformly distributed normal traction versus the normalized half-length of loading region. Results are reported for $a/h=1$, $\rho^{(1)}=\rho^{(2)}=1$, and $\nu^{(1)}=\nu^{(2)}=0.3$.

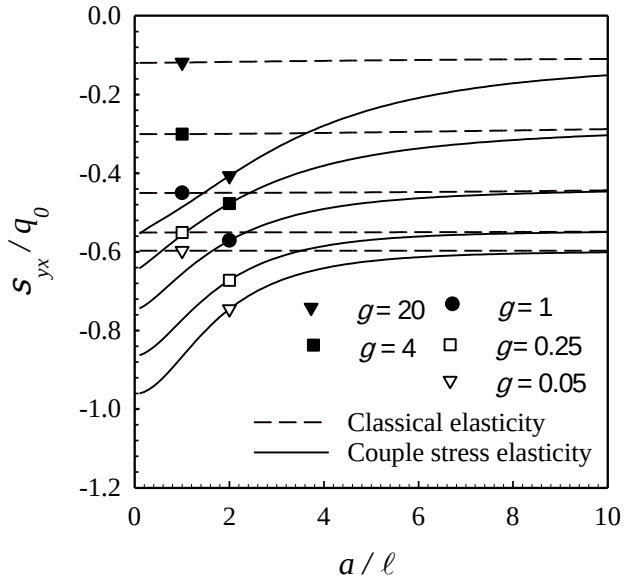

Figure 4.34 Normalized shear stress σ_{yx} at a selected point $x=0$, $y=h/2$ within the elastic layer under uniformly distributed shear traction versus the normalized half-length of loading region. Results are reported for $a/h=1$, $\rho^{(1)}=\rho^{(2)}=1$, and $\nu^{(1)}=\nu^{(2)}=0.3$.

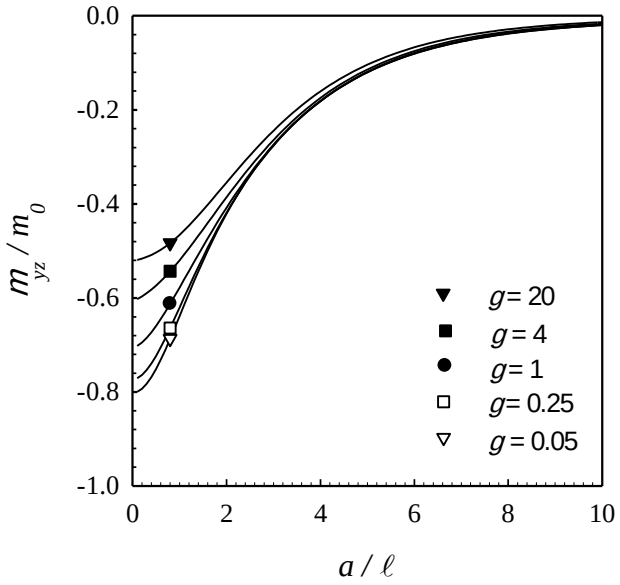

Figure 4.35 Normalized couple stress μ_{yz}/m_0 at a selected point $x=0$, $y=h/2$ within the elastic layer under uniformly distributed couple traction versus the normalized half-length of loading region. Results are reported for $a/h=1$, $\rho^{(1)}=\rho^{(2)}=1$, and $\nu^{(1)}=\nu^{(2)}=0.3$.

4.4 Layered Media Consisting of Periodic Bi-materials

To demonstrate the novel aspect of the present study in handling multi-layered media loaded on the surface with the presence of couple stresses, consider a layered material rested on a rigid base. The layered medium of total thickness H is fabricated by two different elastic materials which are arranged alternately into layers of a periodic structure as shown in Figure 4.36. The elastic shear modulus, Poisson's ratio, the material length scale, and the layer thickness of the first and second materials are denoted by $\mu^{(1)},\nu^{(1)},\ell^{(1)},h^{(1)}$ and $\mu^{(2)},\nu^{(2)},\ell^{(2)},h^{(2)}$, respectively. The layered medium is subjected Hertzian traction over a region $[-a,a]$. In particular, the distribution of the normal traction over a region $[-a,a]$ takes the following form

$$p(x)=p_0\sqrt{a^2-x^2} \tag{87}$$

where p_0 denotes the maximum pressure (also see Figure 4.36). In the simulations, the medium consisting of 10 layers with $h^{(1)}=h^{(2)}$ and with the normalized thickness

$H/\ell_0 = 1$ is chosen and the following two scenarios, one associated with $\bar{\mu}^{(1)} = 0.5\bar{\mu}^{(2)} = 1$, $\nu^{(1)} = \nu^{(2)} = 0.25$, $\rho^{(1)} = \rho^{(2)} = 1$ and the other corresponding to $\bar{\mu}^{(1)} = 2\bar{\mu}^{(2)} = 2$, $\nu^{(1)} = \nu^{(2)} = 0.25$, $\rho^{(1)} = \rho^{(2)} = 1$, are considered. It is remarked that the top layer is made of a stiffer material and a more flexible material for the first and the second scenarios, respectively.

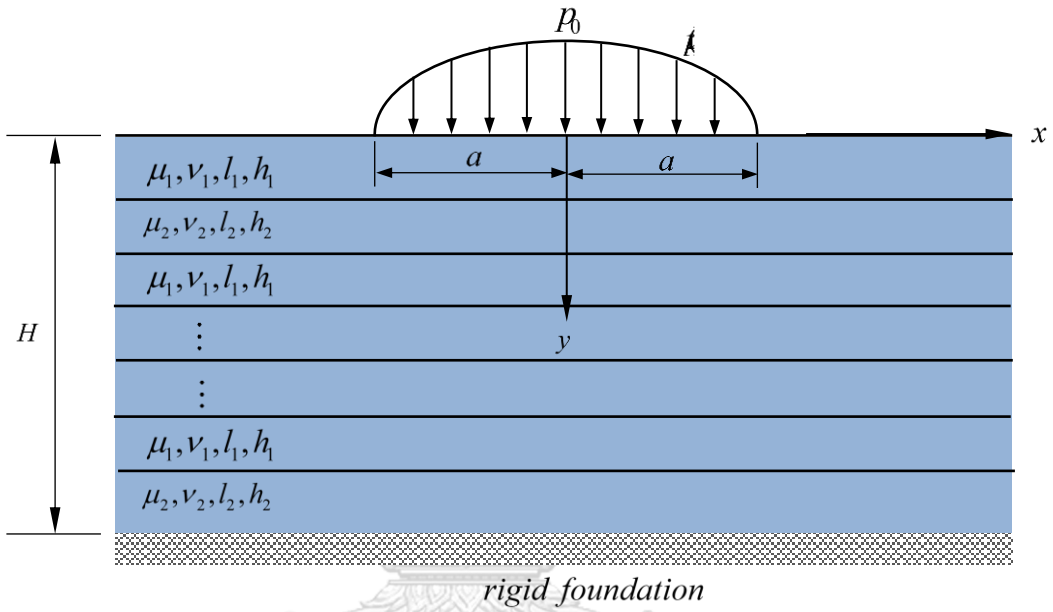

Figure 4.36 Schematic of two-dimensional layered medium consisting of two different materials arranged alternately and rested on rigid foundation. The layered medium shown is subjected to Hertzian traction over the region $[-a, a]$.

จุฬาลงกรณ์มหาวิทยาลัย
CHULALONGKORN UNIVERSITY

Results for the horizontal and vertical displacements and the rotations along the top surface (i.e., along $y = 0$), the vertical displacement along the line of symmetry (i.e., along $x = 0$), the force stresses and couple stresses along the bottom surface (i.e., along $y = H$), and certain components of force and couple stresses along the line of symmetry are reported for both scenarios in Figures 4.37-4.39, Figure 4.40, Figures 4.41-4.46, and Figures 4.47, respectively. Solutions predicted by the classical theory of linear elasticity are also reported, per necessary, for the sake of comparison. From obtained results, it is seen that the presence of couple stresses significantly alter the elastic field (both the displacements and stresses) from that predicted by the size-independent elasticity theory. In particular, it tends to stiffen the

medium. Also, it is found that the surface displacements and rotations for the case with the stiffer layer lying on the top are slightly lower than those of the other case. Similary to the computed force stresses (i.e., σ_{xx}, σ_{xy}, σ_{yx}, and σ_{yy}) at the bottom surface for the two cases (associated with the stiffer and more flexible layer lying on the top) that are also different on a small scale for both classical and size-dependent linear elasticity theories. However, couple stresses (i.e., μ_{xz} and μ_{yz}) measurement at the bottom of the layer for the case of stiffer layer laminated first is higher than another case. It is also seen from results shown in Figures 4.40 and 4.47 that the rate of decay along the depth of the bi-material layer is higher when the maerial becomes more flexible.

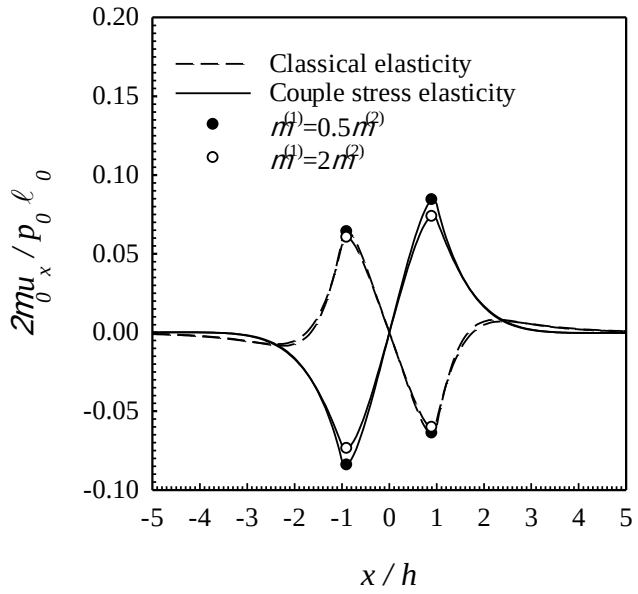

Figure 4.37 Normalized horizonal displacement u_x along the top surface of the periodic bi-materials layered medium under Hertzian loading. Results are reported for $a/H = 1$, $\rho^{(1)} = \rho^{(2)} = 1$, and $\nu^{(1)} = \nu^{(2)} = 0.25$.

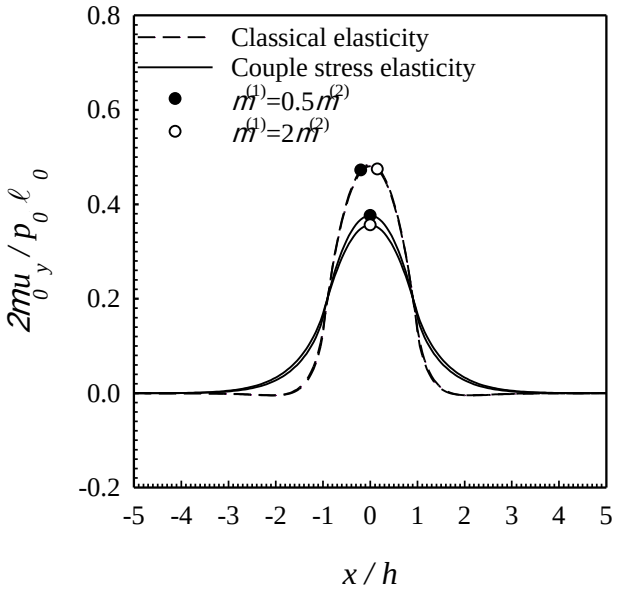

Figure 4.38 Normalized vertical displacement u_y along the top surface of the periodic bi-materials layered medium under Hertzian loading. Results are reported for $a/H=1,\ \rho^{(1)}=\rho^{(2)}=1$, and $\nu^{(1)}=\nu^{(2)}=0.25$.

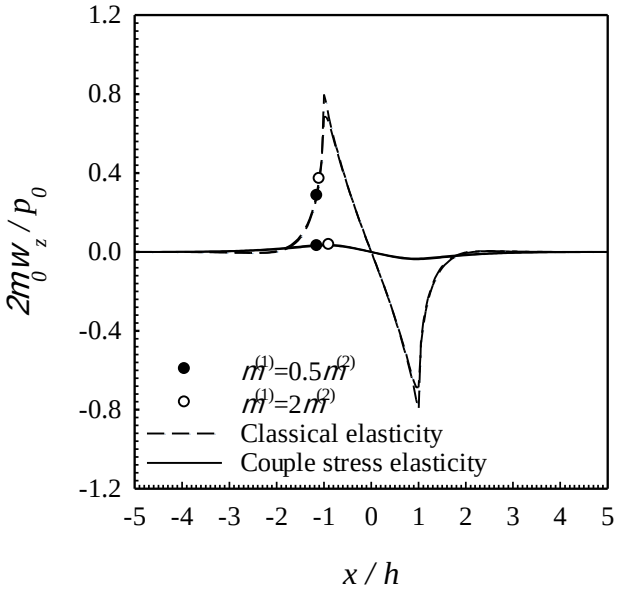

Figure 4.39 Normalized rotation ω_z along the top surface of the periodic bi-materials layered medium under Hertzian loading. Results are reported for $a/H=1$, $\rho^{(1)}=\rho^{(2)}=1$, and $\nu^{(1)}=\nu^{(2)}=0.25$.

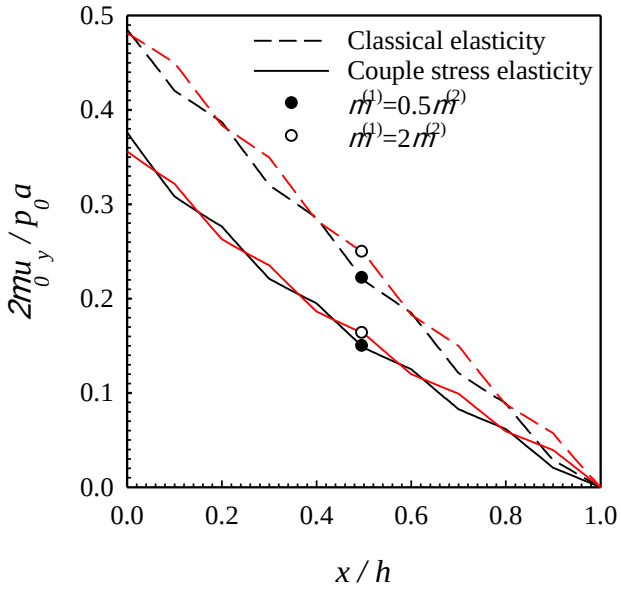

Figure 4.40 Normalized vertical displacement u_y along line of symmetry the periodic bi-materials layered medium under Hertzian loading. Results are reported for $a/H=1,\ \rho^{(1)}=\rho^{(2)}=1$, and $\nu^{(1)}=\nu^{(2)}=0.25$.

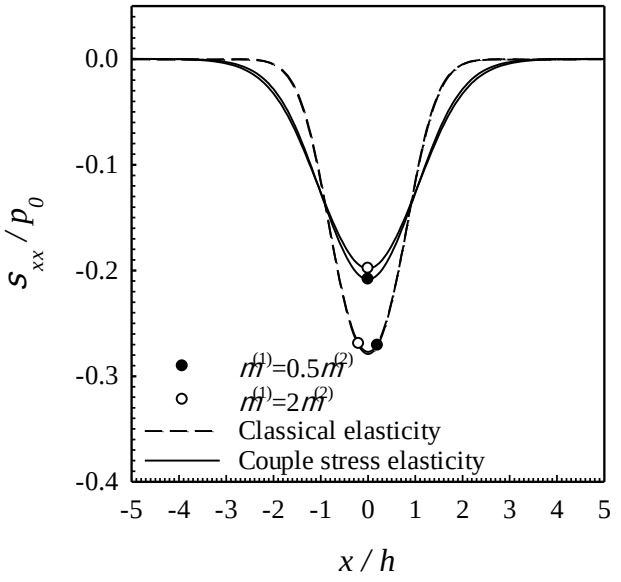

Figure 4.41 Normalized horizontal stress σ_{xx} along the bottom surface of the periodic bi-materials layered medium under Hertzian loading. Results are reported for $a/H=1,\ \rho^{(1)}=\rho^{(2)}=1$, and $\nu^{(1)}=\nu^{(2)}=0.25$.

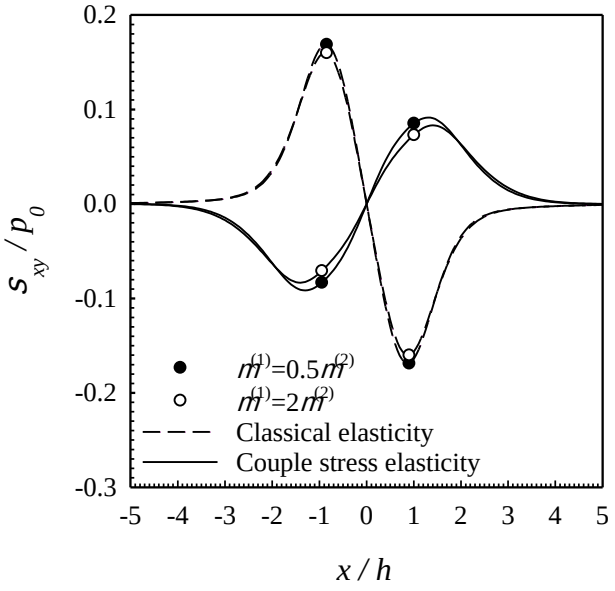

Figure 4.42 Normalized shear stress σ_{xy} along the bottom surface of the periodic bi-materials layered medium under Hertzian loading. Results are reported for $a/H=1$, $\rho^{(1)}=\rho^{(2)}=1$, and $\nu^{(1)}=\nu^{(2)}=0.25$.

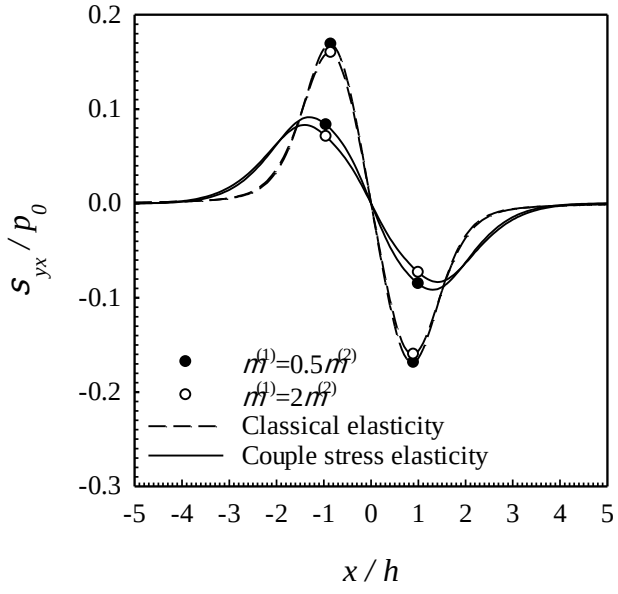

Figure 4.43 Normalized shear stress σ_{yx} along the bottom surface of the periodic bi-materials layered medium under Hertzian loading. Results are reported for $a/H=1$, $\rho^{(1)}=\rho^{(2)}=1$, and $\nu^{(1)}=\nu^{(2)}=0.25$.

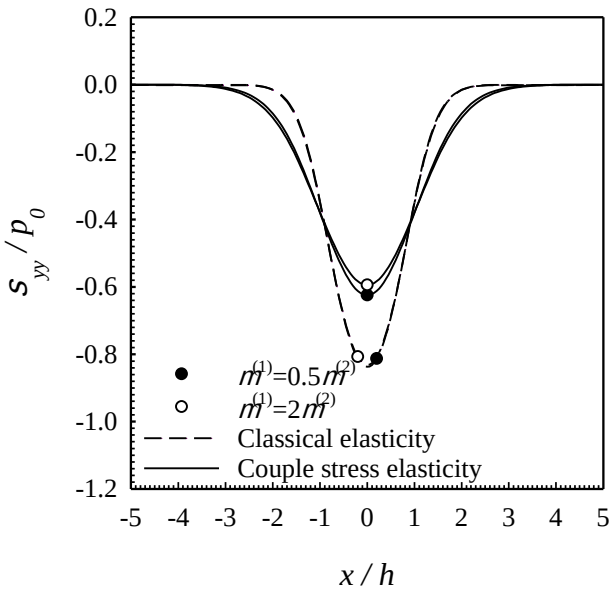

Figure 4.44 Normalized vertical stress σ_{yy} along the bottom surface of the periodic bi-materials layered medium under Hertzian loading. Results are reported for $a/H=1,\ \rho^{(1)}=\rho^{(2)}=1$, and $\nu^{(1)}=\nu^{(2)}=0.25$.

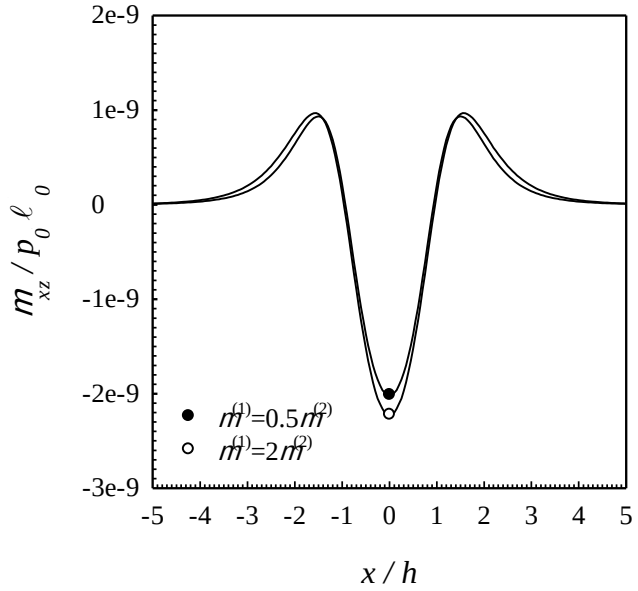

Figure 4.45 Normalized couple stress μ_{xz} along the bottom surface of the periodic bi-materials layered medium under Hertzian loading. Results are reported for $a/H=1$, $\rho^{(1)}=\rho^{(2)}=1$, and $\nu^{(1)}=\nu^{(2)}=0.25$.

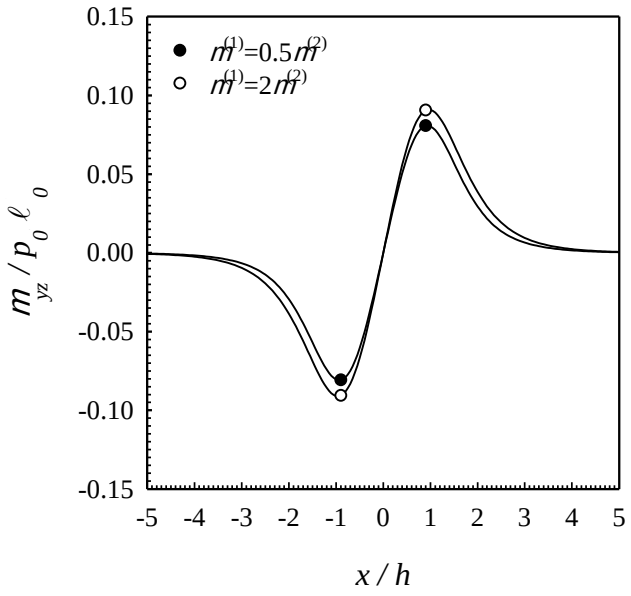

Figure 4.46 Normalized couple stress μ_{yz} along the bottom surface of the periodic bi-materials layered medium under Hertzian loading. Results are reported for $a/H=1$, $\rho^{(1)}=\rho^{(2)}=1$, and $\nu^{(1)}=\nu^{(2)}=0.25$.

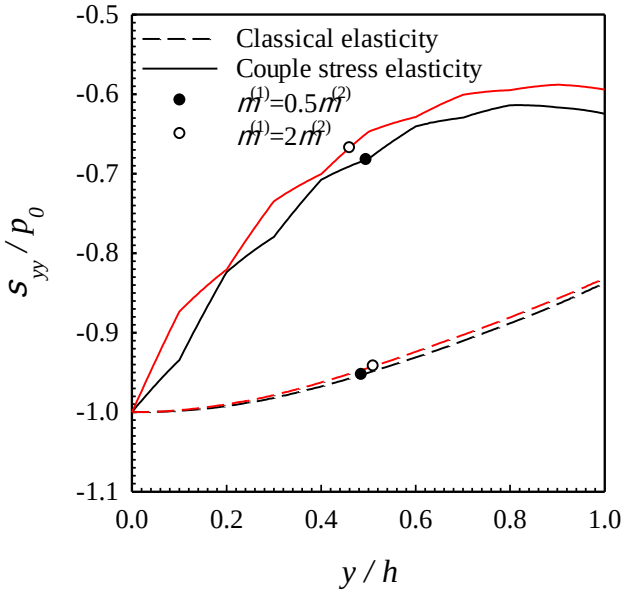

Figure 4.47 Normalized vertical stress σ_{yy} along line of symmetry of the periodic bi-materials layered medium under Hertzian loading. Results are reported for $a/H=1$, $\rho^{(1)}=\rho^{(2)}=1$, and $\nu^{(1)}=\nu^{(2)}=0.25$.

4.5 Functionally Graded Layer on Rigid Base

As a final example, consider a single layer medium of thickness h, rested on a rigid base and subjected to a uniformly distributed load p_0 over the region $[-a,a]$ as shown schematically in Figure 4.48. The medium is made of a functionally graded material with its properties varying across the thickness of the layer. In particular, the graded material properties, considered in the numerical study, are assumed in the following linear, exponential, and quadratic forms

$$A(y) = A_{(0)}\left(1+\alpha\frac{y}{h}\right) \tag{88}$$

$$A(y) = A_{(0)}\left(1+\alpha\right)^{y/h} \tag{89}$$

$$A(y) = A_{(0)}\left(1+\alpha\left(\frac{y}{h}\right)^2\right) \tag{90}$$

where $A = A(y)$ denotes the value of the material parameter at any depth y, $A_{(0)}$ is the value of the material parameter at the top surface (i.e., $y=0$), and α is a grading constant. It is worth noticing that the grading constant α appearing in (88)-(90) can be written as

$$\alpha = \frac{A_{(1)}-A_{(0)}}{A_{(0)}} = \frac{A_{(1)}}{A_{(0)}} - 1 \tag{91}$$

where $A_{(1)}$ denotes the value of the material parameter at the bottom surface (i.e., $y=h$).

จุฬาลงกรณ์มหาวิทยาลัย
Chulalongkorn University

To simulate the mechanical response of this functionally graded layer, within the context of the proposed scheme, the medium is first portioned into N identical sub-layers and each sub-layer is then represented by a homogeneous layer whose material properties are taken from those at the middle of the sub-layer. It is apparent that such approximation improves as N increases and finally converges to the functionally graded layer as the number of sub-layers is sufficiently large. For this particular problem, it is found that $N=100$ is adequate to ensure the convergence of the predicted solutions.

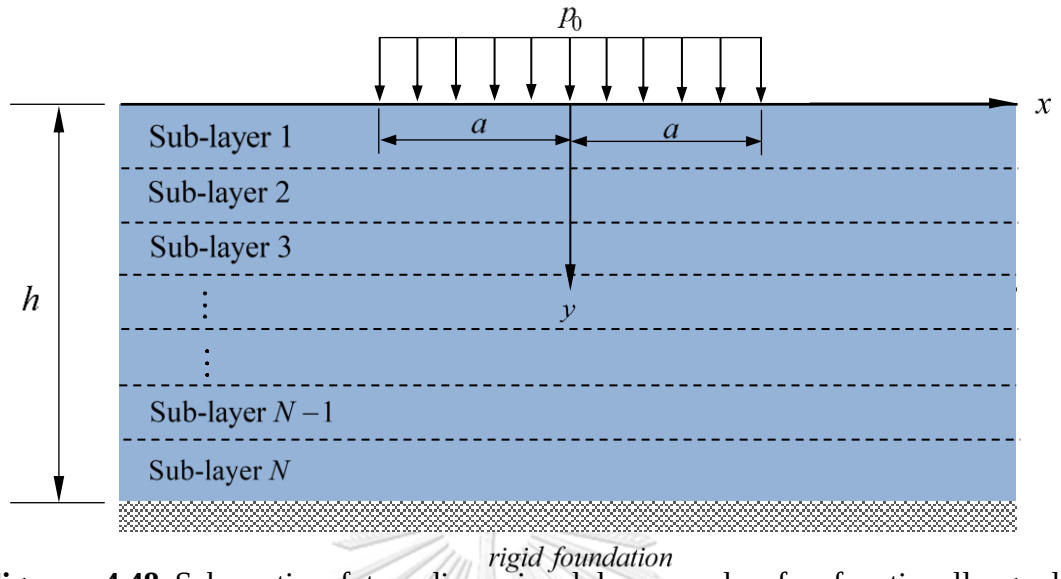

Figure 4.48 Schematic of two-dimensional layer made of a functionally graded material and subjected to uniformly distributed normal traction p_0. The layer is discretized into N identical sub-layers.

In a numerical evaluation, the thickness of the layer is taken as $h/\ell_0 = 1$ and the shear modulus, Poisson's ratio or characteristic length of the material is chosen and graded according to (88)-(90) while the remaining two material parameters are taken to be uniform across the layer. For the sake of brevity, only results for the vertical displacement u_y at top surface (i.e., $y = 0$), the shear stress σ_{yx} at bottom surface (i.e., $y = h$), the horizontal stress σ_{xx} and the vertical stress σ_{yy} along the line of symmetry (i.e., $x = 0$) in indeterminate couple stress theory are reported and compared for the chosen values of the grading constant α and grading function forms (88)-(89) in Figures 4.49-4.51, 4.52-4.54, 4.55-4.57, and 4.58-4.60, respectively.

It can be seen from the results that when the grading constant and gradation function are used differently, the predicted fields diverge from each other. This deviate trend can be observed better in the case of initial material parameter at the surface is much higher than the other end. The small gap of variation in material parameter between the two surface (i.e. small gradation constant α) provides insignificant change in the field quatities no matter which gradation function used as the values that generated by every form are about the same. Especially in the case of

the gradation of characteristice length ℓ, all the results from the different cases are scarcely told apart. However, for the case of Poisson's ratio gradation, the horizontal stress σ_{xx} has become greatly sensitive to the change eventhough the gap of gradation is not large.

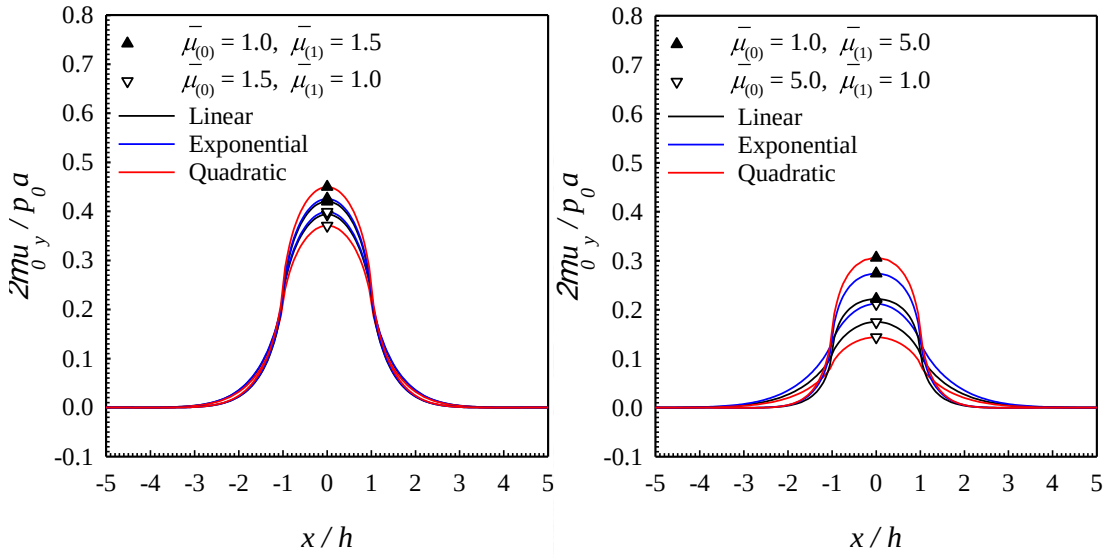

(a) (b)

Figure 4.49 Normalized vertical displacement u_y at the top surface of (a) small different between $\bar{\mu}_{(0)}$ and $\bar{\mu}_{(1)}$, and (b) large different between $\bar{\mu}_{(0)}$ and $\bar{\mu}_{(1)}$ medium under uniformly distributed normal traction. Results are reported for $a/h = 1$, $\nu = 0.3$, $\rho = 1$, and various grading functions.

จุฬาลงกรณ์มหาวิทยาลัย
Chulalongkorn University

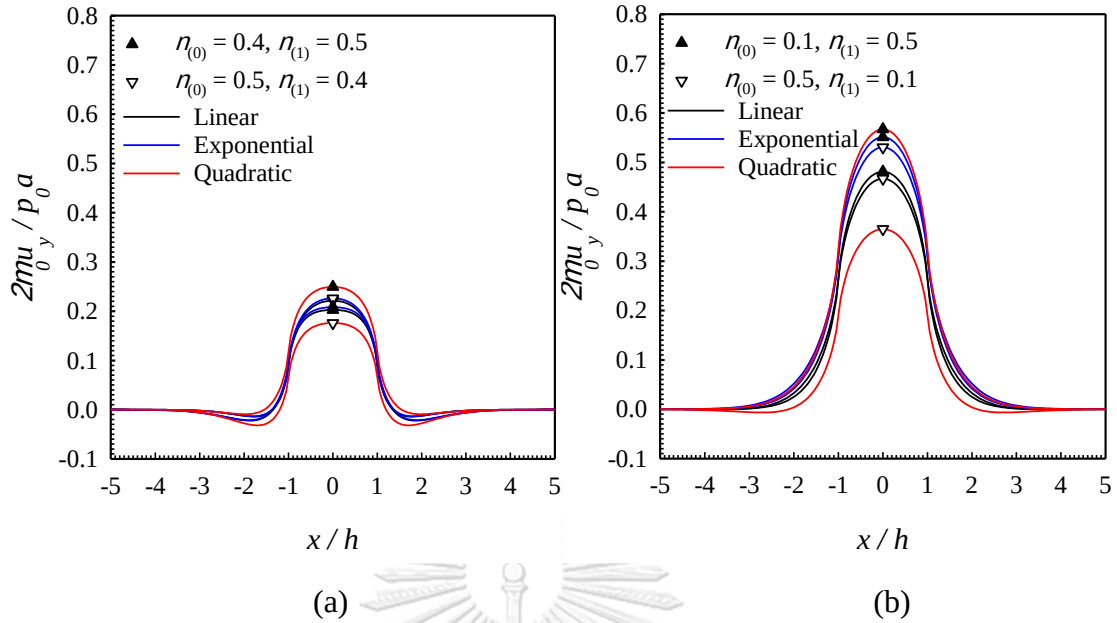

(a) (b)

Figure 4.50 Normalized vertical displacement u_y at the top surface of (a) small different between $\nu_{(0)}$ and $\nu_{(1)}$, and (b) large different between $\nu_{(0)}$ and $\nu_{(1)}$ medium under uniformly distributed normal traction. Results are reported for $a/h=1$, $\bar{\mu}=1$, $\rho=1$, and various grading functions.

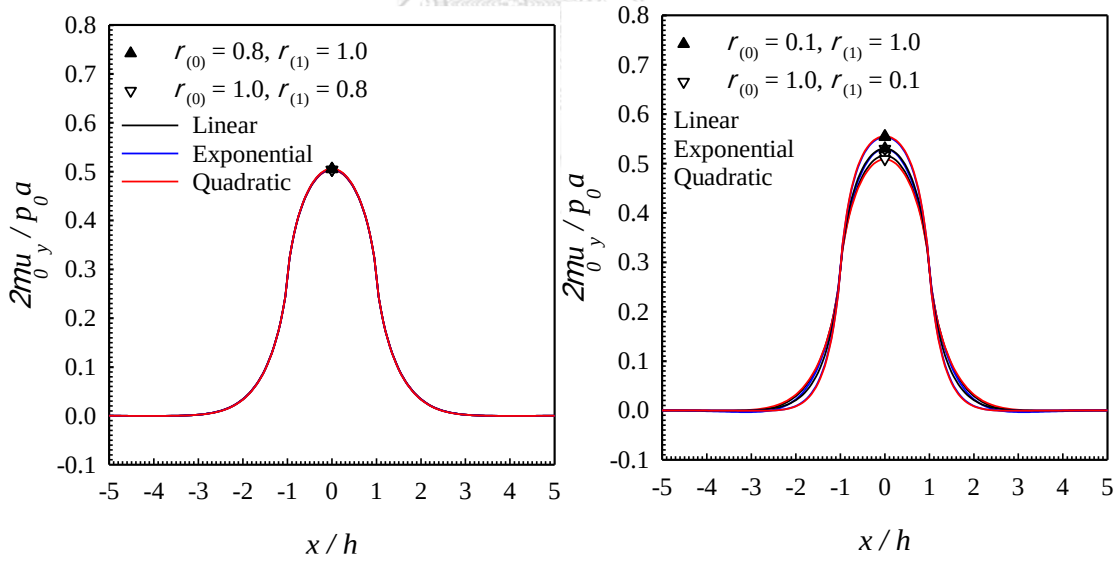

(a) (b)

Figure 4.51 Normalized vertical displacement u_y at the top surface of (a) small different between $\rho_{(0)}$ and $\rho_{(1)}$, and (b) large different between $\rho_{(0)}$ and $\rho_{(1)}$ medium under uniformly distributed normal traction. Results are reported for $a/h=1$, $\bar{\mu}=1$, $\nu=0.3$, and various grading functions.

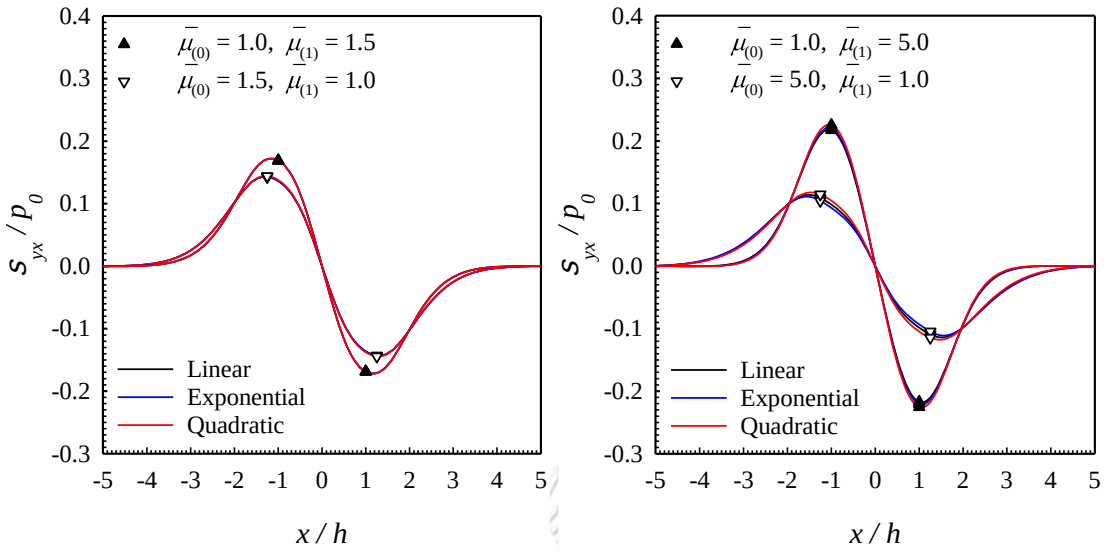

(a) (b)

Figure 4.52 Normalized shear stress σ_{yx} at the bottom surface of (a) small different between $\bar{\mu}_{(0)}$ and $\bar{\mu}_{(1)}$, and (b) large different between $\bar{\mu}_{(0)}$ and $\bar{\mu}_{(1)}$ medium under uniformly distributed normal traction. Results are reported for $a/h=1$, $\nu=0.3$, $\rho=1$, and various grading functions.

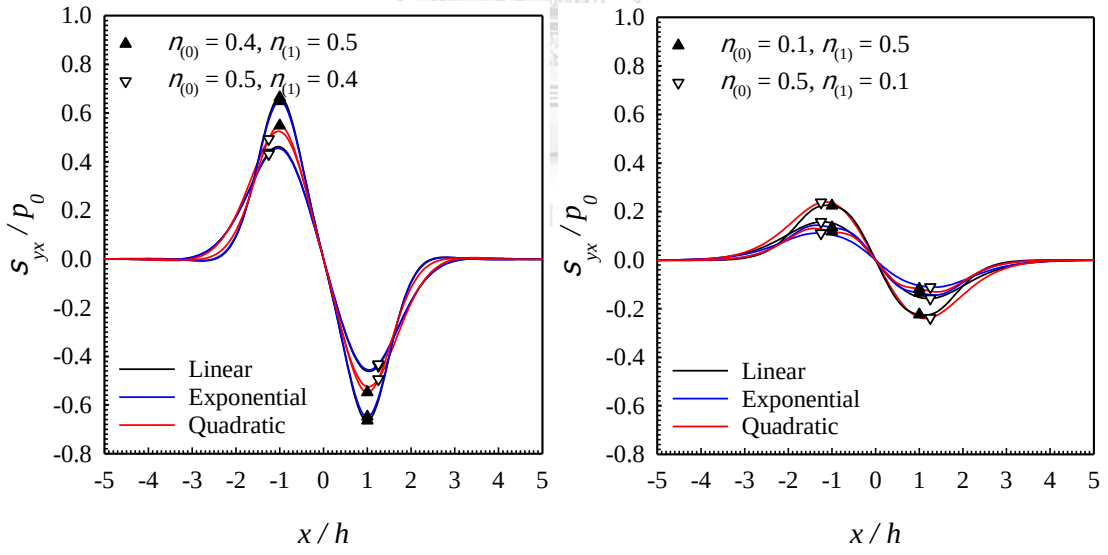

(a) (b)

Figure 4.53 Normalized shear stress σ_{yx} at the bottom surface of (a) small different between $\nu_{(0)}$ and $\nu_{(1)}$, and (b) large different between $\nu_{(0)}$ and $\nu_{(1)}$ medium under uniformly distributed normal traction. Results are reported for $a/h=1$, $\bar{\mu}=1$, $\rho=1$, and various grading functions.

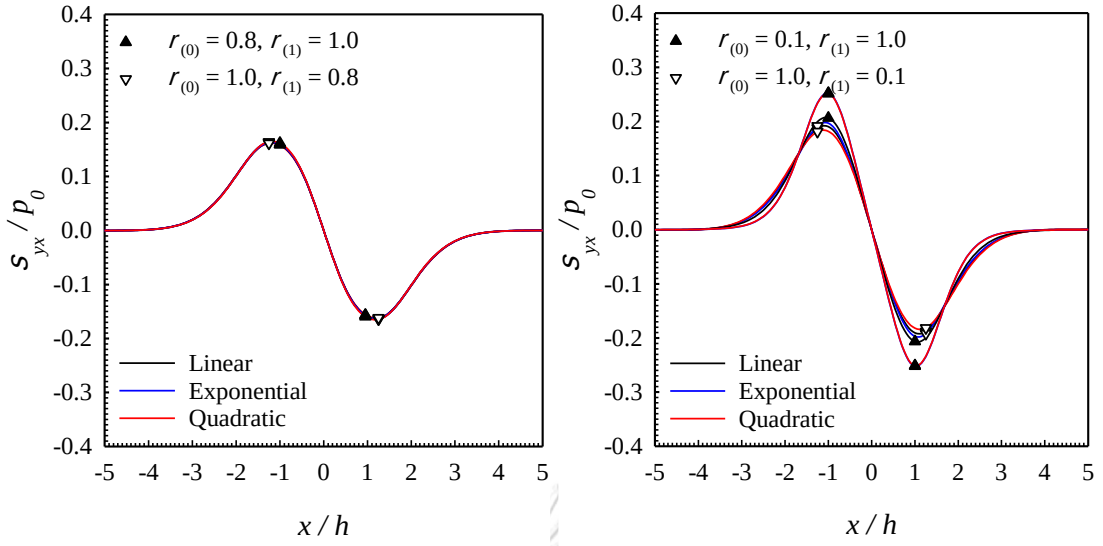

(a) (b)

Figure 4.54 Normalized shear stress σ_{yx} at the bottom surface of (a) small different between $\rho_{(0)}$ and $\rho_{(1)}$, and (b) large different between $\rho_{(0)}$ and $\rho_{(1)}$ medium under uniformly distributed normal traction. Results are reported for $a/h=1$, $\bar{\mu}=1$, $\nu=0.3$, and various grading functions.

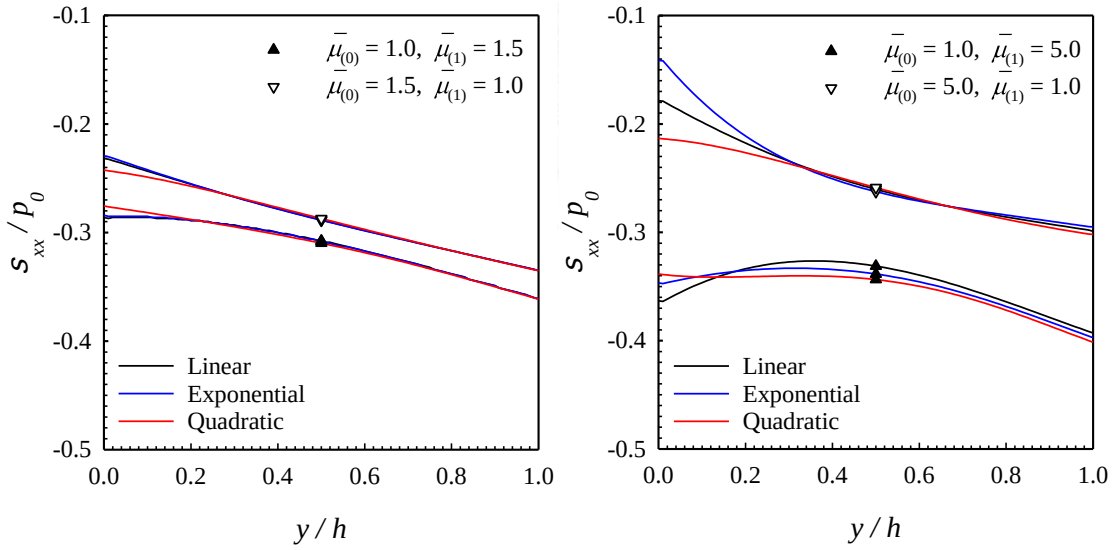

(a) (b)

Figure 4.55 Normalized horizontal stress σ_{xx} along the line of symmetry for (a) small different between $\bar{\mu}_{(0)}$ and $\bar{\mu}_{(1)}$, and (b) large different between $\bar{\mu}_{(0)}$ and $\bar{\mu}_{(1)}$ medium under uniformly distributed normal traction. Results are reported for $a/h=1$, $\nu=0.3$, $\rho=1$, and various grading functions.

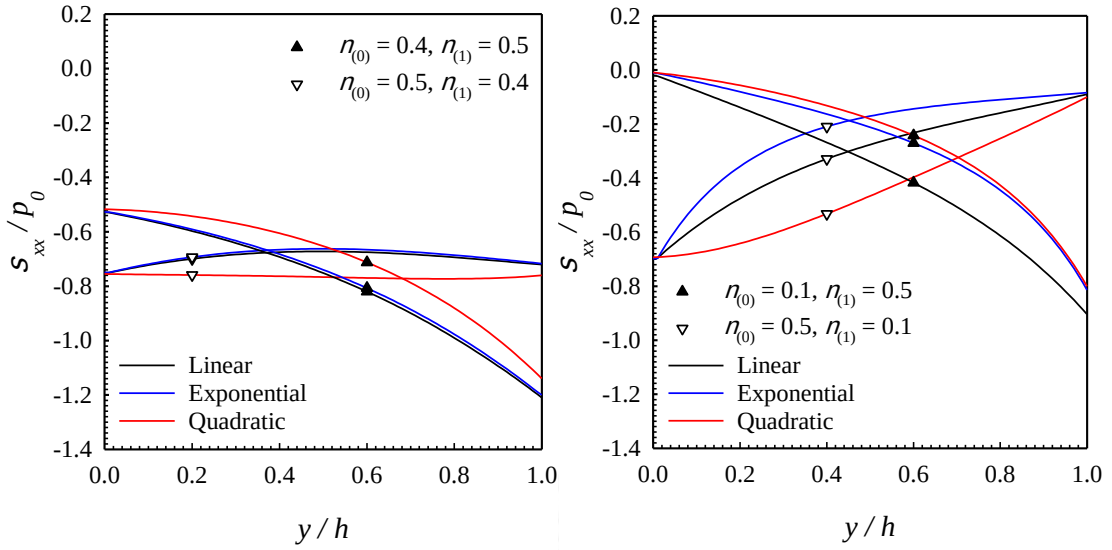

(a) (b)

Figure 4.56 Normalized horizontal stress σ_{xx} along the line of symmetry for (a) small different between $\nu_{(0)}$ and $\nu_{(1)}$, and (b) large different between $\nu_{(0)}$ and $\nu_{(1)}$ medium under uniformly distributed normal traction. Results are reported for $a/h=1$, $\bar{\mu}=1$, $\rho=1$, and various grading functions.

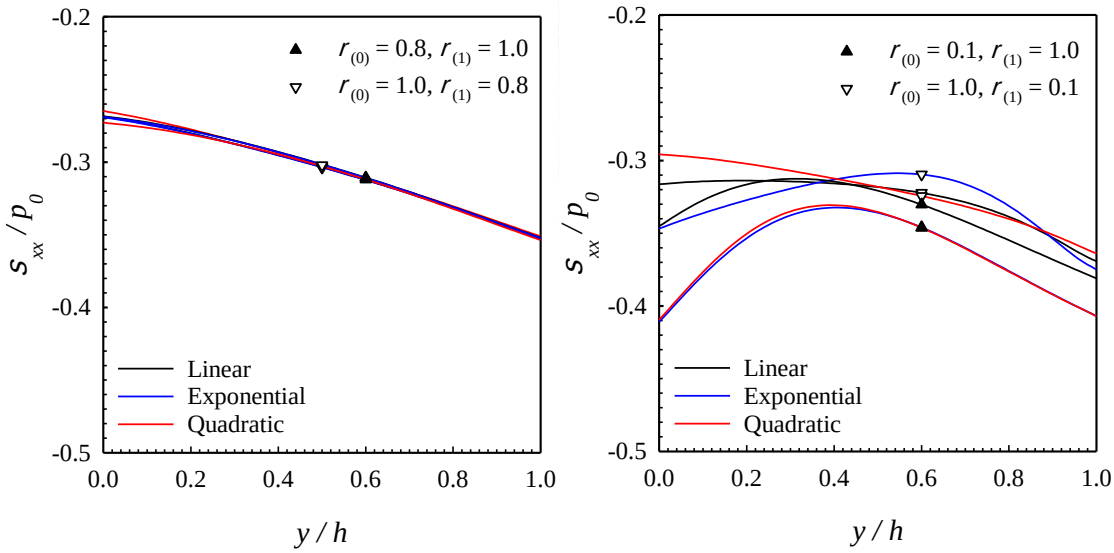

(a) (b)

Figure 4.57 Normalized horizontal stress σ_{xx} along the line of symmetry for (a) small different between $\rho_{(0)}$ and $\rho_{(1)}$, and (b) large different between $\rho_{(0)}$ and $\rho_{(1)}$ medium under uniformly distributed normal traction. Results are reported for $a/h=1$, $\bar{\mu}=1$, $\nu=0.3$, and various grading functions.

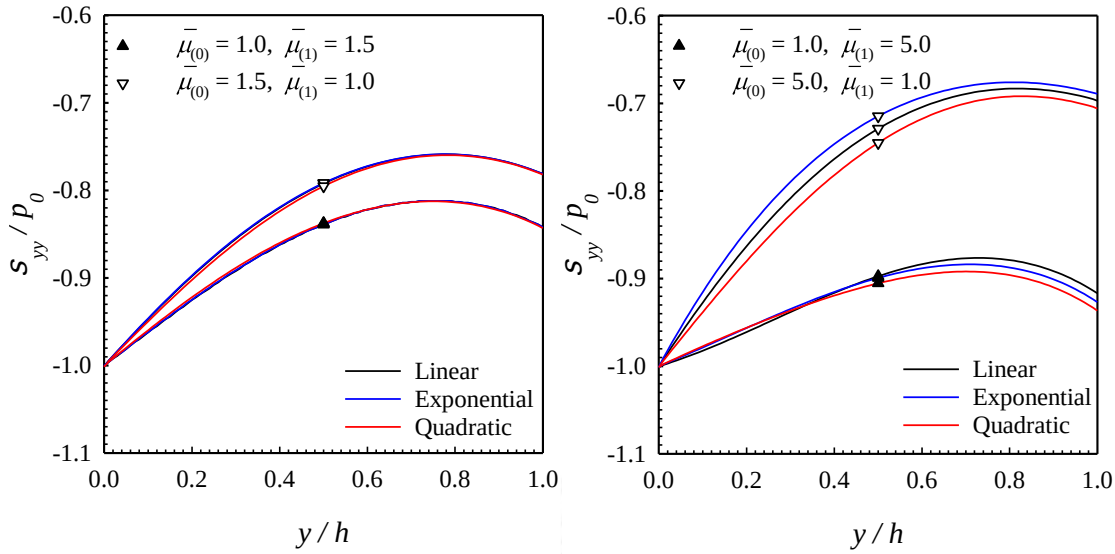

Figure 4.58 Normalized vertical stress σ_{yy} along the line of symmetry for (a) small different between $\bar{\mu}_{(0)}$ and $\bar{\mu}_{(1)}$, and (b) large different between $\bar{\mu}_{(0)}$ and $\bar{\mu}_{(1)}$ medium under uniformly distributed normal traction. Results are reported for $a/h=1$, $\nu=0.3$, $\rho=1$, and various grading functions.

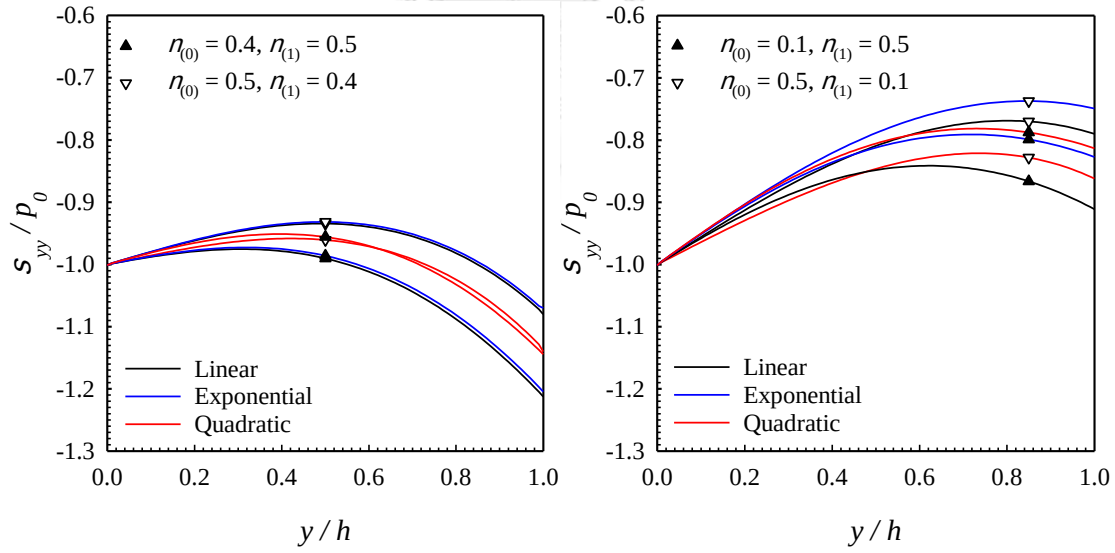

Figure 4.59 Normalized vertical stress σ_{yy} along the line of symmetry for (a) small different between $\nu_{(0)}$ and $\nu_{(1)}$, and (b) large different between $\nu_{(0)}$ and $\nu_{(1)}$ medium under uniformly distributed normal traction. Results are reported for $a/h=1$, $\bar{\mu}=1$, $\rho=1$, and various grading functions.

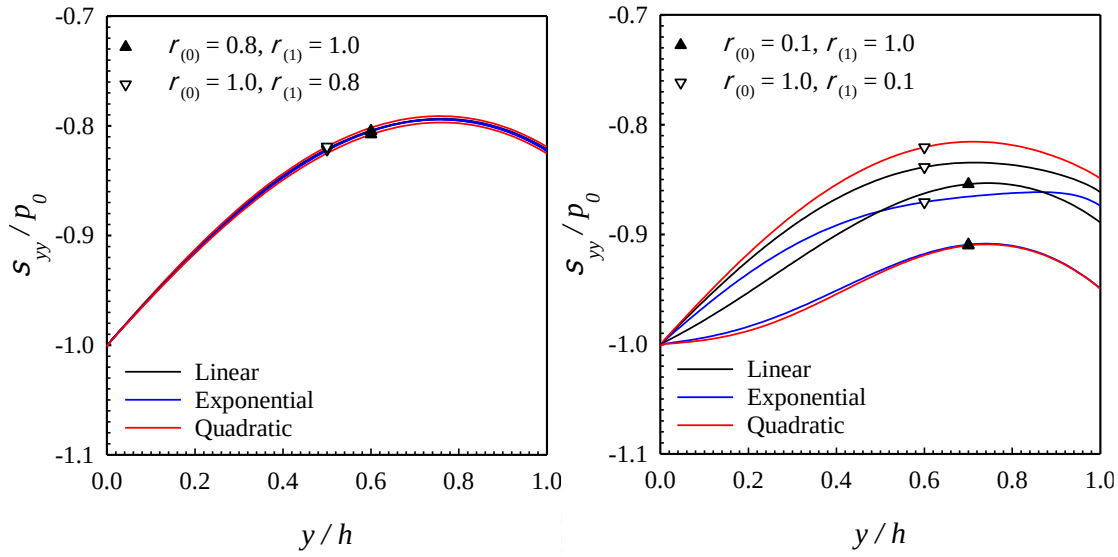

Figure 4.60 Normalized vertical stress σ_{yy} along the line of symmetry for (a) small different between $\rho_{(0)}$ and $\rho_{(1)}$, and (b) large different between $\rho_{(0)}$ and $\rho_{(1)}$ medium under uniformly distributed normal traction. Results are reported for $a/h = 1$, $\bar{\mu} = 1$, $\nu = 0.3$, and various grading functions.

จุฬาลงกรณ์มหาวิทยาลัย
Chulalongkorn University

CHAPTER 5
CONCLUSION

A set of fundamental solutions of a two-dimensional, elastic, layered medium under arbitrarily distributed loadings at the surface has been established by taking the material micro-structure into account. The indeterminate couple stress theory has been selected to form the mathematical model with the appearance of the material length scale and, in addition, to formulate the key equations governing the elastic field within each layer. An analytical solution procedure, based mainly upon the method of Fourier integral transform, has been successfully adopted to obtain the closed form general solution of the elastic field of each layer in the Fourier transform space. Such results have been further applied to construct the stiffness equation for each layer. Upon enforcing the continuity and equilibrium conditions along the material interfaces between layers together with a standard assembly procedure, it leads to a final system of equations governing nodal quantities along the interfaces of the whole layered medium. An efficient numerical quadrature has been implemented to carry out all involved integrals resulting from Fourier transform inversion.

Results from a comprehensive numerical study, upon the comparison with available benchmark cases, has confirmed the correctness of the formulation and the corresponding solution procedure. It has also been found that as the length of the loading region is comparable to the internal material characteristic length (induced by the integration of the couple stresses within the medium); the predicted solutions become size dependent and deviate significantly from those predicted from the size-independent continuum mechanics. As the size of the loading region becomes sufficiently large or relatively small in comparison with the internal material length scale, the size dependent characteristics disappears. However, for the latter case, while the size dependence cannot be observed, responses predicted with the presence of the couple stresses are still significantly different from the classical case. Results from various cases confirm the necessity to integrate the size dependent effect into the mathematical model when the influence of material micro-structure becomes significant or, equivalently, the external and internal length scales are comparable.

Resulting from the development in a general framework allowing an arbitrary number of layers with arbitrary thickness and material properties to be treated, the model can be used to simulate a layered medium made of functionally graded materials (FGM).

Although the present study focuses mainly on the layered media excited only by the prescribed surface loadings, the mathematical model has the direct application as the first approximation to investigate the indentation or contact problems where the distribution of the pressure under the indenter is presumed a priori. To offer a better approach, a set of fundamental solutions established for specific loading conditions can be used as the essential basis to formulate a set of equations governing the unknown contact pressure. This task is considered as a nontrivial extension of the current study. In addition, the generalization to treat problems in fully three-dimensional settings is also of crucial interest to further broaden the modelling capability in handling more practical cases.

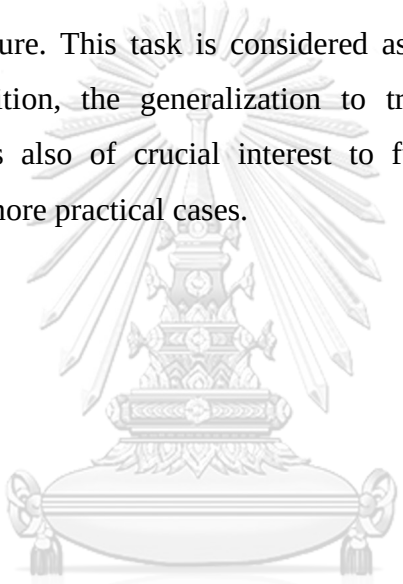

จุฬาลงกรณ์มหาวิทยาลัย
Chulalongkorn University

REFERENCES

Asaro, R. J. and V. A. Lubarda (2006). Mechanics of solids and materials. Cambridge ; New York, Cambridge University Press.

Baxevanakis, K. P., P. A. Gourgiotis and H. G. Georgiadis (2017). "Interaction of cracks with dislocations in couple-stress elasticity. Part I: Opening mode." International Journal of Solids and Structures **118-119**: 179-191.

Baxevanakis, K. P., P. A. Gourgiotis and H. G. Georgiadis (2017). "Interaction of cracks with dislocations in couple-stress elasticity. Part II: Shear modes." International Journal of Solids and Structures **118-119**: 192-203.

Booker, R. and E. Boysen (2005). Nanotechnology for dummies. Hoboken, N.J., Wiley.

Chong, A. C. M. and D. C. C. Lam (1999). "Strain gradient plasticity effect in indentation hardness of polymers." Journal of Materials Research **14**(10): 4103-4110.

Chong, A. C. M., F. Yang, D. C. C. Lam and P. Tong (2001). "Torsion and bending of micron-scaled structures." Journal of Materials Research **16**(04): 1052-1058.

Cosserat, E. and F. Cosserat (1909). Theorie des corps deformables. Paris, Hermann et Fils.

Fleck, N. A., G. M. Muller, M. F. Ashby and J. W. Hutchinson (1994). "Strain Gradient Plasticity: Theory and Experiment." Acta Metallurgica et Materialia **42**(2): 475-487.

Gourgiotis, P. A. and H. G. Georgiadis (2008). "An approach based on distributed dislocations and disclinations for crack problems in couple-stress elasticity." International Journal of Solids and Structures **45**(21): 5521-5539.

Gourgiotis, P. A. and H. G. Georgiadis (2011). "The problem of sharp notch in couple-stress elasticity." International Journal of Solids and Structures **48**(19): 2630-2641.

Gourgiotis, P. A., H. G. Georgiadis and M. D. Sifnaiou (2011). "Couple-stress effects for the problem of a crack under concentrated shear loading." Mathematics and Mechanics of Solids **17**(5): 433-459.

จุฬาลงกรณ์มหาวิทยาลัย

Gourgiotis, P. A. and T. Zisis (2016). "Two-dimensional indentation of microstructured solids characterized by couple-stress elasticity." Journal of Strain Analysis for Engineering Design **51**(4): 318-331.

Grekova, E. F. (2012). "Linear reduced cosserat medium with spherical tensor of inertia, where rotations are not observed in experiment." Mechanics of Solids **47**(5): 538-543.

Hadjesfandiari, A. R. and G. F. Dargush (2011). "Couple stress theory for solids." International Journal of Solids and Structures **48**(18): 2496-2510.

Han, B., X. Yu and J. Ou (2011). Multifunctional and Smart Carbon Nanotube Reinforced Cement-Based Materials. **Nanotechnology in Civil Infrastructure**.

Itou, S. (2013). "Effect of couple-stresses on the stress intensity factors for a crack in an infinite elastic strip under tension." European Journal of Mechanics - A/Solids **42**: 335-343.

Karasudhi, P. (1991). Foundations of solid mechanics. Dordrecht ; Boston, Kluwer Academic Publishers.

Karuriya, A. N. and T. K. Bhandakkar (2017). "Plane strain indentation on finite thickness bonded layer in couple stress elasticity." International Journal of Solids and Structures **108**: 275-288.

Koiter, W. T. (1964). "Couple-stresses in the theory of elasticity. Parts I and II." Proceedings of the Koninklijke Nederlandse Akademie van Wetenschappen **B67**: 17-44.

Liao, F., S. L. Girshick, W. M. Mook, W. W. Gerberich and M. R. Zachariah (2005). "Superhard nanocrystalline silicon carbide films." Applied Physics Letters **86**(17).

Lu, M., H. Xie, H. Huang, J. Zou and Y. He (2013). "Indentation-induced delamination of plasma-enhanced chemical vapor deposition silicon nitride film on gallium arsenide substrate." Journal of Materials Research **28**(8): 1047-1055.

Ma, Q. and D. R. Clarke (1994). "Size dependent hardness of silver single crystals." Journal of Materials Research **10**(04): 853-863.

จุฬาลงกรณ์มหาวิทยาลัย
Chulalongkorn University

Mindlin, R. D. (1963). "Influence of Couple-stresses on Stress Concentrations." Experimental Mechanics **3**(1): 1-7.

Mindlin, R. D. (1964). "Micro-structure in linear elasticity." Archive for Rational Mechanics and Analysis **16**: 51-78.

Mindlin, R. D. and H. F. Tiersten (1962). "Effects of couple-stresses in linear elasticity." Archive for Rational Mechanics and Analysis **11**(1): 415–448.

Muki, R. and E. Sternberg (1965). "The influence of couple-stresses on singular stress concentrations in elastic solids." Zeitschrift für angewandte Mathematik und Physik ZAMP **16**(5): 611–648.

Münch, I., P. Neff, A. Madeo and I.-D. Ghiba (2017). "The modified indeterminate couple stress model: Why Yang et al.'s arguments motivating a symmetric couple stress tensor contain a gap and why the couple stress tensor may be chosen symmetric nevertheless." ZAMM - Journal of Applied Mathematics and Mechanics / Zeitschrift für Angewandte Mathematik und Mechanik **97**(12): 1524-1554.

Neff, P. (2006). "The Cosserat couple modulus for continuous solids is zero viz the linearized Cauchy-stress tensor is symmetric." Zamm-Zeitschrift Fur Angewandte Mathematik Und Mechanik **86**(11): 892-912.

Neff, P., I. Münch, I.-D. Ghiba and A. Madeo (2016). "On some fundamental misunderstandings in the indeterminate couple stress model. A comment on recent papers of A.R. Hadjesfandiari and G.F. Dargush." International Journal of Solids and Structures **81**: 233-243.

Park, H. J., T. Xu, J. Y. Lee, A. Ledbetter and L. J. Guo (2011). "Photonic color filters integrated with organic solar cells for energy harvesting." ACS Nano **5**(9): 7055-7060.

Peng, B., M. Locascio, P. Zapol, S. Li, S. L. Mielke, G. C. Schatz and H. D. Espinosa (2008). "Measurements of near-ultimate strength for multiwalled carbon nanotubes and irradiation-induced crosslinking improvements." Nat Nanotechnol **3**(10): 626-631.

จุฬาลงกรณ์มหาวิทยาลัย
Chulalongkorn University

Qian, D., W. K. Liu and Q. Zheng (2008). "Concurrent quantum/continuum coupling analysis of nanostructures." Computer Methods in Applied Mechanics and Engineering **197**(41-42): 3291-3323.

Ratner, M. A. and D. Ratner (2003). Nanotechnology : a gentle introduction to the next big idea. Upper Saddle River, NJ, Prentice Hall.

Sadd, M. H. (2014). Elasticity : theory, applications, and numerics. Amsterdam ; Boston, Elsevier/AP, Academic Press is an imprint of Elsevier.

Seyyed Fakhrabadi, M. M. (2015). "Size effects on nanomechanical behaviors of nanoelectronics devices based on consistent couple-stress theory." International Journal of Mechanical Sciences **92**: 146-153.

Sneddon, I. N. (1951). Fourier transforms. New York,, McGraw-Hill.

Toupin, R. A. (1964). "Theories of elasticity with couple-stress." Archive for Rational Mechanics and Analysis **17**(2): 85–112.

Vardoulakis, I. (2019). "Cosserat Continuum Mechanics With Applications to Granular Media." Lecture Notes in Applied and Computational Mechanics **87**.

Voigt, W. (1887). "Theoretische Studien uber die Elastizitatsverhaltnisse der Krystalle." Abhandlungen der Königlichen Gesellschaft der Wissenschaften zu Göttingen **34**: 3-51.

Wong, E. W., P. E. Sheehan and C. M. Lieber (1997). "Nanobeam Mechanics: Elasticity, Strength, and Toughness of Nanorods and Nanotubes." Science **277**: 1971-1975.

Yang, C., C. Ji, W. Shen, K.-T. Lee, Y. Zhang, X. Liu and L. J. Guo (2016). "Compact Multilayer Film Structures for Ultrabroadband, Omnidirectional, and Efficient Absorption." ACS Photonics **3(4)**: 590-596.

Yang, F., A. C. M. Chong, D. C. C. Lam and P. Tong (2002). "Couple stress based strain gradient theory for elasticity." International Journal of Solids and Structures **39**(10): 2731-2743.

Yang, Y. T., K. L. Ekinci, X. M. H. Huang, L. M. Schiavone, M. L. Roukes, C. A. Zorman and M. Mehregany (2001). "Monocrystalline silicon carbide nanoelectromechanical systems." Applied Physics Letters **78**(2): 162-164.

จุฬาลงกรณ์มหาวิทยาลัย
Chulalongkorn University

Zisis, T. (2018). "Burmister's problem extended to a microstructured layer." Journal of Mechanics of Materials and Structures **13**(2): 203-223.

Zisis, T., P. A. Gourgiotis, K. P. Baxevanakis and H. G. Georgiadis (2014). "Some basic contact problems in couple stress elasticity." International Journal of Solids and Structures **51**(11-12): 2084-2095.

จุฬาลงกรณ์มหาวิทยาลัย
CHULALONGKORN UNIVERSITY

VITA

NAME	Wipavee Wongviboonsin
DATE OF BIRTH	7 Feb 1995
PLACE OF BIRTH	Khon Kaen, Thailand
HOME ADDRESS	Applied Mechanics and Structures Research Unit, Department of Civil Engineering,Faculty of Engineering, Chulalongkorn University, Bangkok, Thailand 10330

จุฬาลงกรณ์มหาวิทยาลัย
CHULALONGKORN UNIVERSITY